Mesoscale Modeling of Sediment Transport and Morphologic Changes at Tidal Inlets: Years 1-3

Prepared by:

Y. Zhang, P.A. Work, and E.J. Hayter
CMI Engineering Department
Clemson University

and

T.W. Kana
Department of Geological Sciences
University of South Carolina

Sponsored by:

Sea Grant
S.C. Sea Grant Consortium

JANUARY 1997

Mesoscale Modeling of Sediment Transport and Morphologic Changes at Tidal Inlets: Years 1–3

by

Y. Zhang, P.A. Work, and E.J. Hayter
Civil Engineering Department
Clemson University

and

T.W. Kana
Department of Geological Sciences
University of South Carolina

Sponsored by:
South Carolina Sea Grant Consortium

January 1997

ABSTRACT

A number of numerical models have been developed as predictive tools for the simulation of morphological changes of tidal inlets. Most of these models were designed for short–term simulation, on the order of days to months. These are referred to as microscale models. However, the prediction of longer–term morphological evolution is desirable for coastal planning and management. A numerical model for longer–term simulation (years to decades) of non–cohesive sediment transport and morphological changes of tidal inlets due to the combined action of waves and currents is developed and presented here. The model includes prediction of shoreline changes adjacent to an inlet and bathymetric changes around the inlet. This "mesoscale" model consists of four modules: a hydrodynamic module, a wave transformation module, a shoreline change module, and a sediment transport module.

The hydrodynamic module is an existing two–dimensional, finite element model (Veeramachaneni and Hayter 1988). This model is used to calculate the velocity field and water surface elevations resulting from astronomical tides in the vicinity of tidal inlets. The calculated hydrodynamic results are saved as time series and are used to construct empirical relations between net sediment transport over a tidal cycle and tidal range at the offshore boundary of the model domain. These empirical relations are then used in the sediment transport module. The shoreline change module (Work and Dean 1995), a "one–line" type model, was modified slightly and used to calculate the shoreline changes adjacent to a tidal inlet caused by longshore sediment transport gradients resulting from breaking waves. The input conditions to the shoreline module are breaking wave heights and directions provided by the wave transformation module. The wave transformation module was developed to include three major wave transformation processes: shoaling, refraction, and wave breaking. Computed breaking wave heights and directions serve as input conditions to the shoreline change module. The input wave heights, periods, and directions for the wave module at the offshore boundary are generated randomly using a Rayleigh probability distribution for the wave heights and periods, and a normal (Gaussian) distribution is assumed for directions. The sediment transport module is used to

compute bathymetric changes due to tidal currents based on established empirical relations. The coefficients of the empirical relations are updated if the maximum calculated bathymetric change of the domain exceeds a specified tolerance. The four modules are linked together and iterated successively.

The mesoscale model was applied to a prototype scale, hypothetical inlet system such as might be found along the South Carolina coast. Comparison of the mesoscale model results to those from a microscale model was conducted over a 178 day time period with no waves. Good agreement was obtained. A long–term (3.3 years) simulation of bathymetric and shoreline changes due to the action of waves and tides was performed.

The mesoscale modeling approach shows promising results through the comparison to the microscale model results and the long–term (3.3 years) simulation. However, verification of the model by field data is necessary. Modular construction of the model allows for easy substitution or modification of model components.

TABLE OF CONTENTS

LIST OF TABLES

LIST OF FIGURES

List of Figures (Continued)

List of Figures (Continued)

Mesoscale Modeling of Sediment Transport and Morphologic Changes at Tidal Inlets: Years 1 – 3

I INTRODUCTION

This report is the second progress report describing the progress–to–date on the research project entitled "Mesoscale modeling of sediment transport and morphologic changes at tidal inlets", a four year project being supported by the South Carolina Sea Grant Consortium. The primary objective of this project is to develop a numerical (computer) model which simulates long–term (year–to–decadal) shoreline changes around tidal inlets. The focus is on inlets typical of the South Carolina coast and similar mesotidal, mixed energy settings.

The first progress report by Work *et al.* (1996) describes the work during the first two years of the project. This report is a slightly modified version of a Master of Science thesis by Zhang (1996) in the Civil Engineering Department at Clemson University, and describes in detail the work accomplished during the first three years. A final technical report will be produced after the fourth and final year of the project.

1.A Problem Statements

Tidal inlets are channels connecting bays or estuaries to open oceans or seas. They are often located between barrier islands which parallel the shoreline and which separate bays or estuaries from oceans. Tidal inlets interrupt the continuity of the shoreline and isolate one beach from another. Currents in the tidal inlet channel originate due to the hydraulic head difference between the bay and ocean induced by astronomical tides. Some typical features of tidal inlets are ebb and flood shoals on the ocean side and bay side of the inlet, respectively (see Figure 1.1). One or both of these shoals may not exist at some inlets. The sizes of these shoals are related to the size of the tidal inlet, tidal range, sediment supply, and other parameters such as wave climate. Ebb shoals are deposits of sediment derived from adjacent beaches and the bays or estuaries. An ebb shoal is formed when sediment is carried offshore by tidal currents flowing out through the inlet. Breaking waves act to push the shoal back to shore. Ebb shoals provide

two important functions for adjacent beaches. First, they act as natural breakwaters, causing waves to break and lose most of their energy before reaching beaches. Second, the ebb shoals can function as a crucial source of sediment to adjacent beaches and provide a natural bridge for sediment to naturally bypass the inlet from one barrier island to another.

Tidal inlets are of vital importance to the economics, environmental resources, transportation and quality of life of surrounding coastal communities. They are the passages that provide hydraulic and ecological links between bays and open seas. Also, tidal inlets provide important navigational access from sheltered waters to seas and oceans for various purposes. An inlet undergoes morphological changes of some types. These changes may include inlet migration, evolution of shoals, and adjacent shoreline changes. Morphological changes of tidal inlets are generally attributed to the action of tidal currents, ocean waves, and longshore currents, along with extreme meteorological phenomena like hurricanes and northeasters. Such changes may simply be perturbations around an equilibrium state of an inlet, dynamic changes in a cyclic morphological change, or a permanent change. The morphological changes of tidal inlets are of interest to coastal engineers and planners. Understanding of tidal inlet processes and evolution help determine whether some kinds of construction measures (i.e., terminal groins, jetties, and offshore breakwaters) are desirable to maintain the stability of an inlet channel and adjacent shorelines.

1.B Objectives of Study

Many numerical models have been developed for simulation of shoreline and morphological changes of tidal inlet systems. These models can be broken into two primary categories, the microscale model and the mesoscale model, according to their simulation time scales. The spatial scale of both types of models may vary greatly. Only those models, however, with a range from one to tens of kilometers are addressed in this study. Each type of model has its own characteristics, modeling techniques, and assumptions. A mesoscale model is intended to perform simulations at long time scales, measured in years or decades, while a microscale model is operated over a relatively short time scale, on the order of hours to months. Common

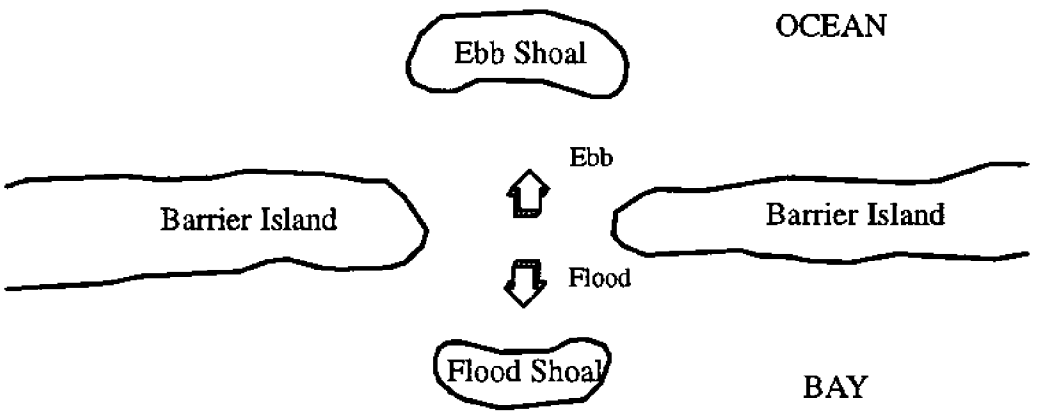

Figure 1.1 Schematized tidal inlet.

computational time steps of the latter are at most tens of minutes. At the present time it is not economically practical to use microscale models to perform longer simulations. Although some mesoscale modeling approaches have been developed in the past years, they still are in the infant stage of development compared to the microscale modeling approaches (De Vriend *et al.* 1993). Furthermore, most existing mesoscale approaches are based on input filtering (input reduction) techniques (De Vriend *et al.* 1993; Steijn *et al.* 1989; Latteux 1992, 1995), which use one or more representative tide and wave conditions instead of a long time series as model input.

The objective of this project is to develop and test a mesoscale numerical modeling approach for prediction of sediment transport and morphological changes at tidal inlets. The model application focuses on a hypothetical tidal inlet system with tidal and wave conditions such as might be found along the coast of South Carolina. The simulation emphasis is placed on bathymetric changes at the inlet and adjacent shoreline changes under the presence of tidal flows and ocean waves.

The physical processes governing morphological evolution of tidal inlets are very complex. It is impossible for a numerical model to include every process occurring in a coastal environment. The selection of physical processes to be included in a numerical model is closely

related to their significance and consideration of computational efforts for a given inlet system. Therefore, some assumptions have to be made in construction of such a numerical model.

The mesoscale model is limited to cohesionless sediment transport. Effects of density stratification on flows are not included. The flow fields within the domain to be modeled are treated as horizontal, two–dimensional flows. Depth–averaged governing equations are used to determine tidal currents. The mesoscale model is developed in submodels (or modules). The first module is for wave transformation. This module simulates the major wave transformation processes of refraction, shoaling and breaking. Wave diffraction and reflection are assumed negligible. Linear wave theory is employed, and refraction induced by mean currents is neglected. The module is intended to provide input to the shoreline change module in the form of breaking wave heights and directions.

The second module computes shoreline changes adjacent to the inlet due to sediment transport driven by breaking waves. The shoreline change module is developed based on the concept of a "one–line model" which assumes that the beach profile simply moves on or off shore without changing shape (e.g., Hansen and Kraus 1989). In addition, another function of the shoreline change module is to calculate the longshore sediment transport flux entering the inlet channel.

The third module is a microscale hydrodynamic module which is used to compute the depth–averaged velocity field and water surface elevations generated by tides. This hydrodynamic information serves as the input data for the construction of empirical relations between the residual (net) sediment transport over a tidal cycle and the corresponding tidal range at each grid node in the sediment transport module, i.e., the fourth module of the mesoscale model. Using those empirical relations, the sediment transport module computes the residual sediment transport and the resulting bathymetric changes over a tidal period corresponding to a given input tidal range. The modules are dependent on one another. To accomplish a long–term simulation of morphological evolution of a tidal inlet system, these modules are linked and run successively.

A comprehensive literature review pertinent to the microscale and mesoscale modeling approaches and prevailing sediment transport formulas is given in Section II. The model description and test results for each module are presented in Section III. In Section IV, the application to the hypothetical inlet system is illustrated. Conclusions drawn from this study and recommendations are included in Section V.

II LITERATURE REVIEW

Comprehensive studies on tidal inlet hydraulics can be found in Brunn (1978), and Mehta and Joshi (1984). These efforts emphasize prediction of flows and sediment transport through an inlet channel under simple hydrodynamic conditions, using analytical methods. In the near field, the ebb flow issuing from an inlet is treated as two–dimensional turbulent jet. Other methods, such as physical and numerical modeling, are desirable for the study of real tidal inlet systems. Buckingham (1984) studied Jupiter Inlet, Florida, using physical modeling technique. Sill *et al.* (1981) and Wells (1988) conducted a series of laboratory studies on the formation of ebb tidal shoals. These studies investigated the effects and relative significance of various factors such as waves, sediment size, tidal prism, and mean water depth on the formation of ebb shoals. With the increasing development of computer and numerical computational techniques, numerical modeling methods are increasing in popularity and viability. The major advantages of numerical modeling over physical modeling are: 1) that numerical models allow easy sensitivity studies on individual variables; 2) that computers, the facilities for numerical modeling, are widely available, and models can be stored and transferred easily for later use at little cost. In the past years, several microscale numerical models have been designed to be capable of predicting bathymetric changes in the vicinity of a tidal inlet under the action of both waves and tides (Veeramachaneni and Hayter 1988, Vemulakoda *et al.* 1987, 1988). These models are limited to relatively short–term (days to months) simulations. Numerical models suitable to longer–term simulation (years to decades) have been developed, but they still are in the infant stage of their development (De Vriend *et al.* 1993). A review of existing microscale and mesoscale models as well as prominent sediment transport equations is presented below.

2.A Microscale Numerical Models

Microscale numerical models reviewed herein have been developed primarily for prediction of bathymetric changes in the vicinity of tidal inlets over a spatial range of 1 to 10 km and a time range of days to months. In order to make the model economical to use, most such models are two–dimensional (depth–averaged). Commonly, such models consider the

effects of both waves and tides on the sediment transport, and consist of several sub–models, such as a hydrodynamic model, a wave model, and a sediment transport model. Obviously, the major limit of the microscale model is that it is not suitable for simulations of long–term (years to decades) bathymetric changes due to its relatively small computational time step (seconds to minutes). The following is a description of some models used for prediction of coastal sediment transport and, in some cases, evolution of tidal inlets.

Seelig and Sorensen (1978) developed a one–dimensional numerical model to investigate the hydraulic characteristics of inlet–bay systems. An idealized inlet–bay system was chosen. The model numerically solves the continuity and momentum equations governing the flow driven by tides in inlet channels. Sediment transport is then computed based on the flow information. The effects of the variation of some parameters on the net and gross sediment transport in an inlet channel were investigated. These parameters include: type of tide, storm surge, bay surface area, channel resistance, and the connection of a second inlet channel. Obviously, this model is unable to predict detailed hydrodynamic and morphological changes beyond the inlet channel. But, it is useful tool for understanding the effects of some factors on sediment transport characteristics in an inlet channel.

The CWSTM–H model (Veeramachaneni and Hayter 1988) was developed for prediction of cohesionless sediment transport at tidal inlets due to the combined action of waves and currents. The CWSTM–H model consists of three modules: hydrodynamics (specifically, shallow water barotropic flow), wave transformation, and cohesionless sediment transport. The flow module, coupled to the wave transformation module, is used to calculate the barotropic flow field in the vicinity of tidal inlets. The hydrodynamic module solves the depth–averaged, shallow water wave equations using a finite element scheme. The wave module simulates refraction and shoaling of small amplitude gravity waves (CERC 1984). A wave ray method is used to obtain the direction, wave length, and wave height throughout the domain. The sediment transport module calculates bed load transport induced by the flow field using an empirical procedure developed by Vincent *et al.* (1981). CWSTM–H has been used to simulate

both a prototype–scale hypothetical inlet system as well as Murrell's Inlet, South Carolina. For the hypothetical inlet system, the model was run for a period of 400 hours (about 17 days).

Vemulakonda *et al.* (1988) developed the Coastal and Inlet Processes (CIP) modeling system to numerically simulate the sediment transport at tidal inlets. This system consists of a series of models for tides and storm surge, waves, wave–induced currents and setup, and non–cohesive sediment transport. For tidal and storm surge computation, a long wave model known as WIFM (Butler 1980) is used. This model employs an alternating direction, implicit, finite–difference scheme. The monochromatic wave transformation model of Ebersole (1985) considers combined refraction and diffraction via the "mild slope" equation. Wave climate in deep water or at the offshore boundary of the numerical grid is given as input. The model computes wave height, wave length and wave direction at discrete points throughout the domain. In the surf zone, the model of Dally *et al.* (1984) is used to calculate wave transformation. The sediment transport model considers noncohesive sediments. Two regions, the open coast region away from the tidal inlet and the vicinity of the tidal inlet, are delineated for sediment transport computations because of different properties of sediment transport in these two regions. The open coast region is further divided into two zones, the area within the surf zone and the area beyond the surf zone. Within the surf zone, wave breaking and the resulting energy dissipation play a dominant role in sediment transport. The approach of Bagnold (1966) is used in this zone. Beyond the surf zone, the tractive force of the currents causes the sediment transport. Thus, the method of Ackers and White (1973) is followed after appropriate modification for the presence of waves. In the region near the inlet, the flow and bathymetry are highly complicated. Tidal currents are a major mechanism comparable to wave–induced currents. Here, the method of Ackers and White (1973) is also used to compute the transport. The CIP model can simulate the details of bathymetric change over time at tidal inlets. However, the CIP model is limited to the simulation of relatively short–term events due to the fact that the current model requires a relatively small time step to maintain stability in the model. The CIP system has been applied to two inlets, St. Marys Inlet, Florida, and Oregon Inlet, North Carolina.

Andersen *et al.* (1988) developed a two–dimensional, morphological model to describe the erosion/deposition pattern from man–made changes such as the introduction of structures or dredging in an area subject to combined wave and current action. The model simulates the morphological evolution in the area beyond the surf zone where the sediment transport is driven by the combination of waves and currents rather than breaking waves. The two sub–models, a hydrodynamic model and a wave model, are not directly coupled. The model methodology makes feasible prediction of bathymetric changes over relatively long time durations up to 32 months. The procedure used in the model is the following: after the hydrodynamic calculations are updated, the bathymetry used in updating the hydrodynamics is re–calculated based on both the new and former hydrodynamics. The rate of change in the hydrodynamic field is then extrapolated to predict the bathymetry at a given later time. This method implies that a linear relationship between hydrodynamics and bathymetric change exists. Thus, a sensitivity analysis is needed to determine the proper time step for calculation of bathymetric changes. The model has been used to predict the morphological evolution at a cooling water intake.

A simulation system (Maruyama 1988) has been developed to predict the nearshore sediment transport under the coupling of sea bottom topography, waves and currents. This system consists of three sub–models: wave propagation, nearshore current induced only by waves, and bathymetric change due to currents. This system does not consider currents induced by tides. Current induced wave refraction is also neglected. In the current model, the radiation stress due to waves is considered. The bottom friction equation by Nishimura (1982) is used when waves and currents coexist. In the topography model the continuity equation with diffusion by Watanabe *et al.* (1984) is employed. The sediment transport rate formula by Tanaka and Shuto (1981) is suitable for the case of coexisting waves and currents as used in the system. To save computing time, different grids for wave and current calculations are used. The model simulation time is on the order of ten days.

Vincent (1992) developed a two–dimensional, finite–difference, depth–averaged numerical model (USF SCOUR model) for predicting sediment transport in a tidal inlet.

Vincent's model consists of two sub–models, a hydrodynamic model and a sediment transport model. The hydrodynamic model computes tidal and wave–induced currents. Through scaling the transport up or down, this model considers the effects of contraction and expansion from subgrid features such as pilings or channels on the effective area of flow between adjacent grids. In the sediment transport model, the Engelund and Hansen (1967) equation for total sediment load is selected for the computation of sediment transport due to prior success for tidal inlet modeling (Zarillo and Park 1987; Ross 1991) and high recommendation based on comparison to other formulas. Vincent's model accounts for the contributions to sediment transport from the actions of waves and currents, but does not include the interaction of waves and currents. The model was applied to Johns Pass, Florida, and the simulated hydrodynamics and sediment transport trends were in general agreement with documented observations. Vincent's model is limited to simulation of short–term changes at tidal inlets due to a small computational time step. For Johns Pass, the length of the simulation was 14 days and the computational time step used was 1.5 seconds.

Wang *et al.* (1992) developed a nearshore morphological model. This model has three submodels: wave, nearshore current and sediment transport and bottom change model. Two approaches were tested in wave transformation calculation (shoaling, refraction, diffraction and breaking waves): the Winer (1990) and Lee and Wang (1992) wave models. The depth–integrated momentum equations (Ebersole and Dalrymple 1979) were solved for the velocity and water surface setup due to waves in the current model. The ADI (Alternating Direction Implicit) finite difference scheme was used in the current model. A sediment transport equation by Ohnaka and Watanabe (1990) which includes transport due to mean current and wave induced turbulence was employed. Three submodels are fully coupled. The model was compared with large wave tank data, the SBEACH beach profile model (Larson and Kraus 1989), and physical model results for Sebastian Inlet, FL (Wang *et al.* 1991, 1992). This numerical model does not account for tidal effects.

The GENESIS model (Hansen and Kraus 1989) was developed to simulate shoreline change produced by longshore sediment transport gradients at the coast over a large range of space and time. The longshore extent of a typical modeled reach can be 1 to 100 km, and the time frame of a simulation can be 1 to 100 months. GENESIS is usually used to calculate the shoreline change resulting from placement of coastal structures such as groins, jetties, detached breakwaters and seawalls as well as beach fills. The fundamental assumption of this model is that the shape of the beach profile does not change. Thus, one contour can describe the change of the beach plan form and volume. This is called a "one–line model". The basic assumptions of the model make it flexible and simple to use in the simulation of shoreline change. However, the model is not suitable for the simulation of tidal inlet systems because the model is developed only to describe longshore sediment transport by breaking waves well away from tidal inlets.

The SBEACH model (Larson and Kraus 1989) was developed to simulate the storm–induced changes in beach profiles. SBEACH describes the cross shore sediment transport and assumes that the longshore gradient of the longshore sediment transport rate is negligible for the modeled beach profile and, as a result, is not appropriate for use near a tidal inlet. The other basic assumptions of the model are that beach profile change is mainly governed by breaking, short–period waves, and that an equilibrium beach profile will result if forcing is held constant for infinite time. The model consists mainly of two parts, a wave model and a sediment transport model. The wave model calculates wave height and setup within the surf zone (Dally *et al.* 1985). The sediment transport rate is calculated using different relationships for different portions of the surf zone. The transport rate formulas are obtained from the results of prototype–scale laboratory experiments, i.e., large wave tank experiments, which are a reproduction of near–prototype conditions. The mass conservation equation is applied to compute the beach profile change. The finite difference approach is used in the model. The SBEACH model can be applied for situations dominated by cross–shore transport. However, it is not suitable for application when appreciable longshore gradients of longshore sediment transport exist, as is common near a tidal inlet.

2.B Mesoscale Numerical Models

De Vriend *et al.* (1993) and Stive and De Vriend (1995) summarize the state–of–the–art approaches to numerical modeling of long–term coastal evolution. Various approaches are classified as input filtering (input reduction), model reduction and behavior oriented modeling. Among the three approaches, the input reduction technique is used more often than other two. The idea of the input reduction is to select a limited number of representative tides and/or waves as the input to a microscale model for a long–term simulations to reduce computational intensity. Typically, the selection of representative tides is to take a complete tidal record over the period of interest and compute the residual (net) sediment transport in a number of critical points of the model domain. Then a limited number of representative tides is chosen, such that the residual (net) sediment transport at these points is reproduced.

Steijn *et al.* (1989) developed a numerical model for simulation of morphological evolution in the coastal environment. The model consists of a wave model, a current model and a sediment transport model. The wave model, named HISWA model, takes into account the effects of refraction due to bathymetric features and currents, and diffraction. Wave breaking is also considered. A current model is applied to compute currents induced by waves and tides. A curvilinear grid is used for a good representation of the simulated geometry. The sediment transport model is called COMOR. Several transport formulae such as Bailard (1986), CERC (1984), Bijker (1967) or van Rijn (1984) can be used in the model. But, among these formulas, only the Bailard (1986) formula can account for both cross–shore and longshore transport. In order to reduce computational effort and make the model run for a longer time, a technique of schematization of input data is introduced. This results in a limited number of representative sets of input data for the model, each with its own weight factor. Thus, the computational effort is reduced greatly and it becomes feasible to simulate long–term coastal morphological changes. Similar to the Steijn *et al.* (1989) technique of input reduction, Latteux (1987, 1992, 1995) proposes techniques for the selection of representative tides and their accuracy.

Chesher *et al.* (1995) described the HR Wallingford coastal area model, PISCES. This model contains three constituent submodules: wave propagation, current and sediment transport and morphological updating. The PISCES model was originally designed for relatively short– and medium–term modeling. To enable practical application, input filtering (reduction) and a so–called process filtering were introduced for long–term simulation. The process filtering technique is to reduce the calls to specific submodels of a model system, such that the computational time is saved. In an application to Keta Lagoon, connecting the Gulf of Guinea at Keta, Ghana, the process filtering technique was applied to reduce the calls to a bathymetry updating submodel through calculation of the residual sediment transport induced by tides over a tidal cycle. It is evident that the process filtering technique becomes more effective if it is used for a hydrodynamic submodel that usually consume the most computing time among the other submodels. As another application example, a detached breakwater case was simulated. An innovative method was developed in order to extend the applicability of the model to the long–term. Using the PISCES process–based model, the trend in the bathymetric changes during the initial stage of the morphological simulation is identified. Then, time–history bed profiles over this period are fitted to an exponential function and future bed changes are extrapolated. The bathymetry results after 300 hours using the extrapolation approach are compared to the results from the PISCES model with full morphodynamic updating method. The accuracy of this approach depends on how far in time the bathymetry will be extrapolated. This approach exhibits promising potential for long–term simulation, but needs to be tested further, as stated by Chesher *et al.* (1995).

Broker *et al.* (1995) applied the process filtering approach to simulation of coastal morphology. The approach focuses on the hydrodynamic model, a submodel of the modeling system. The procedure is to 1) "warm up" the hydrodynamic model and calculate the sediment transport field and the bottom change rates; 2) run the hydrodynamic model for a period of time corresponding to a so–called "morphological time step"; 3) re–calculate the sediment transport field based on updated bathymetry within the morphological time step; 4) compute the wave

field every k morphological time steps, where k is an arbitrary integer. In this modeling system, there are three types of wave models, elliptic mild–slope model, a parabolic mild–slope model and a spectral nearshore wind–wave model. This model system was applied to a systematic study on the morphological response to shore–parallel breakwaters.

2.C Sediment Transport Equations

A number of formulas for predicting sediment transport rate can be found. Most of these formulas have been developed for noncohesive sediment transport in steady uniform flow conditions. Because of the complexity of sediment transport processes, it is impossible to establish a formula purely theoretically. This section is intended to provide an overview of some prominent sediment transport equations. An equation which is the most suitable for this study will be selected.

Sediment transport rate is commonly subdivided into bed load and suspended load. Bed load is defined as the part of the load moving on, or near, the bed by rolling, saltation, or sliding. Suspended load moves in suspension.

The Du Boys formula (1879) is one of the oldest empirical bed load equations expressed in terms of shear stress.

$$q_b = C_d \tau_o (\tau_o - \tau_c) \tag{2.1}$$

where

q_b = bed load sediment transport rate (kg/m/sec),

C_d = characteristic sediment coefficient,

τ_o = shear stress on the bottom (kg/m^2),

τ_c = critical shear stress(kg/m^2).

Relations for C_d and τ_c are given in metric units as follows:

$$C_d = \frac{0.17}{d^{3/4}} \qquad (m^3/kg/sec) \tag{2.2}$$

$$\tau_c = 0.061 + 0.093d \qquad (kg/m^2) \tag{2.3}$$

where d = diameter of sand in millimeters.

The relations in English units are

$$C_d = \frac{0.173}{d^{3/4}} \qquad (\text{ft}^6/\text{lb}^2/\text{sec}) \qquad (2.4)$$

$$\tau_c = 0.0125 + 0.019d \qquad (\text{lb}/\text{ft}^2) \qquad (2.5)$$

The unit for d is still in millimeters.

Shields (1936) proposed a non–dimensional bed load sediment transport equation based on excess shear stress.

$$\frac{q_b(\gamma_s/\gamma - 1)}{q\gamma S} = 10\frac{\tau_0 - \tau_c}{(\gamma_s - \gamma)d} \qquad (2.6)$$

where

q = flow discharge per unit width,

γ_s = specific weight of sand,

γ = the specific weight of water,

S = slope of water surface.

This equation is dimensionless and any system of units can be used. The left hand side of the equation may be interpreted as being the dimensionless bed–load transport rate, and the right hand side the dimensionless excess shear stress.

The Meyer–Peter–Muller (1948) equation was developed based on flume experimental data with a wide range of sand sizes and flow depths. The Meyer–Peter–Muller equation has been used widely in Europe.

$$\left[\frac{q_b(\gamma_s - \gamma)}{\gamma_s}\right]^{2/3}\left(\frac{\gamma}{g}\right)^{1/3}\frac{0.25}{(\gamma_s - \gamma)d_m} = \frac{(k/k')^{3/2}\gamma RS}{(\gamma_s - \gamma)d_m} - 0.047 \qquad (2.7)$$

The parameters k and k', which are reciprocals of Manning's roughness coefficients, are given by

$$U = k\, R^{2/3} S^{1/2} \tag{2.8}$$

$$U = k'\, R^{2/3} (S')^{1/2} \tag{2.9}$$

where

S' = energy gradient caused by grain roughness,

U = average velocity,

R = hydraulic radius,

d_m = mean sediment size.

The Einstein–Brown (1950) equation, given below, is a modification of the 1942 Einstein formula by Rouse, Boyer, and Laursen presented in a chapter by Brown (1950).

$$\Phi = 40\left(\frac{1}{\Psi}\right)^3 \qquad \text{where} \quad \Phi < 5.5 \quad (\tau_* > 0.182) \tag{2.10}$$

$$0.456\Phi = e^{-0.391\Psi} \qquad \text{where} \quad \Psi > 5.5 \tag{2.11}$$

in which

$$\Phi = \frac{q_b}{\gamma_s F[g(s-1)d^3]^{1/2}} \tag{2.12}$$

$$\Psi = \frac{(\gamma_s - \gamma)d}{\tau_0} \tag{2.13}$$

$$F = \left[\frac{2}{3} + \frac{36\nu^2}{gd^3(s-1)}\right]^{1/2} - \left[\frac{36\nu^2}{gd^3(s-1)}\right]^{1/2} \tag{2.14}$$

where

ν = kinematic viscosity,

s = specific gravity of sand,

d = median sediment size.

Bagnold (1966) proposed an equation for bed load and suspended load transport based on a stream power approach. This states that the rate of work for sediment transport is equal to the product of stream power (i.e. τu) and an efficiency.

$$q_t = q_b + q_s = \left(\frac{\gamma}{\gamma_s - \gamma}\right)\tau_o u\left(\frac{e_b}{\tan\alpha} + 0.01\frac{u}{w_s}\right) \qquad (2.15)$$

where

q_s = suspended load transport rate,

w_s = sediment fall velocity,

α = a coefficient of dynamic solid friction,

e_b = bed load efficiency factor,

e_s = suspended load efficiency factor.

The efficiency factors and friction factor can be found graphically as functions of mean velocity and non–dimensional shear stress, respectively.

Colby (1984) proposed a graphical method to calculate total sediment transport as a function of mean flow velocity, depth, mean sediment size, water temperature and concentration of fine sediment (silt and clay). Calculations for sediment transport rate by the graphical method are valid only for the condition of sediment size between 0.2 mm and 0.3 mm, temperature of 60 °F, and negligible fine sediment concentration. For other cases, correction factors, k_1, for water temperature, k_2 for concentration of fine sediment and k_3 for sediment size, are introduced. Then the corrected sediment transport rate q_t is given by

$$q_t = [1 + (k_1 k_2 - 1)\ 0.01 k_3]\ q_{s1} \qquad (2.16)$$

where

q_{s1} = uncorrected sediment transport rate determined by given graphical relationships.

Engelund–Hansen (1967) applied the concept of stream power used by Bagnold (1966) to propose their sediment transport equation:

$$f\,\phi = 0.1\ (\tau_*)^{5/2} \qquad (2.17)$$

in which

$$f = \frac{2gRS}{U^2} \tag{2.18}$$

$$\phi = \frac{q_s}{\gamma_s[(s-1)gd^3]^{1/2}} \tag{2.19}$$

$$\tau_* = \frac{\tau_0}{(\gamma_s - \gamma)d} \tag{2.20}$$

where

f = friction factor,

ϕ = non–dimensional sediment transport rate,

$\tau*$ = Shields stress.

After substitution of the equations above, the Engelund–Hansen equation can be rewritten as:

$$C_s = 0.05\left(\frac{s}{s-1}\right)\frac{US}{[(s-1)gd]^{1/2}}\frac{RS}{(s-1)d} \tag{2.21}$$

where

C_s (=Q_s/Q) is the sediment concentration by weight.

Ackers and White (1973) also used Bagnold's stream power concept to relate sediment transport rate to the mobility number F_g :

$$C_s = c\ s\ \frac{d}{R}\left(\frac{U}{U_*}\right)^n\left(\frac{F_g}{A} - 1\right)^m \tag{2.22}$$

where n, c, A and m are empirical coefficients. The mobility number is given by:

$$F_g = \frac{U_*{}^n}{[gd(s-1)]^{1/2}}\left[\frac{U}{(32)^{1/2}\log(10R/d)}\right]^{1-n} \tag{2.23}$$

Sediment size is expressed as a non–dimensional grain diameter d_g:

$$d_g = d\left[\frac{g(s-1)}{\nu^2}\right]^{1/3} \tag{2.24}$$

Values of the coefficients are given in Table 2.1.

Table 2.1. Coefficients of Ackers–White equation.

$d_g > 60$	$60 > d_g > 1$
$n = 0$	$n = 1 - 0.243\ \ln(d_g)$
$A = 0.17$	$A = 0.23/(d_g)^{1/2} + 0.14$
$m = 1.5$	$m = 9.66/d_g + 1.34$
$c = 0.025$	$c = \exp\ [2.86 \ln(d_g) - 0.434\ (\ln(d_g))^2 - 8.13]$

Yang (1972, 1984) relates sediment concentration to the rate of energy dissipation of flow, which can be expressed in the product of velocity and slope, i.e., unit stream power.

$$\log(C_s) = 5.435 - 0.286 \log\frac{w_s d}{\nu} - 0.457 \log\frac{U_*}{w_s} + \left(1.799 - 0.409 \log\frac{w_s d}{\nu} - 0.314 \log\frac{U_*}{w_s}\right) \log\left(\frac{US}{w_s} - \frac{U_c S}{w_s}\right) \tag{2.25}$$

where

C_s = parts per million by weight,

w_s = sediment fall velocity,

U_* = friction velocity,

U_c = average flow velocity for incipient sediment motion.

This incipient velocity normalized by the fall velocity can be determined by the following equations:

$$\frac{U_c}{w_s} = \frac{2.5}{\log(U_* d/\nu) - 0.06} + 0.66, \qquad 1.2 < \frac{U_* d}{\nu} < 70 \tag{2.26}$$

$$\frac{U_c}{w_s} = 2.05, \qquad 70 \leq \frac{U_* d}{\nu} \tag{2.27}$$

Yang (1984) developed an equation for gravel transport:

$$\log(C_s) = 6.681 - 0.633 \log\frac{w_s d}{\nu} - 4.816 \log\frac{U_*}{w_s} + \left(2.784 - 0.305 \log\frac{w_s d}{\nu} - 0.282 \log\frac{U_*}{w_s}\right) \log\left(\frac{US}{w_s} - \frac{U_c S}{w_s}\right) \tag{2.28}$$

The equations for sand and gravel are the same in form but employ different values of the coefficients. The equation for sand should be used if sediment size is less than 2 mm; otherwise, the equation for gravel is used.

The equations above were established under steady flow conditions and do not include the effect of waves. Some sediment transport equations accounting for the influences of wave both inside and outside the surf zone are discussed below.

The Bijker equation (1967) can be used for the calculation of sediment transport due to waves and currents. Bijker's bed load equation is stated as:

$$q_b = 5\, d \frac{U}{C} g^{1/2} \exp\left[\frac{-0.27 \Delta d C^2}{\mu U^2}\left(1 + \frac{1}{2}\left(\xi \frac{u_b}{U}\right)^2\right)^{-1}\right] \tag{2.29}$$

$$\Delta = \frac{\varrho_s - \varrho}{\varrho} \tag{2.30}$$

$$\mu = \left(\frac{C}{C_{90}}\right)^{3/2} \tag{2.31}$$

$$\xi = C\left(\frac{f_w}{2g}\right)^{1/2} \tag{2.32}$$

where

u_b = the amplitude of orbital velocity near the sea bed,

ξ = Bijker parameter,

μ = ripple factor,

Δ = relative apparent density of bed material,

ϱ_s, ϱ = the density of sediment and water, respectively,

C = Chezy coefficient,

C_{90} = Chezy coefficient based on d_{90},

f_w = wave friction factor.

The Bailard equation (1986) can be expressed in the sum of four terms:

$$\vec{q}_t = \vec{q}_{bo} - \vec{q}_{bs} + \vec{q}_{so} - \vec{q}_{ss} \tag{2.33}$$

in which

$$\vec{q}_{bo} = \frac{c_f \varepsilon_b}{g(s-1)\tan\phi}\left\langle |\vec{u}|^2 \vec{u} \right\rangle \tag{2.34}$$

$$\vec{q}_{bs} = \frac{c_f \varepsilon_b \tan\beta}{g(s-1)\tan^2\phi}\left\langle |\vec{u}|^3 \vec{i} \right\rangle \tag{2.35}$$

$$\vec{q}_{so} = \frac{c_f \varepsilon_s}{g(s-1)w_s}\left\langle |\vec{u}|^3 \vec{u} \right\rangle \tag{2.36}$$

$$\vec{q}_{ss} = \frac{c_f \varepsilon_s^2 \tan\beta}{g(s-1)w_s^2}\left\langle |\vec{u}|^5 \vec{i} \right\rangle \tag{2.37}$$

where

c_f = friction coefficient,

u = velocity near the bottom due to waves and currents,

ϕ = angle of repose of sediment,

β = bottom slope,

i = unit vector directed up–slope,

w_s = the sediment fall velocity,

ε_b = efficiency of bedload transport,

ε_s = efficiency of suspended sediment transport,

$< >$ = time average over many waves.

The first subscripts b and s in the four terms of the total transport rate indicate bedload and suspended transport, respectively; while the second subscripts s and o indicate the effect of slope and horizontal bottom, respectively.

Vincent *et al.* (1981) introduced their bedload sediment transport equation based on experimental data conducted previously by Kalkanis (1964) and Abou–Seida (1965). Vincent *et al.* interpreted that the rate of accumulation of sediment in recessed traps in oscillating sediment beds is a measure of the average concentration of bed–load per unit area during the period of oscillation for which Shields stress exceeds the threshold Shields stress. The transport rate predicted by this equation matches the experimental data of Manohar (1955).

$$q_b = (0.09 \pm 0.03)(\tau_* - \tau_{*_c})\ u \tag{2.38}$$

where τ_*, τ_{*_c} = Shield's number and threshold Shield's number. It is noted that the coefficient in the equation has a unit of length (cm).

Because there exist a large number of sediment transport formulas, a reliable formula suitable to the specific physical condition must be selected. In addition to the theoretical basis of a formula, the suitability of a formula should be judged by the comparison of predictive sediment transport discharge with lab or field data. Some quantitative evaluations of formulas have been conducted by a number of researchers. As an example, Yang (1982) conducted the comparison of seven formulas with laboratory and river and stream data. These formulas include Colby (1984), Ackers and White (1973), Engelund and Hansen (1967), Shen and Hung (1972), Yang (1982), and Maddock (1976). The evaluation indicated that the formulas proposed by Yang, Engelund and Hansen, and Ackers and White were the most competent. All three

formulas were expressed in dimensionless terms and derived from the concept that sediment transport is related to the energy dissipation of the flow. Additionally, Vincent (1992) stated that consistently ranked among the most accurate by a number of researchers are the formulas proposed by Ackers and White (1973) and Engelund and Hansen (1967). Furthermore, Vemulakonda *et al.* (1987, 1988) successfully applied the Ackers and White equation to the modeling of morphology of St. Marys Inlet, Florida, and Oregon Inlet, North Carolina. The Ackers and White equation is selected as the preferred equation in this study.

III MODEL DESCRIPTION

Morphological changes at a tidal inlet are the result of sediment transport gradients arising mainly through the combined action of tides and wind–generated waves. The mechanisms of sediment transport are quite different from region to region in such an area. In an inlet channel, flows are generated primarily by the difference of water surface elevation between the ocean and bay side. This elevation difference is caused by astronomical tides, which have a semi–diurnal period of 12.42 hours on the east coast of the United States. Sediment in the inlet channel is transported primarily seaward and bayward by ebb and flood tidal currents, respectively. Wave–induced currents are assumed negligible compared to tidal currents in the channel. Inside the surf zone, oblique breaking waves striking shores generate longshore and cross–shore currents. The longshore currents move sediment along the shoreline, forming the littoral drift. Gradients of longshore sediment transport rate yield shoreline changes. Cross–shore currents cause sediment transport in the direction normal to the shoreline, and contribute to the formation of one or more longshore bars parallel to the shoreline. Outside the surf zone, sediment is transported by combined wave and tidal currents. Wave–induced orbital velocities act to mobilize the sediment. The sediment is suspended and then transported by the mean currents. If wave action becomes negligible or does not exist, the sediment is carried by the tidal currents if it exceeds a threshold value.

The physical phenomenon of sediment transport in the vicinity of a tidal inlet is extremely complicated. The factors affecting the morphologic changes of tidal inlets are numerous, some natural and some man–made. Unfortunately, it is not possible to include all factors and resultant processes contributing to sediment transport in a microscale or mesoscale model. Assumptions and simplifications of some processes must be made to reduce computational efforts for long–term simulation of an inlet system. These are described below.

3.A Assumptions

First, effects of density stratification are neglected. It is assumed that two–dimensional (depth–averaged) continuity and momentum equations are valid for the modeling of the flow field and sediment transport.

Second, monochromatic, small amplitude, progressive surface gravity waves are assumed. Wave transformation processes of shoaling, refraction and wave breaking are included in this study. Refraction due to currents and diffraction are assumed negligible.

Third, sediment transport outside the surf zone is assumed to be due to tidal currents only. On the basis of the small amplitude wave theory, the variation of wave orbital velocity near the bed is sinusoidal. If only waves are present, there is no net sediment transport. Even if a second order effect is considered, the transport is very small. This, however, is not always the case in the field. Waves act as a stirring agent, making sediment available for transport by a current which may be incapable of even initiating sediment movement by itself. The major reason to make this assumption is because it is believed that tidal effects on sediment transport are much larger than those of waves in the vicinity of tidal inlets outside the surf zone (Bruun 1978).

Fourth, it is assumed that there is no sediment transport at the offshore boundary. This boundary condition can be true as long as the offshore boundary of the domain is set far enough from the shoreline that no sediment transport occurs because of typically very low mean current velocities.

Fifth, two main processes contributing to the bathymetric change in the vicinity of the inlet are considered. One is the sediment transport derived from the adjacent shores by the longshore transport due to breaking waves. The other is the sediment transport driven by tidal currents outside the surf zone. The two processes are illustrated in Figure 3.1.

3.B Wave Transformation Module

As waves approach a coast they change in height and direction as a result of a number of wave transformation processes. These processes, due to spatial variations in bathymetry and

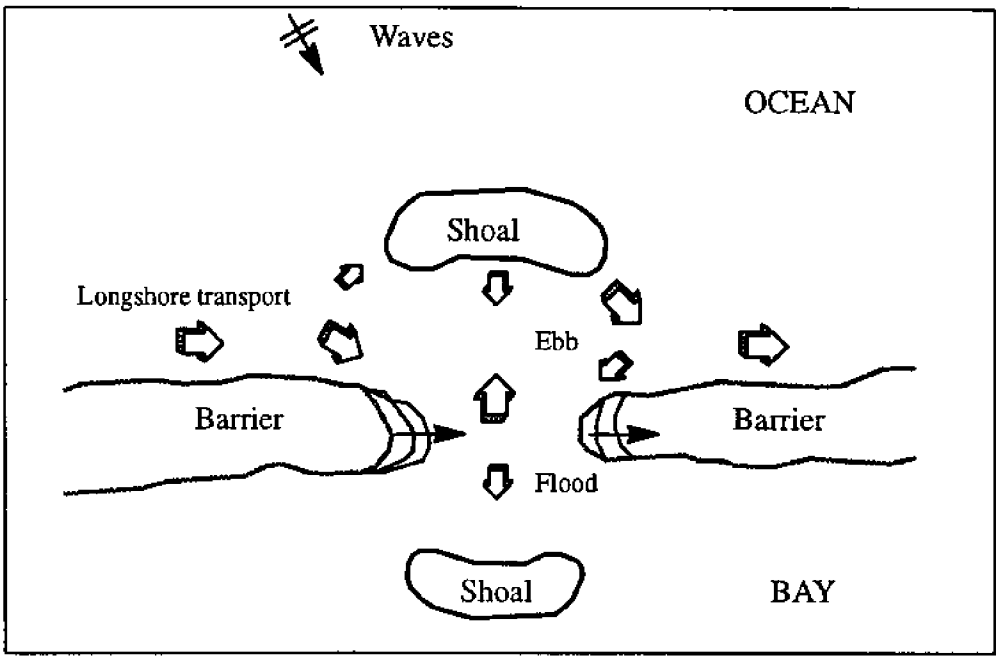

Figure 3.1 Schematized sediment transport at tidal inlet.

mean currents, may include shoaling, refraction, diffraction, breaking, and reflection. Modeling of wave transformation processes can be very complicated or relatively simple, depending on modeling strategies to be used and complexity of simulated conditions. For a simplistic case where bottom contours are straight and parallel with no mean currents, Snell's law governs the wave transformation processes of shoaling and refraction. Wave heights and directions can be determined analytically. For a case of irregular bathymetry, the two–dimensional equations governing wave transformation are more realistic than Snell's law. For instance, Work *et al.* (1996) investigated features of a number of existing numerical wave models including REFRACT (Dalrymple 1988), RCPWAVE (Ebersole *et al.* 1986), NLMSE (Kaihatu and Kirby 1992), REFDIF/S (Kirby and Ozkan 1994) and STWAVE (Resio 1993). Tests were done using the REFRACT model and the NLMSE model. In addition to processes of shoaling and refraction, diffraction was included in all of these wave models except the REFRACT model. Most of the models used a non–linear wave theory or a non–linear dispersion relation.

In this study, the primary purpose of the wave transformation module is to provide input breaking wave conditions for shoreline change modeling. Since simulations at time scales of

years to decades are desired, the wave transformation modeling is limited to monochromatic waves with the transformation processes of shoaling, refraction and wave breaking included. A simple representation of wave breaking is adopted. The interaction of tidal currents and waves is not included. This approach trades an increase in computational speed for a slight decrease in realism.

3.B.1 Governing Equations for Wave Transformation Module

The coordinate system and a finite difference grid used in this module are illustrated in Figure 3.2. The equation solved in this module are given below.

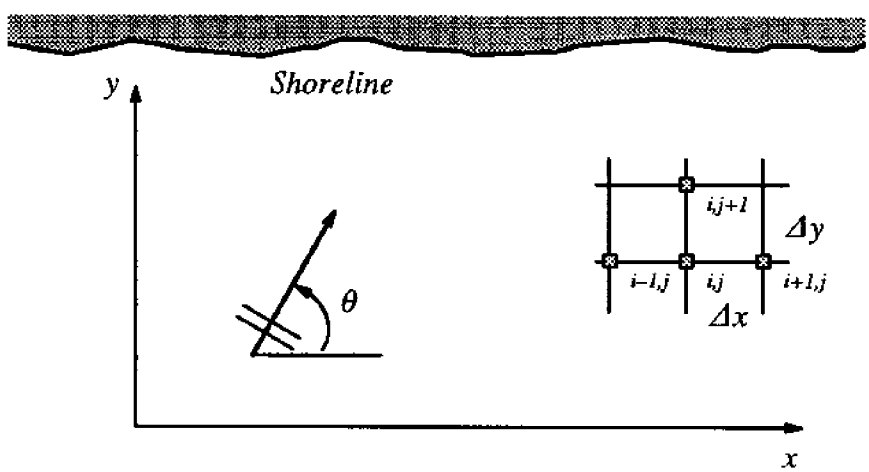

Figure 3.2 Coordinate system for wave modeling.

The equation for irrotationality of wave number:

$$\frac{\partial}{\partial x}\left(\frac{\sin\theta}{C}\right) - \frac{\partial}{\partial y}\left(\frac{\cos\theta}{C}\right) = 0 \tag{3.1}$$

Wave energy conservation equation (Dean and Dalrymple 1984):

$$\frac{\partial}{\partial x}\left(H^2 C_g \cos\theta\right) + \frac{\partial}{\partial y}\left(H^2 C_g \sin\theta\right) = 0 \tag{3.2}$$

The linear wave theory dispersion relation:

$$\sigma^2 = gk \tanh kh \tag{3.3}$$

where

x, y = longshore and onshore coordinate, respectively,

θ = wave angle,

C = wave celerity, $C = \frac{\sigma}{k}$

σ = wave angular frequency, $\sigma = \frac{2\pi}{T}$

T = wave period,

k = wave number, $k = \frac{2\pi}{L}$

L = wave length,

H = wave height,

C_g = group speed expressed as:

$$C_g = \frac{C}{2}\left[1 + \frac{2kh}{\sinh 2kh}\right] \tag{3.4}$$

3.B.2. Finite Difference Equations for Wave Transformation Module

A finite difference numerical method proposed by Koutitas (1988) is used to solve the governing equations above. The explicit finite difference equation for wave angle is expressed as:

$$\theta_{i,j+1} = \cos^{-1}\left\{\left[\frac{\Delta y}{2\Delta x}\left(\frac{\sin\theta_{i+1,j}}{C_{i+1,j}} - \frac{\sin\theta_{i-1,j}}{C_{i-1,j}}\right) + \frac{\cos\theta_{i,j}}{C_{i,j}}\right] C_{i,j+1}\right\} \tag{3.5}$$

The finite difference equation for wave height is given by:

$$H^2_{i,j+1} = \frac{1}{\left(C_g \sin\theta\right)_{i,j+1}}\left[\left(H^2 C_g \sin\theta\right)_{i,j} - \frac{\Delta y\left[\left(H^2 C_g \cos\theta\right)_{i+1,j} - \left(H^2 C_g \cos\theta\right)_{i-1,j}\right]}{2\Delta x}\right] \tag{3.6}$$

The stability of this procedure is dependent on the values of Δx and Δy as well as the wave celerity. The value of θ is between 0 and π.

3.B.3 Boundary Conditions

To solve the system of finite difference equations above, initial and boundary conditions must be specified. The following boundary conditions are employed:

1. Since the domain to be modeled is large, parallel contours are assumed on the updrift and downdrift domain boundaries.
2. Wave heights, wave periods and directions are input uniformly on the offshore boundary where the water depth is relatively deep and the longshore variation is relatively small.

3.B.4 Input Wave Climate

It is observed that wave height, period and direction in the field vary randomly with time, and the probability of occurrence for each appear to follow certain distributions. Generally, wave height in deep water follows a Rayleigh distribution. Wave period was also assumed to follow a Rayleigh distribution, and wave direction a normal distribution. The Rayleigh probability density functions for wave height and period can be expressed as (Dean and Dalrymple 1984):

$$f(H) = \frac{2H}{H^2_{rms}}\exp\left[-\left(\frac{H}{H_{rms}}\right)^2\right] \tag{3.7}$$

$$f(T) = \frac{2T}{T^2_{rms}}\exp\left[-\left(\frac{T}{T_{rms}}\right)^2\right] \tag{3.8}$$

where

H = wave height,

T = wave period,

H_{rms}, T_{rms} = the root mean square values of wave height and period, respectively.

These are expressed as:

$$H_{rms} = \sqrt{\frac{1}{N}\sum_{i=1}^{N} H_i^2} \tag{3.9}$$

$$T_{rms} = \sqrt{\frac{1}{N}\sum_{i=1}^{N} T_i^2} \tag{3.10}$$

The relationship between the mean value and the root mean square value of wave height is given as

$$\overline{H} = 0.886 H_{rms} \tag{3.11}$$

The same relationships are assumed to hold for wave period. The normal distribution function for wave direction is given by

$$f(\theta) = \frac{1}{2\pi\sigma}\exp\left[-\frac{1}{2}\left(\frac{\theta - \overline{\theta}}{\sigma_1}\right)^2\right] \tag{3.12}$$

where

θ = wave direction,

σ_1 = standard deviation,

$\overline{\theta}$ = mean wave direction.

Using given mean wave height and period, mean wave direction, and the standard deviation of wave direction, two subroutines are run to generate random wave heights, periods, and directions following the prescribed probability distribution for the wave transformation module.

To verify these two subroutines, comparisons of the density distribution of 5000 numbers generated by the subroutines to theoretical expressions are illustrated in Figure 3.3. Bars in the

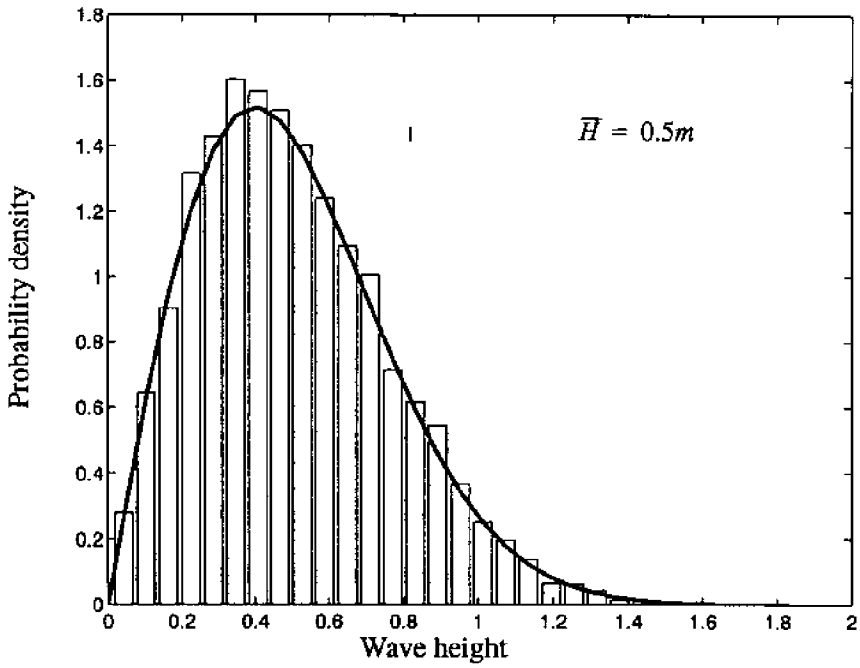

(a) Rayleigh distribution for wave height

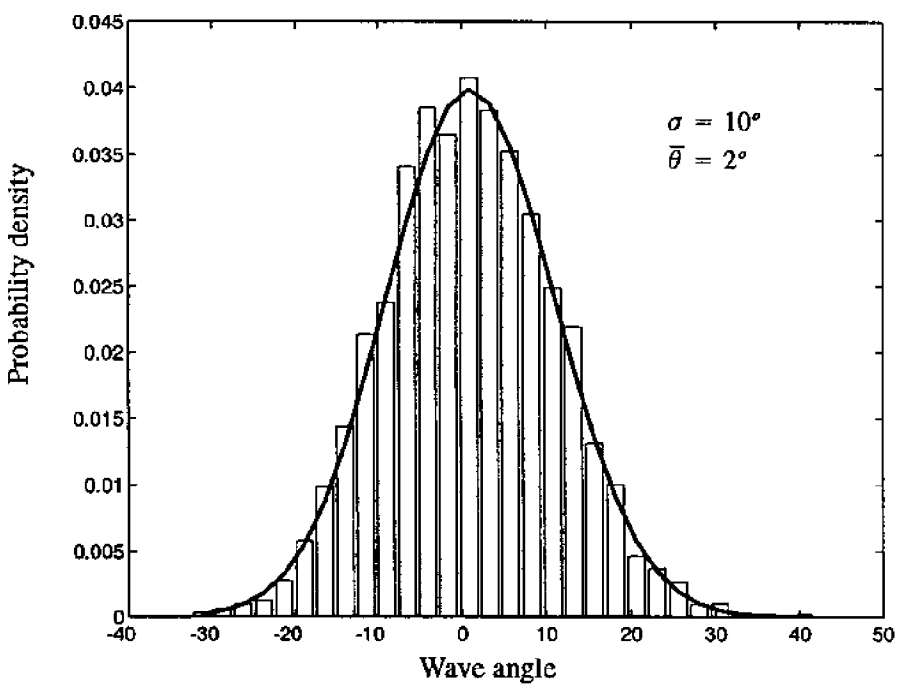

(b) Normal distribution for wave direction

Figure 3.3 Probability density distribution of input wave climate of wave model.

figures represent the results generated by the subroutines, and solid lines are theoretical distribution curves. A good agreement is indicated.

3.B.5 Wave Breaking Criterion

If the calculated wave height is greater than 78% of the water depth, the wave height is set to 78% of water depth (McCowan 1894). This criterion is simple and is commonly used in wave transformation calculations. It is noted that the criterion neglects any dependence on wave period and beach slope.

3.B.6 Applicability of Wave Module

The wave module was tested by simulating a hypothetical case. The calculated wave height vectors for two constant incoming wave angles are shown in Figure 3.4. The figure indicates that the wave heights increase and wave directions tend to turn toward bottom contours as waves propagate on the varying bathymetry with a gradual decrease in water depth.

Additionally, wave heights calculated by the wave module were compared to the analytical solution (Snell's law and conservation of energy) at two sections, A–A' and B–B', as shown in Figures 3.5. and 3.6. The ordinates in these figures are the ratio of the local wave height to the input wave height at the offshore boundary. Variable x_b in the abscissa denotes the distance from the offshore boundary to the wave breaking points. At section A–A' where contours are locally straight and parallel, Snell's law is valid. The calculated wave heights match the analytical solution given by Snell's law. At section B–B', the calculated wave heights are higher than the analytical solution near the wave breaking points where Snell's law becomes less valid because of longshore bathymetric gradients. Thus, deviations will arise when Snell's law is applied to the case where bottom contours are not straight and parallel.

For a given domain to be modeled, the water depth usually becomes shallower gradually as waves approach the shoreline. If a relatively coarse numerical wave transformation model grid is used, wave breaking will occur between nodes. In this case, if the wave height or direction at a neighboring node is directly taken as the breaking wave height or direction, a considerable deviation from the "real" value may arise. To more accurately determine the breaking wave

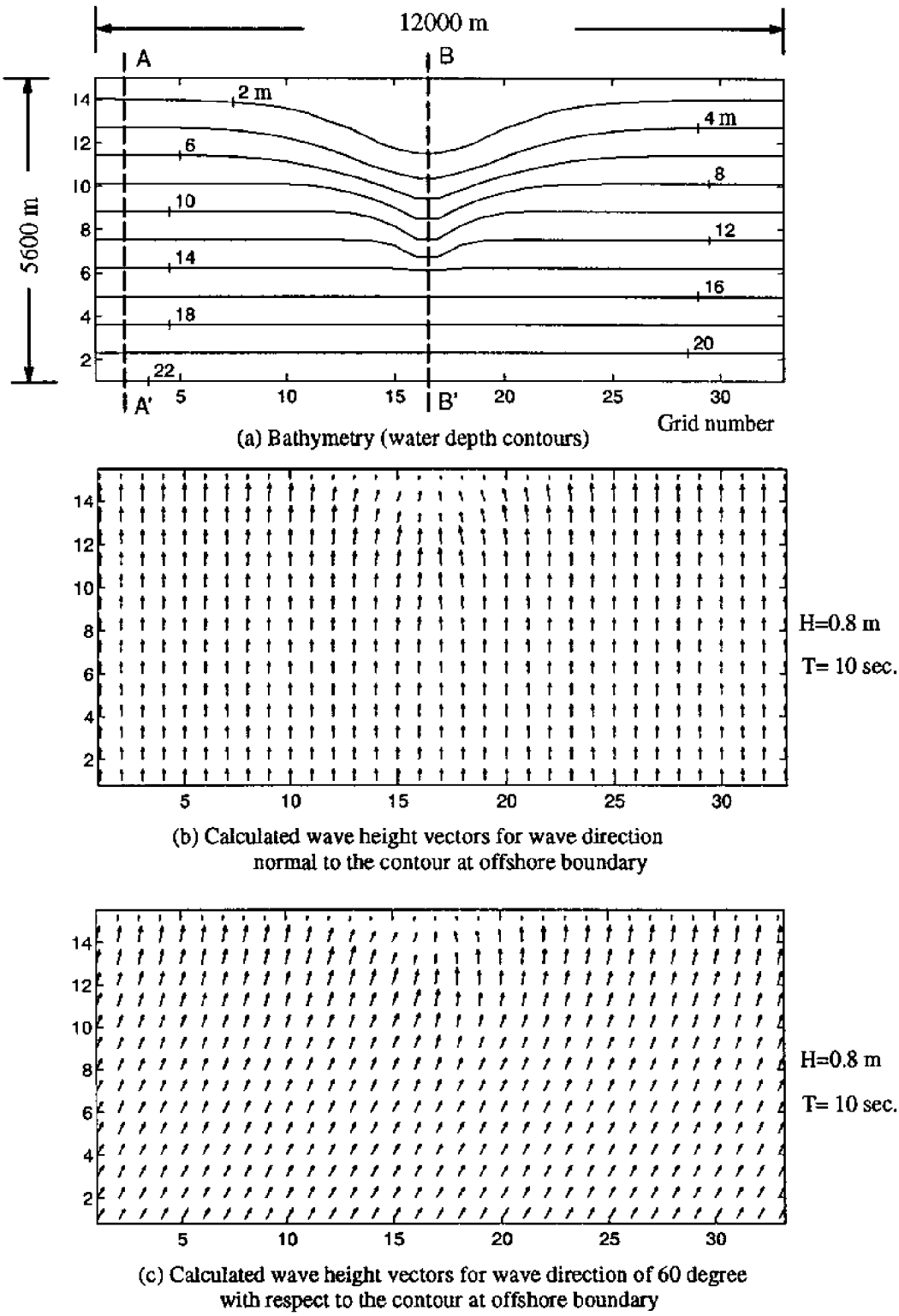

Figure 3.4 Bathymetry and calculated wave vectors for wave modeling tests.

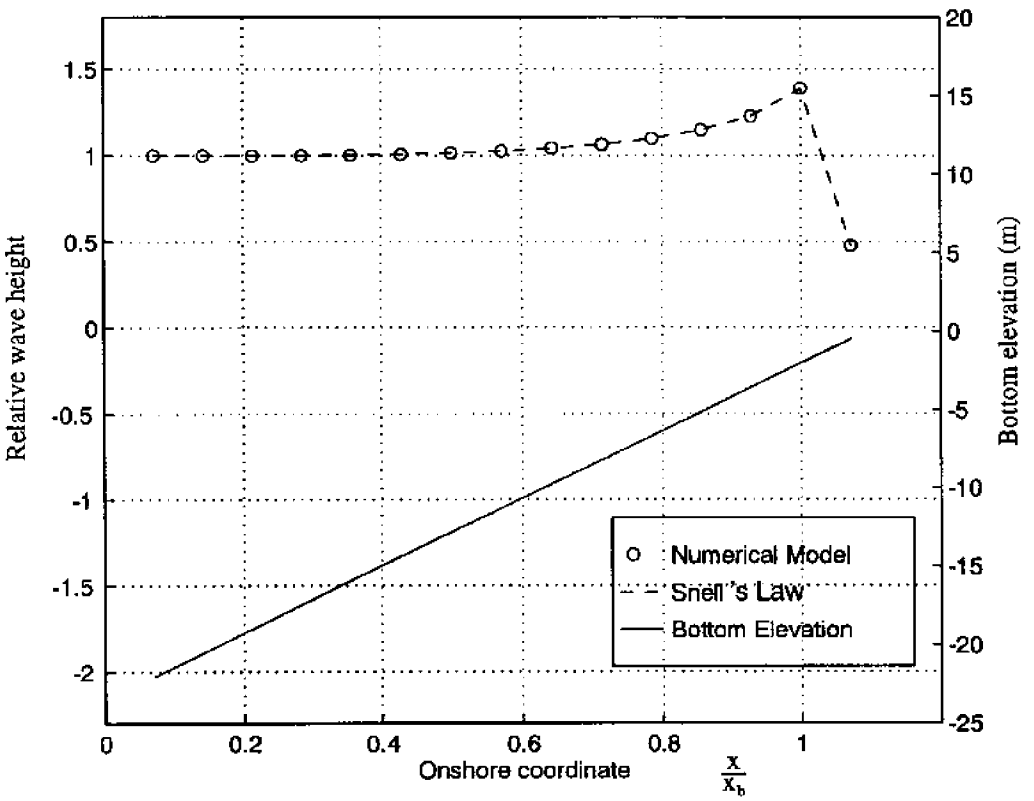

Figure 3.5 Comparison of numerical model results with analytical results (at section A–A') for shore parallel contours.

height and direction, the wave module is designed to be able to automatically split the coarse grid of the region where wave breaking may occur into a finer grid. The breaking wave height and direction are then determined using an interpolation method, based on values of wave heights and directions at neighboring nodes.

3.C Shoreline Change Module

Shoreline change is assumed to be the result of longshore gradients of longshore sediment transport, produced by waves that strike the shore at an oblique angle. Longshore sediment transport varies with wave angle and wave energy (wave height). In this study, a shoreline model (Work and Dean 1995) was used to simulate the shoreline changes in the vicinity of a tidal inlet due to the action of breaking waves. The shoreline model was also used to

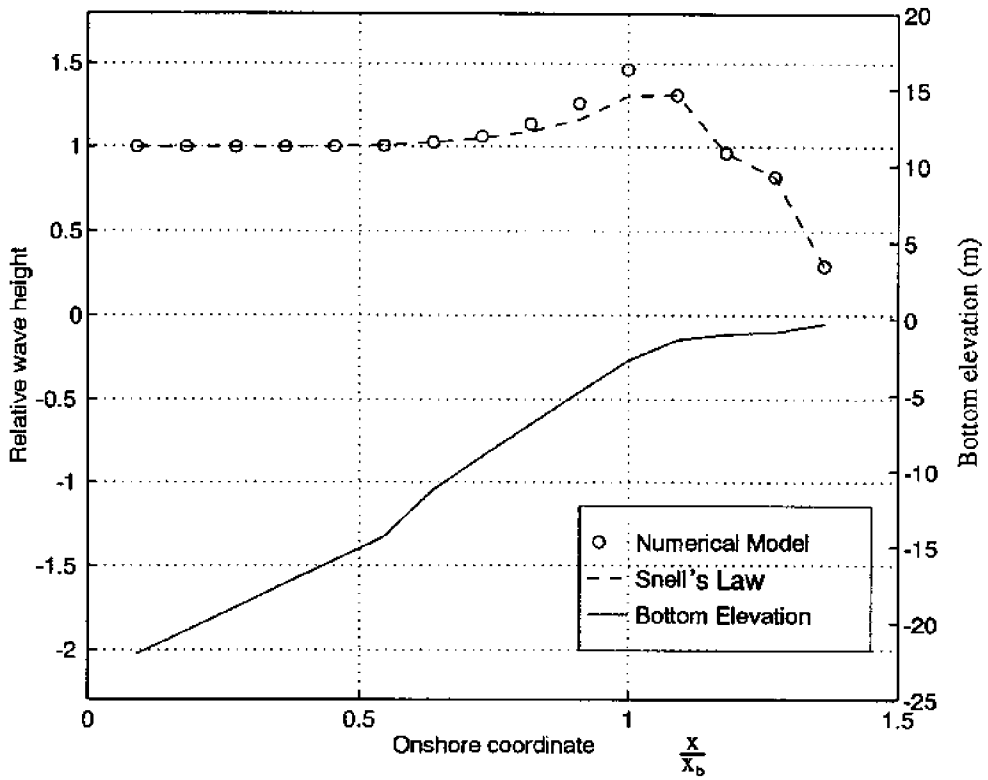

Figure 3.6 Comparison of numerical model results with Snell's law at section B–B').

calculate the amount of longshore sediment transport entering into the mouth of an inlet channel on the ocean side. The transport may contribute to the formation of ebb shoals and inlet migration. Among the assumptions of this module, the most important is that the beach profile simply moves onshore or offshore without change of shape. This type of model is called a "one–line" model, since only the position of one bathymetric contour need be known. The mean waterline contour is typically modeled. The GENESIS model (Hansen and Kraus 1989) is an example of this type of model.

3.C.1 Governing Equations

The coordinate system for the shoreline model is shown in Figure 3.7.

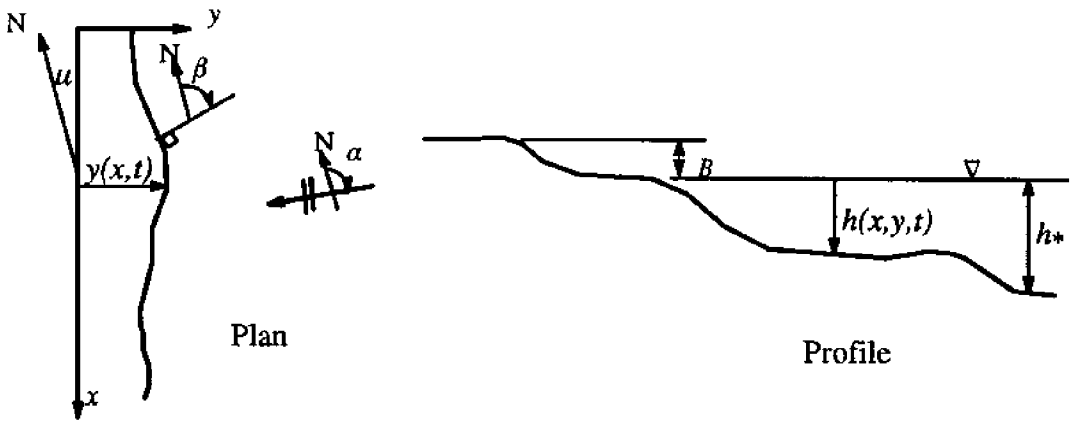

Figure 3.7 Coordinate system for shoreline change model.

The continuity equation of the shoreline module is expressed as:

$$\frac{\partial y}{\partial t} + \frac{1}{h_* + B}\frac{\partial Q}{\partial x} = 0 \tag{3.13}$$

where;

y = distance from the baseline to the mean waterline

h_* = "depth of closure" for longshore sediment transport. (The maximum water depth where significant sediment transport occurs due to the action of waves)

B = berm height

Q = longshore sediment transport rate (volume/time)

x = longshore coordinate.

The longshore sediment transport rate is determined by:

$$Q = \frac{KH_b^{5/2}}{8(s-1)(1-p)}\left(\frac{g}{\varkappa}\right)^{1/2} \sin(\beta - \alpha_b)\cos(\beta - \alpha_b) \tag{3.14}$$

where

K = an empirical constant, typically taken as 0.77

H_b = breaking wave height

s = sediment specific gravity

p = sediment porosity

$\varkappa$ = ratio of wave height to water depth at breaking

α_b = wave angle at breaking

β = shoreline angle with respect to the north (see Figure 3.7).

3.C.2 Finite Difference Equations

For some simple cases, the "one–line" model governing equations can be solved analytically. Numerical approaches become useful tools for complicated cases, especially for time dependent boundary conditions. Here an explicit numerical approach is used to solve the equations above. The coordinate system for the numerical scheme is shown in Figure 3.8. The domain is divided into a series of cells. The longshore sediment transport equation (Equation 3.14) is used to calculate sediment fluxes into and out of each cell. The continuity equation is then solved to compute the shoreline change.

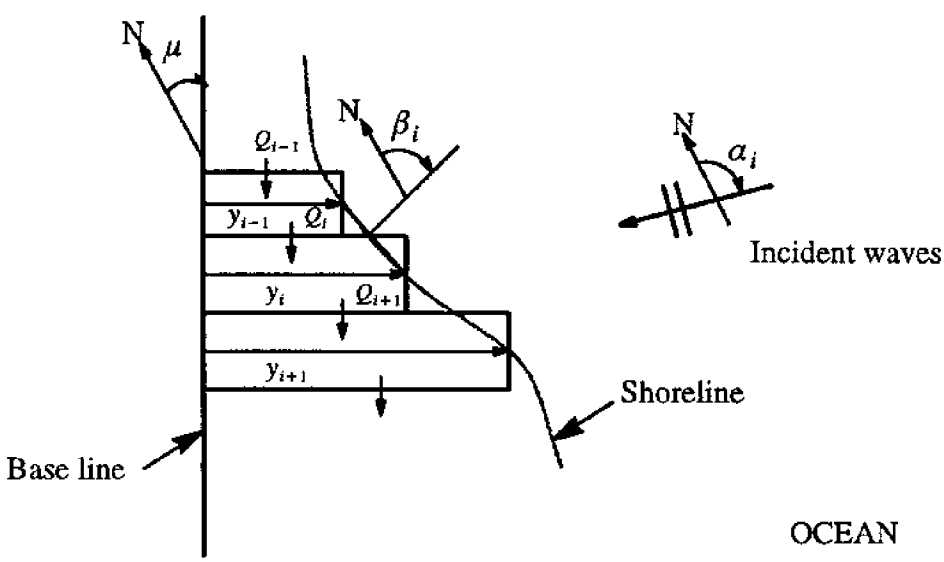

Figure 3.8 Coordinate system for numerical model.

The finite difference equations are given by:

$$Q_i^n = \frac{K\left(H_{bi}^n\right)^{5/2}}{8(s-1)(1-p)}\left(\frac{g}{\varkappa}\right)^{1/2}\sin\left(\beta_i^n - \alpha_{bi}^n\right)\cos\left(\beta_i^n - \alpha_{bi}^n\right) \tag{3.14}$$

$$\beta_i^n = \mu + \frac{\pi}{2} - \tan^{-1}\left[\frac{y_i^n - y_{i-1}^n}{x_i - x_{x-1}}\right] \tag{3.15}$$

$$y_i^{n+1} = y_i^n - \frac{\Delta t}{\Delta x(h_* + B)}\left(Q_{i+1}^n - Q_i^n\right) \tag{3.16}$$

where n denotes the time step level, and i the spatial node number.

3.C.3 Boundary Conditions

From the finite difference equations above, boundary conditions related to either Q or y need to be specified. At the two ends of the shoreline domain, the boundary conditions can be specified in many ways depending on features of the problem. Pinned boundary conditions are commonly use if pronounced shoreline change is sufficiently far from the ends of the domain. This boundary condition is equivalent to zero longshore transport gradient at the ends. Another option for boundary conditions at the ends is to set zero longshore transport. In this study, the simulated shoreline domain may not be long enough, and as such, both boundary conditions may not be completely applicable. Therefore, a boundary condition is used in which the longshore transport gradient at each of the two longshore boundaries of the domain is the same as that at the immediately adjacent node. This can be expressed using a finite difference formulation as:

$$\frac{Q_2 - Q_1}{\Delta x_1} = \frac{Q_3 - Q_2}{\Delta x_2} \tag{3.17}$$

$$\frac{Q_N - Q_{N-1}}{\Delta x_N} = \frac{Q_{N-1} - Q_{N-2}}{\Delta x_{N-1}} \tag{3.18}$$

The longshore sediment transport rates Q_1 and Q_N at the two longshore boundaries of the

shoreline domain can be determined based on Equations 3.17 and 3.18, respectively. Figure 3.9 illustrates the specification of these shoreline boundary conditions giving in Equations 3.17 and 3.18.

Figure 3.9 Illustration of the boundary conditions expressed by Equations 3.17 and 3.18.

3.C.4 Calculation of Sediment Transport into Inlet Channel

When the sediment transported by longshore currents reaches an inlet, the longshore transport rate will start to decrease due to the increase in depth and cessation of wave breaking or reduction in wave height. It is difficult to specify longshore sediment transport at an inlet. A boundary condition of zero longshore sediment transport adjacent to the inlet channel is not realistic for an unstabilized inlet. Thus, a permeable boundary condition is proposed as schematized below (See Figure 3.10).

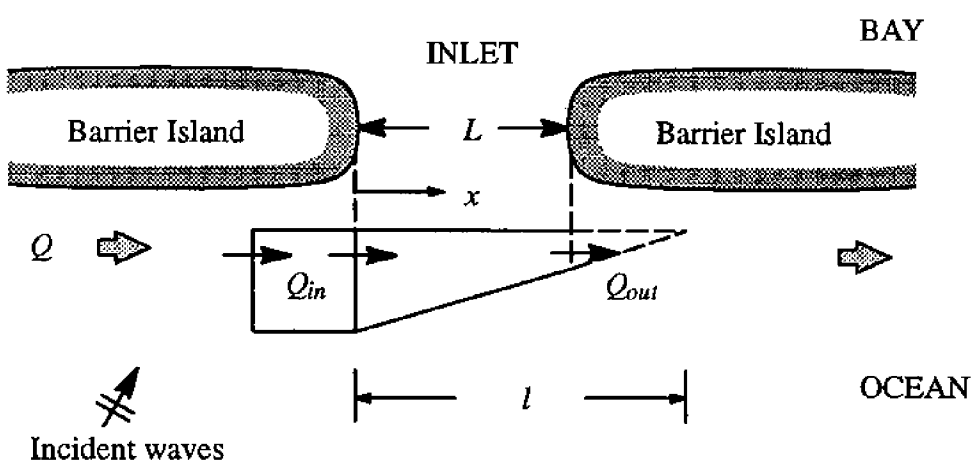

Figure 3.10 Assumed distribution of longshore transport rate across inlet.

When the direction of longshore sediment transport rate near the inlet is to the right, i.e., $Q>0$ (see Figure 3.10),

$$Q(x) = Q_{in}\left(1 - \frac{x}{l}\right) \qquad \text{for } 0 < x < L \tag{3.19}$$

$Q(x)$ was calculated in the standard manner for $x > L$.

The value of l can be adjusted to control the behavior of shoreline and bathymetric changes. If the value of l is less than the inlet width L, this means that Q_{out} is equal to zero and all longshore sediment transport is deposited in the inlet. In the limit as l goes to zero, the expression above equates to a groin boundary condition, that is, Q_{in} goes to zero. The linear variation of Q will lead to a uniform deposition of longshore sediment transport in the inlet. The rate of deposition is directly proportional to the sediment transport gradient across the inlet channel. The representation of the longshore transport boundary condition at an inlet described above needs to be tested with field data for validation.

3.C.5 Comparison of Shoreline Module to Analytical Solutions

If the governing equations for the shoreline change model are linearized, a diffusion equation can be obtained. For some cases with simple boundary conditions, the equation can be solved analytically. Before the shoreline module was linked with the other modules, it was verified by comparison to analytical solutions for two cases.

Case 1: Schematized beach nourishment project

It is assumed the input breaking wave climate is constant in time and space. The initial condition, boundary conditions, and the analytical solution are as follows (Larson *et al.* 1992):

$$y(x,0) = w \qquad |x| \le \frac{l}{2}$$

$$y(x,0) = 0 \qquad |x| > \frac{l}{2}$$

$$y(\pm\ \infty, t) = 0$$

$$y(x,t) = \frac{w}{2}\left\{ \text{erf}\left[\frac{l}{4\sqrt{Gt}}\left(\frac{2x}{l}+1\right)\right] - \text{erf}\left[\frac{l}{4\sqrt{Gt}}\left(\frac{2x}{l}-1\right)\right]\right\} \qquad (3.20)$$

where

w = width of rectangular beach nourishment in offshore direction

l = length of rectangular beach nourishment in longshore direction

G = longshore diffusivity, which can be expressed as

$$G = \frac{K H_b^{5/2}}{8(s-1)(1-p)(h_* + B)}\left(\frac{g}{\varkappa}\right)^{1/2} \qquad (3.21)$$

The comparison for the schematized beach nourishment project after 30 and 180 days is illustrated in Figure 3.11. Good agreement is found between the shoreline module results and the analytical solution.

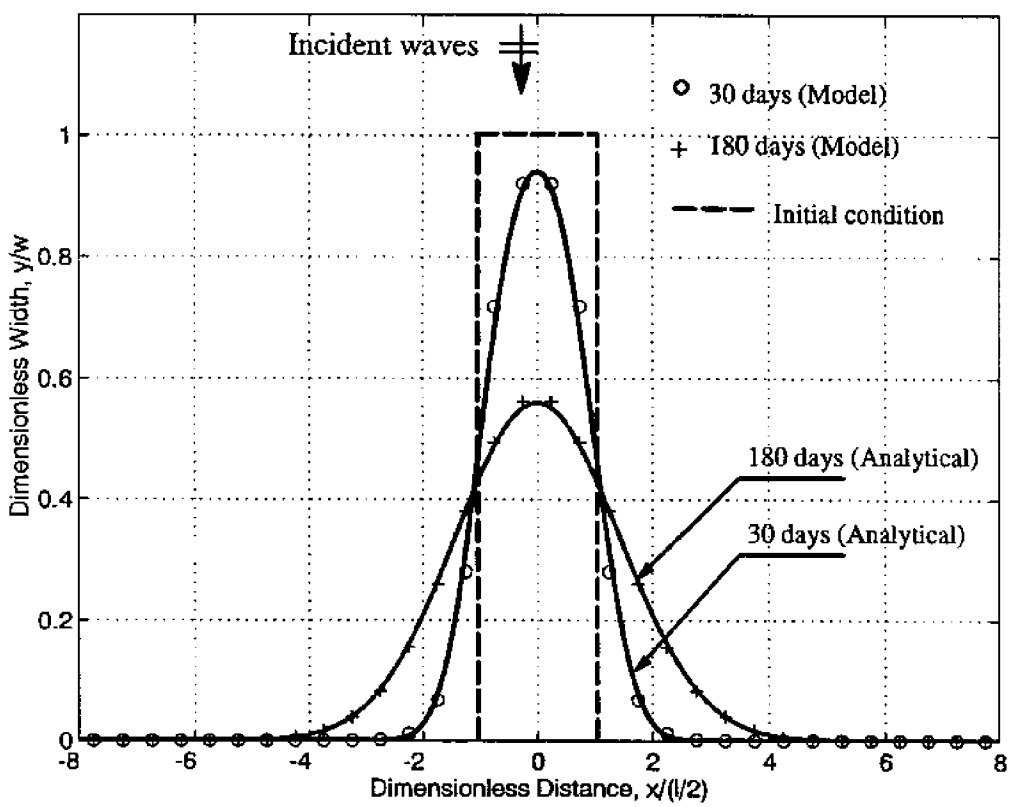

Figure 3.11 Comparison of model results with analytical solution for beach nourishment case (breaking wave height = 0.8 m, wave period = 6 sec.).

Case 2: Groin

It is assumed that a groin is placed on an initially infinite straight beach. No sediment bypasses the groin. A constant incident wave condition is also assumed. The initial conditions, boundary conditions, and solution are given below.

$$y(x,0) = 0$$

$$Q(0,t) = 0$$

$$y(\pm\ \infty, t) = 0$$

$$y(x,t) = \tan\ (\pi - \alpha_b)\left[\sqrt{\frac{4Gt}{\pi}}\ \exp\left(\frac{-x^2}{4Gt}\right) - x\ \text{erfc}\left(\frac{x}{\sqrt{4Gt}}\right)\right] \qquad (3.22)$$

The analytical solution and the numerical model results are shown in Figure 3.12.

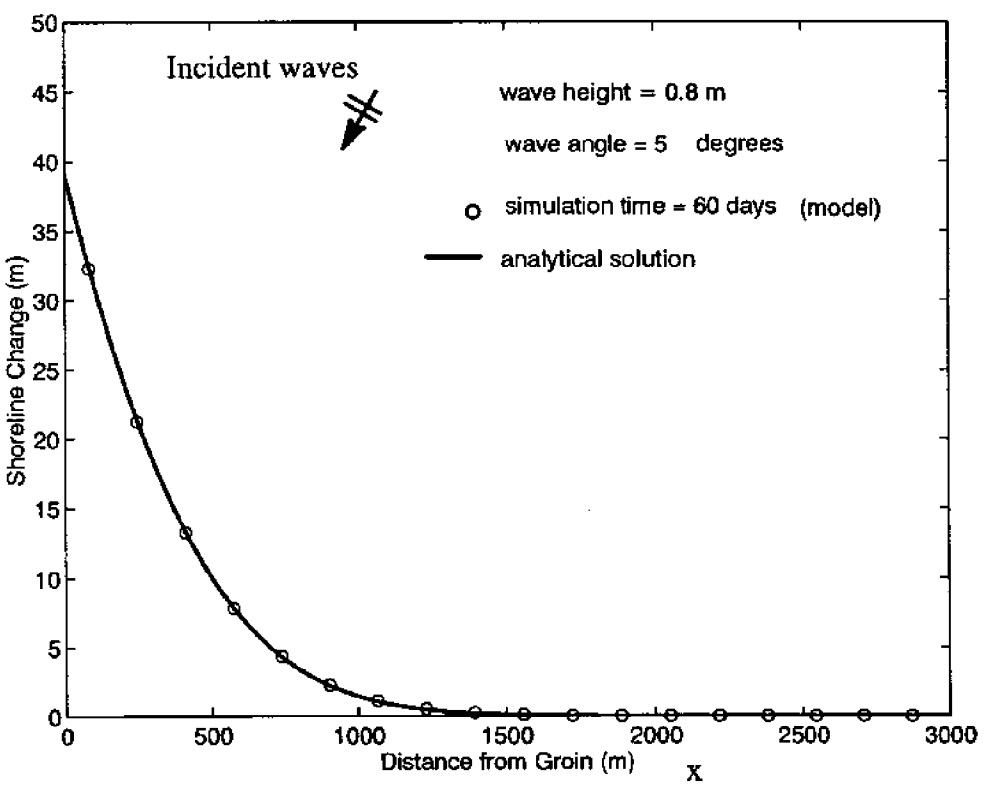

Figure 3.12 Comparison of model results with analytical solution for beach with groin.

3.D Microscale Hydrodynamic Module

As described in the section describing the objectives of the study, the mesoscale modeling relies heavily on some time series of hydrodynamic information, such as velocity and water depth at each location in the solution domain, provided by a microscale module. The hydrodynamic module of a microscale model named CWSTM–H (Veeramachaneni and Hayter 1988), with slight modifications, was used for this purpose. The CWSTM–H model itself, designed for short–term simulations, consists of three modules: a hydrodynamic module, a wave transformation module, and a sediment transport module. The three modules are coupled and executed in succession. It is capable of simulating both hydrodynamics and bathymetric changes in a coastal environment.

The governing equations for the hydrodynamic module are the shallow–water, long–wave equations describing two–dimensional, depth–averaged flows. They are given by: continuity equation:

$$\frac{\partial \eta}{\partial t} + \frac{\partial [U(h+\eta)]}{\partial x} + \frac{\partial [V(h+\eta)]}{\partial y} = 0 \tag{3.23}$$

Momentum equations in x and y directions:

$$\frac{\partial U}{\partial t} + U\frac{\partial U}{\partial x} + V\frac{\partial U}{\partial y} = -g\frac{\partial \eta}{\partial x} + \frac{1}{\varrho}\left(\frac{\partial \tau_{xx}}{\partial x} + \frac{\partial \tau_{yx}}{\partial y}\right) + \frac{\tau_1}{\varrho(h+\eta)} - f\,V \tag{3.24}$$

$$\frac{\partial V}{\partial t} + U\frac{\partial V}{\partial x} + V\frac{\partial V}{\partial y} = -g\frac{\partial \eta}{\partial y} + \frac{1}{\varrho}\left(\frac{\partial \tau_{xy}}{\partial x} + \frac{\partial \tau_{yy}}{\partial y}\right) + \frac{\tau_2}{\varrho(h+\eta)} + f\,U \tag{3.25}$$

where

U, V = depth–averaged velocity in x and y directions, respectively

η = water surface deviation from still water level

h = water depth

ϱ = water density

τ_{ij} = internal turbulent shear stress tensor

τ_i = external forces: bottom friction

f = Coriolis coefficient.

As shown in the equations above, the primary factors influencing flows near inlets, such as bottom friction, internal (turbulent) shear stresses, Coriolis force, and water surface slope, are included in the hydrodynamic module of the CWSTM–H microscale model.

A finite element approach using quadratic, triangular or rectangular elements is utilized to numerically solve the hydrodynamic governing equations in the CWSTM–H model. Other features and a detailed description of the CWSTM–H model are described by Veeramachaneni and Hayter (1988).

The use of a pre– and post–processor program (FASTTABS) allowed easy construction of the finite element grid, input of geometric and boundary conditions, and graphical viewing of model results (velocity field, water head, and bottom elevation changes).

3.E Sediment Transport Module

3.E.1 Background

A microscale tidal inlet model is intended for short–term (days to months) numerical simulation of morphological evolution of tidal inlet systems. Such a model is not yet a practical tool for long–term (years to decades) simulations. The primary reason is that microscale models commonly are run using a small time step (on the order of tens of minutes), which is dictated by computational stability requirements. Thus, a mesoscale model with a relatively large time step is desired for such a task. All existing mesoscale modeling approaches reviewed in this study attempt to reduce computational efforts to make a long–term simulation possible and more economical.

One long–term modeling approach presently in use is called the "input filtering (reduction) technique" (De Vriend *et al.* 1993). The idea of this approach is to select a limited number of representative sets of tide and/or wave data as the input to a microscale model run to reduce computational intensity. The input filtering technique can be used to parameterize tide and wave conditions. For tidal input filtering, the idea of selecting representative tides is to take

a complete tidal record of interest and then compute the mean sediment transport at a number of important points in the modeled domain. Then a limited number of representative tides (perhaps only one representative tide) is selected such that the mean sediment transport is reproduced. It has been found that the representative tide is slightly higher than the mean tide if only one representative tide (sometimes called the "morphological tide") is used (De Vriend 1993). This approach can greatly reduce the computational effort. In fact, this approach implies the assumption that the shape of the tidal curve is more or less uniform throughout the whole area of concern, such that the selected tide is representative of the whole domain, not only for a single point. Obviously, the accuracy of this approach is heavily dependent on how the representative data set is chosen. In this study, emphasis is placed on the reduction of the number of the calls to the hydrodynamic module, which is the most expensive of the model components. The mesoscale modeling approach is described below.

3.E.2 Mesoscale Modeling Approach

As indicated earlier, microscale models for simulation of coastal morphology typically consist of three modules: a flow module, a wave transformation module, and a morphodynamic (or sediment transport) module. The hydrodynamic modules (flow and wave modules) are called after each time step. Computing effort will be reduced if the number of calls to the microscale hydrodynamic module can be reduced. The approach described herein is based largely on this premise. Additionally, because it is assumed that sediment transport outside the surf zone is induced solely by tidal currents, the mesoscale modeling approach was developed based on this assumption.

The tidal effects on sediment transport are represented by periodic boundary conditions at the offshore boundary. As a result, the residual (i.e., time–averaged) sediment transport over each tidal cycle at each point within the computational domain is closely related to the known driving forces represented by the tidal ranges at the offshore boundary. Empirical relations between the residual sediment transport at each location in the domain and the tidal range at the offshore boundary can be established using regression techniques. Once these empirical

relations are obtained, the residual or net sediment transport over a tidal cycle at each node is known for a given tidal range at the offshore boundary. Furthermore, the bottom change at each node can be calculated using the known net transport and a sediment conservation equation. Successive iterations can be performed according to the input of a series of tidal ranges. The time step employed in this approach is one semi–diurnal tidal period (12.42 hours), much larger than the typical microscale model time step. A detailed description of this approach is presented below.

3.E.3 Sediment Transport Module Grid

To reduce computing effort, a simple finite difference scheme using the concept of a "control volume" is used for the calculation of bottom changes in the mesoscale module. Because of the difference in computational algorithms between the finite difference method in the mesoscale module and the finite element method used in the microscale hydrodynamic module, the arrangements of nodes of the two module grids are different. The relationship between the two grids is shown in Figure 3.13. Square grids are used in both modules, and the grid size is the same. In the microscale module, variables (velocity components and the water surface elevation) are computed at the eight nodes composing each element. In the mesoscale module, those variables are saved only at the four mid–side nodes of each element. For the finite difference scheme, each square element can be regarded as a control volume where the sediment conservation equation is applied. There are two sediment transport components (x and y) directions at each node. Only the component normal to the side of the element contributes to the bottom change of each element, as illustrated in Figure 3.13.

3.E.4 Construction of Empirical Relations

The basis of the mesoscale modeling approach is to establish empirical relations between residual (net) sediment transport over a tidal cycle and the corresponding tidal range at the offshore boundary. Empirical relations are constructed using the hydrodynamic results from the microscale model. As a first step, the microscale hydrodynamic module is run for one lunar month and the velocity components and water depth are saved at each node of the mesoscale

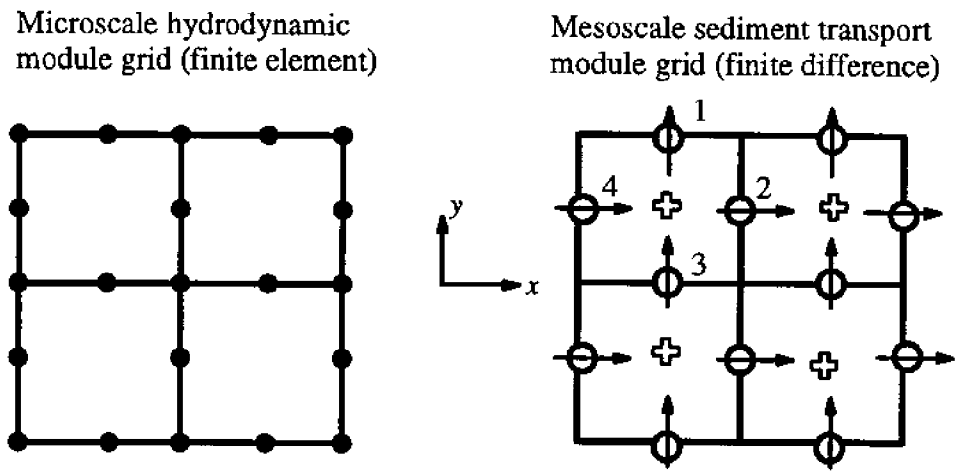

Figure 3.13 Relationship between microscale hydrodynamic module and sediment transport module grids.

model grid at a certain time interval, for instance, every 30 minutes of simulation time. The time interval for saving data is not necessarily equal to the computational time step of the microscale module, and normally is larger. Since both spring and neap tides occur over one lunar month, the simulation time of one lunar month is selected in constructing the empirical relations.

Using the calculated velocities and water depths for one lunar mouth from the microscale module, the sediment transport rate at each node is calculated using a sediment transport formula and stored as an one lunar month time series. A sketch of a typical time series of tide–induced sediment transport rate in a particular coordinate direction is illustrated in Figure 3.14. Since sediment movement changes direction in correspondence with the direction of flow stress acting on the sediment particles, there are positive and negative components of sediment transport within a tidal cycle. Two volumes, Q_{R+} and Q_{R-}, (see Figure 3.14) for each tidal cycle can be obtained by integrating separately the positive and negative parts of the curve using the trapezoid integration method. The residual sediment transport (net sediment transport) over one tidal cycle, Q_R, is the sum of Q_{R+} and Q_{R-}. At some nodes there may be no positive sediment

transport, no negative sediment transport, or no sediment transport at all. The method of integration presented above is still valid for these cases.

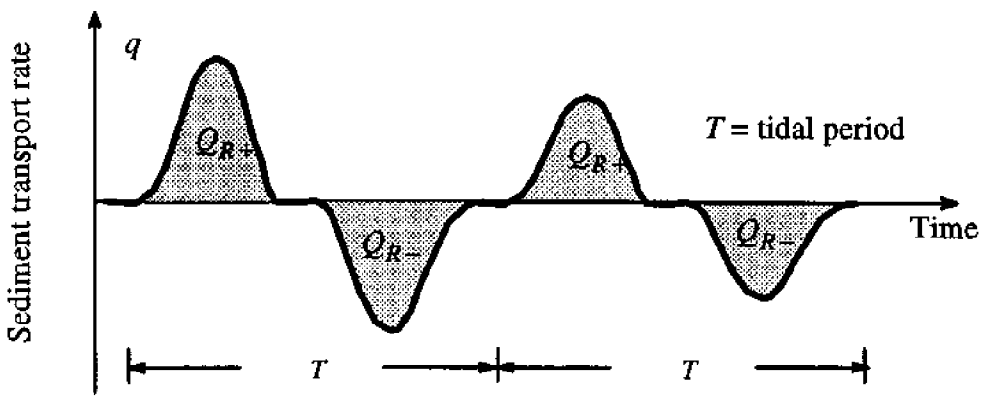

Figure 3.14 Typical time series of sediment transport rate.

The sediment transport rate is proportional to the flow shear stress acting on sediment particles, and the shear stress is a function of the tide–induced flow velocity. The relation between the velocity and tidal stage is generally non–linear. Thus, a quadratic empirical relation between the residual sediment transport over a tidal cycle and the tidal range at the offshore boundary is assumed as follows:

$$Q_R = a + b\,\zeta + c\,\zeta^2 \tag{3.26}$$

where

Q_R = the residual sediment transport (in volume of sediment) over a tidal cycle

ζ = tidal range at the offshore boundary

a, b, c= coefficients.

Finally, the coefficients a, b, and c in Equation 3.26 are determined by a regression method (James 1977). In the next chapter empirical relations and fitted curves at two points in the domain of a hypothetical case are illustrated. Basically the coefficients a, b, and c are space– and time–dependent. The value of each coefficient will be zero at some locations where the flow velocities are always less than the threshold velocity initiating sediment.

3.E.5 Bottom Elevation Change

Once the empirical relations are established between the residual sediment transport and the tidal range at the offshore boundary, the residual sediment transport over each tidal cycle corresponding to the input tidal range at the offshore boundary can be calculated at each node. Based on the sediment conservation equation, the bottom changes are computed with a large time step (one tidal period). The sediment conservation equation is given by (Chang 1992)

$$\frac{\partial z}{\partial t} + \frac{\partial q_x}{\partial x} + \frac{\partial q_y}{\partial y} = 0 \tag{3.27}$$

where

z = bottom elevation;

q_x, q_y = sediment transport rate in x and y directions, respectively.

The finite difference equation for the sediment conservation equation above is expressed below:

$$\Delta z_b = -\left(\frac{Q_{R2} - Q_{R4}}{\Delta x} + \frac{Q_{R1} - Q_{R3}}{\Delta y}\right) \tag{3.28}$$

where

Δz_b = bottom change over one tidal cycle

Q_{Ri} = residual sediment transport per unit width over one tidal cycle (Components 1,2,3,4 are illustrated in Figure 3.13)

Δx, Δy = grid sizes in the x and y directions, respectively.

The cumulative bathymetric change at each node can be obtained by summing the bathymetric change during each mesoscale time step. This implies that the bathymetric change anywhere in the domain is so small that the flow field is not influenced considerably during the mesoscale modeling period. If the bathymetry changes "significantly", the previously established empirical relations based on the microscale hydrodynamic module results become invalid since the velocity field is modified by bathymetric changes. At this point, the microscale hydrodynamic model must be re–run for another lunar month using the new bathymetry to recompute the coefficients of the empirical relations. In this study, the microscale module is

re–run to compute the velocity field when the relative bottom change at any point in the domain exceeds a certain tolerance. The selection of this tolerance is somewhat arbitrary. A larger value of the tolerance results in less run time of the mesoscale model, a smaller value less difference between the mesoscale and microscale approaches.

3.F Linkage of Modules

The four modules of the mesoscale model, the microscale hydrodynamic module, wave transformation module, shoreline change module, and sediment transport module rely on one another. In a long–term simulation, these modules are linked together and iterated successively. A flow chart of the procedure explained below is shown in Figures 3.15 and 3.16.

1. The input data set for the model is formed. This includes geometry, initial bathymetry, boundary conditions, and forcing (tides and waves).
2. The microscale module is run for one lunar month to provide hydrodynamic data (time series of velocity and water depth) for construction of the empirical relations used in the sediment transport module.
3. The empirical relations are determined between local residual sediment transport and tidal range at the offshore boundary.
4. The sediment transport module is run with a time step of 12.42 hours (one tidal period) until the relative bottom change at any node in the domain over the current mesoscale modeling period exceeds a specified tolerance. A tolerance of 15% was chosen for this study.
5. The wave transformation module is run on the same time frame as the mesoscale module for 6 hours. The input wave climate at the offshore boundary changes every 6 hours, provided by the random number generating subroutine programs.
6. The shoreline change module is run for 6 hours. In addition to the calculation of shoreline changes, this module computes the amount of the littoral drift entering the inlet channel and resulting bathymetric change.
7. Steps 5 and 6 are repeated until the run time is equal to that of the mesoscale module.
8. Combine the calculated bathymetry results from the mesoscale module and the shoreline change module and modify the bathymetry. The updated bathymetry results are used for the new bathymetry input to the wave transformation module.
9. Steps 2 through 8 are repeated until the required run time is reached.

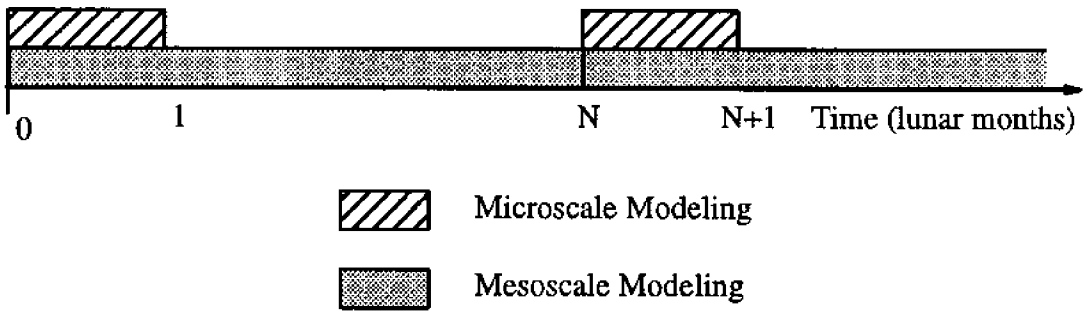

Figure 3.15 Schematized procedure for mesoscale and microscale modeling.

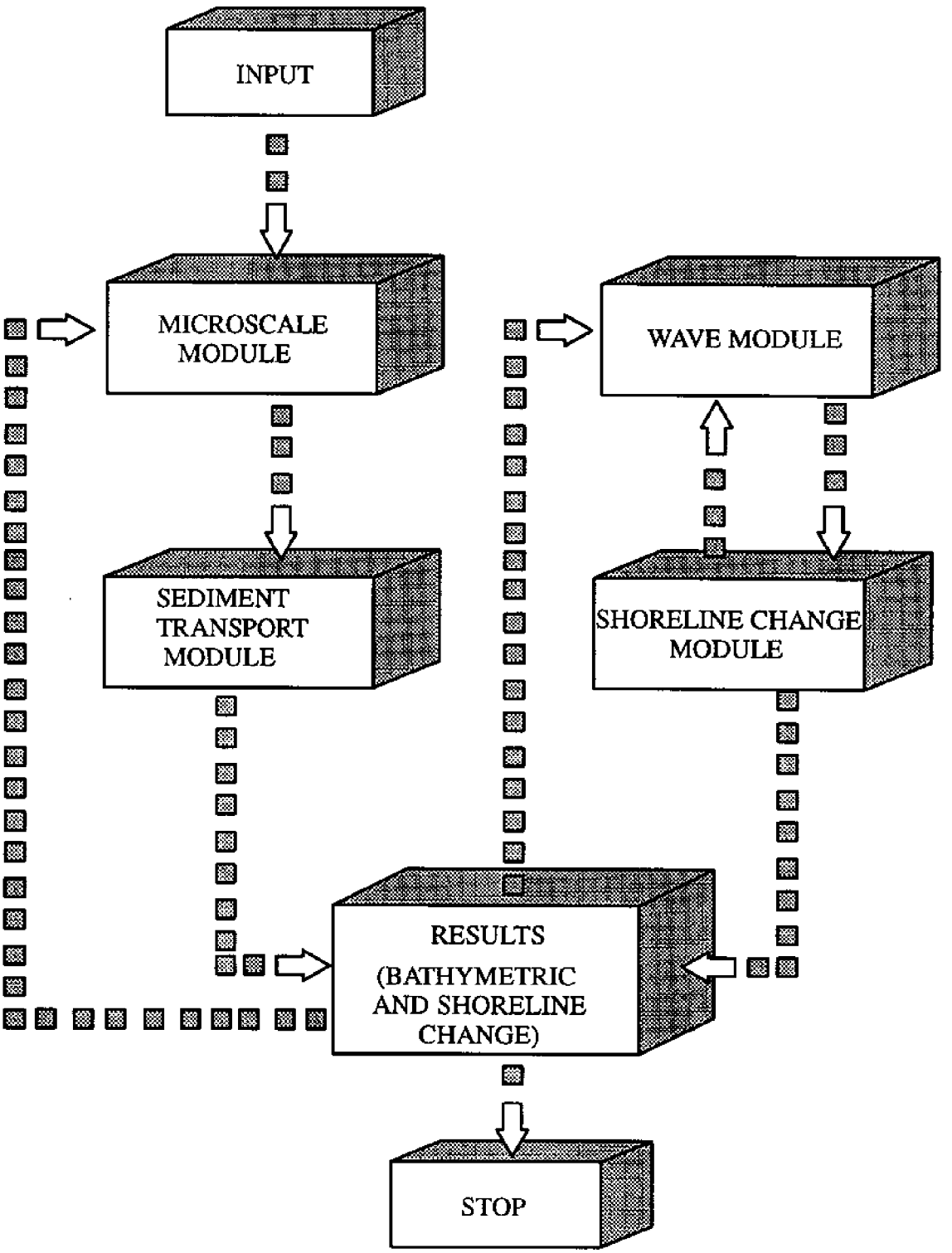

Figure 3.16 Flow chart illustrating linkage of component modules.

IV COMPARISON AND APPLICATION

To demonstrate the ability for simulating long–term morphological changes at a tidal inlet system, the mesoscale model was applied to a hypothetical inlet system at prototype scale. The model results were compared to the results from the CWSTW–H microscale model with no waves. In this chapter, the comparison is discussed, and the results of a long–term run are presented.

4.A Simulation Domain

The hypothetical inlet system consists of a tidal inlet, 1,100 m wide and 1,500 m long, connecting a closed bay and an open ocean. The total length of the straight shoreline plus the tidal inlet is 12,000 m. The total width of the domain, from the solid boundary on the bay side to the offshore boundary on the ocean side, is 9,750 m. The area of the ocean is two–thirds of the whole domain. An initial flat bottom was used in the bay, with a constant bottom elevation of –4 m MSL. The bottom elevation at the offshore ocean boundary is –22.5 m MSL. Figures 4.1 and 4.2 show three dimensional and plan views of the modeled domain, along with bottom contours and the computational grid used. The thick lines on the edges of the domain in Figure 4.2 represent solid boundaries.

The domain was uniformly discretized into 832 square elements with the side length of 375 m. As described in Chapter 3, the number of nodes in the microscale and mesoscale grids was not equal, in spite of having the same number of elements.

4.B Comparison of Mesoscale to Microscale Model Results

As described in the previous chapter, the mesoscale model relies on a microscale model. If waves are not considered, the bathymetric changes calculated by the mesoscale model are an approximation to the calculated results by the microscale model for the same initial and boundary conditions. To examine the validity of the mesoscale modeling approach, the mesoscale model results were compared to the microscale model results. Obviously comparison of model results to field data sets from a real inlet would be preferable, but such data at the

required resolution in space and time, with known tide and wave conditions, are not currently available.

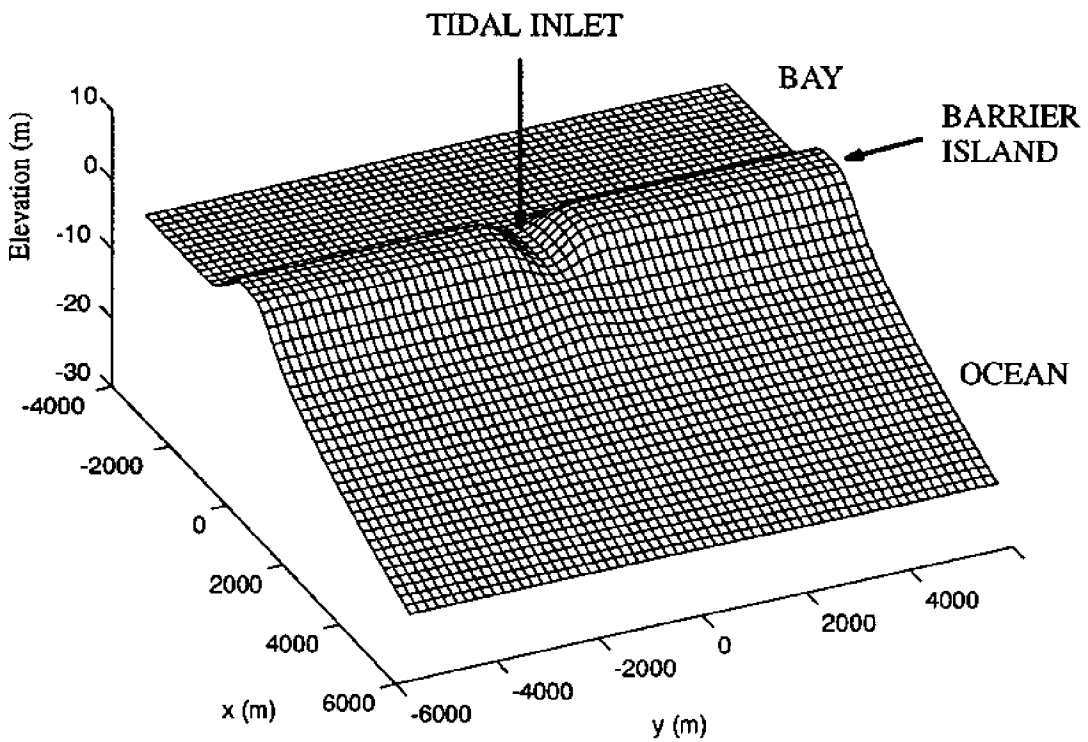

Figure 4.1 Three–dimensional view of initial bathymetry of simulated domain.

In the comparison, wave action was not considered in the computation of the bathymetric change. The wave module of the CWSTM–H microscale model was switched off. For the microscale model, the water surface elevations at all open water boundaries were prescribed. They were given by a time series of tidal stages which were generated using harmonic analysis of the NOS predicted tide at the entrance to Charleston Harbor, South Carolina. Figure 4.3 illustrates a portion of the tidal stage and the tidal range time series. The Ackers and White formula (1973) given in the literature review was used to compute the sediment transport rate.

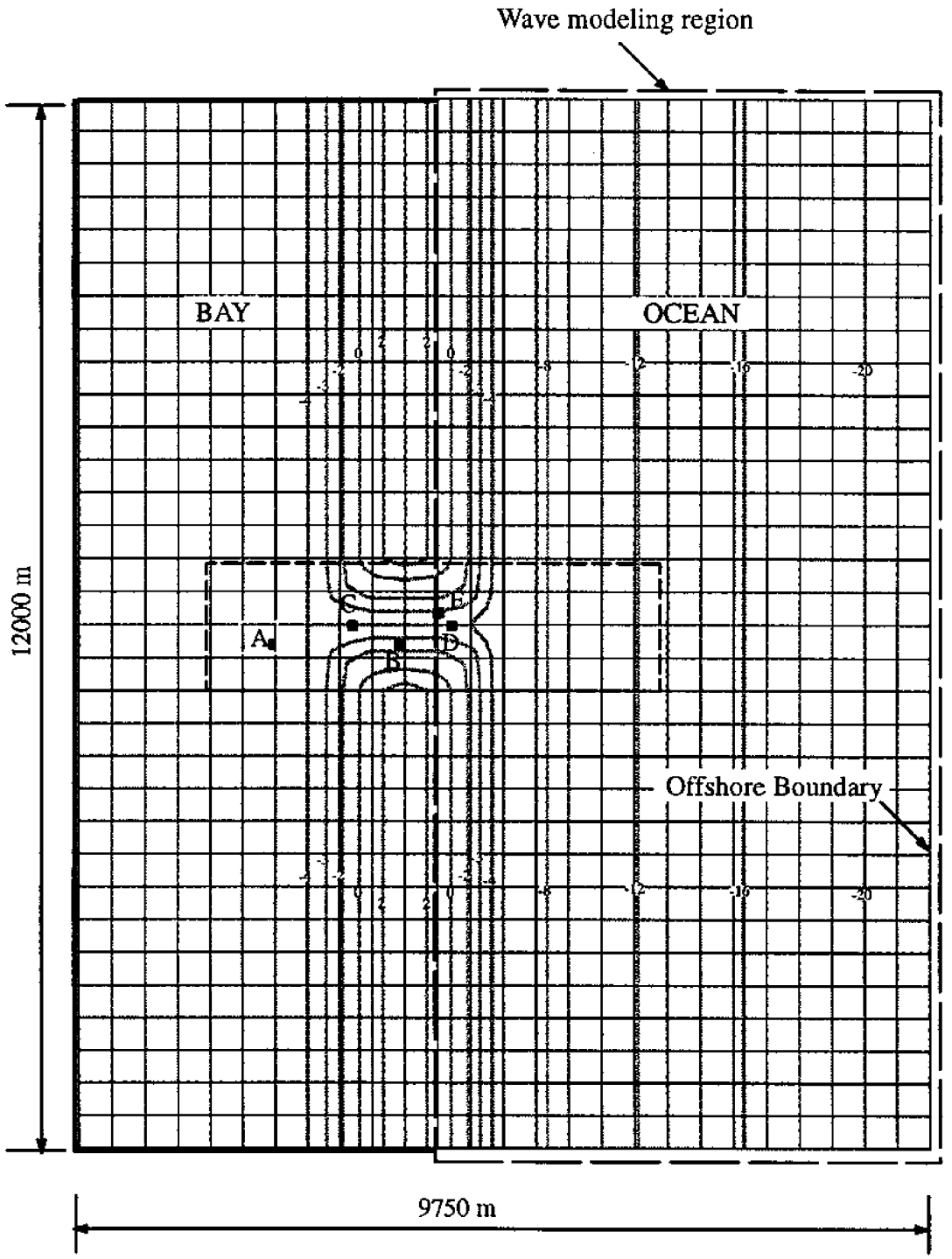

Figure 4.2 Plan view of simulated domain.

The sediment size used is 0.3 mm, with a sediment specific gravity of 2.7 and the angle of repose of 30°. A Nikuradse's roughness value of 0.2 was used.

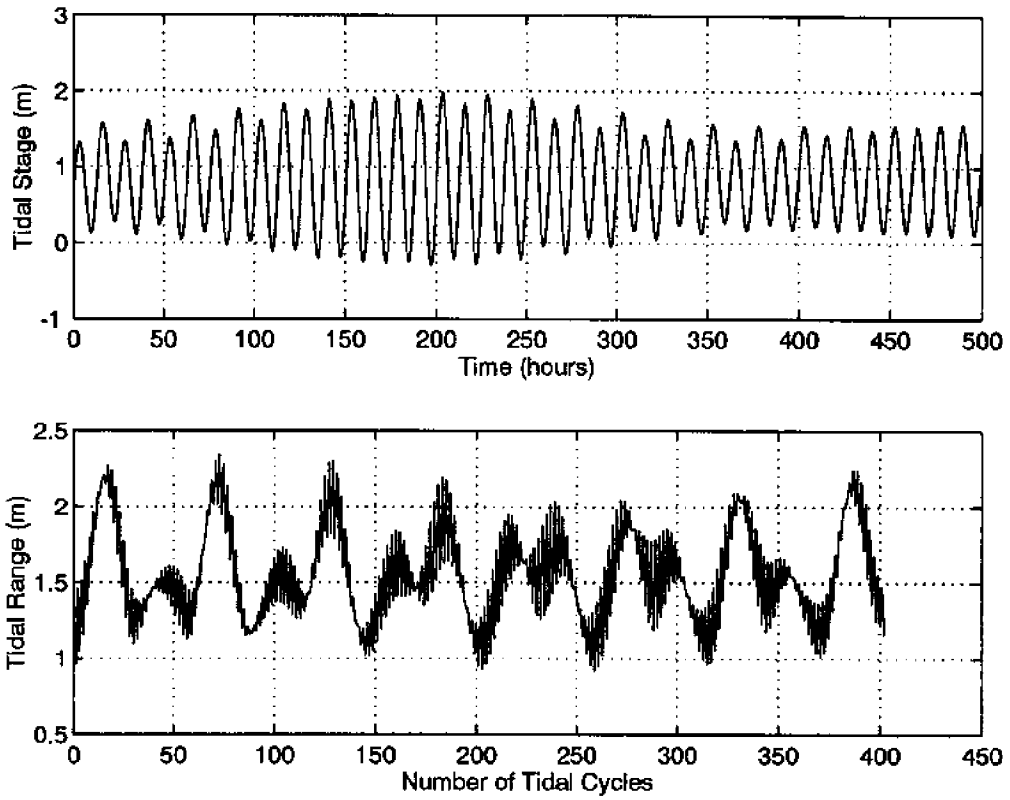

Figure 4.3 Input tidal stage and tidal range at offshore boundary.

The microscale model was independently run for 178 days using a time step of 5 minutes. The calculated results (velocity field, water depths, and bottom elevation changes) were saved every 30 minutes. The upper plots in Figures 4.4, 4.5, and 4.6 show 3–dimensional views of the bathymetry computed by the microscale model after 60, 119, and 178 days, respectively. These figures show only the results in a region in the inlet channel, since there is no significant change beyond that region. This region is illustrated in Figure 4.2 with a box of thick dashed lines. The two plots in Figure 4.7 show 3–dimensional views of the initial bottom elevation and the calculated bottom elevation after 178 days in the same region, respectively. Furthermore, a contour plot of the calculated bathymetric change after 178 days is also shown in the upper plot of Figure 4.8.

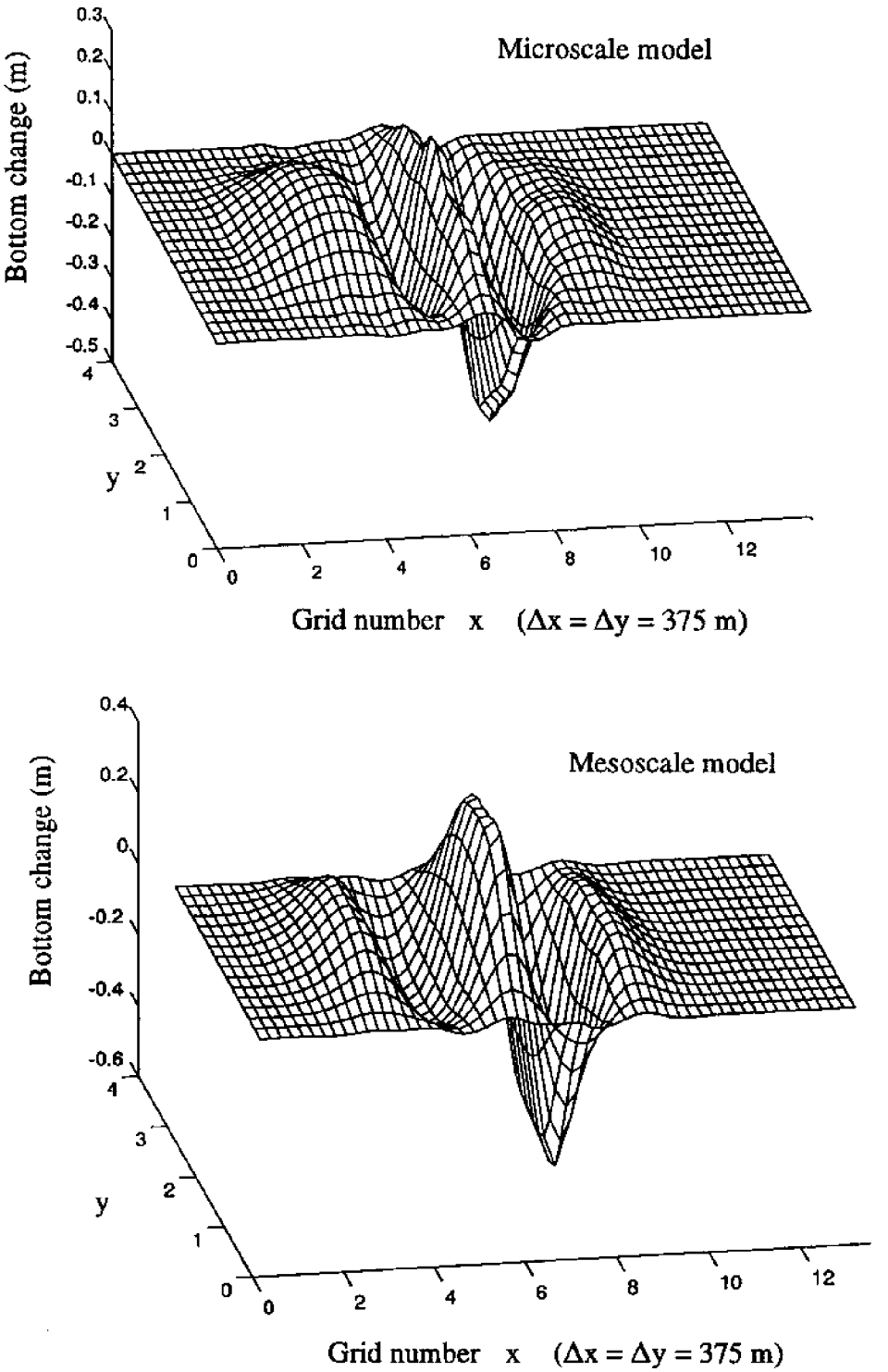

Figure 4.4 Comparison of mesoscale model results to microscale model results after 60 days.

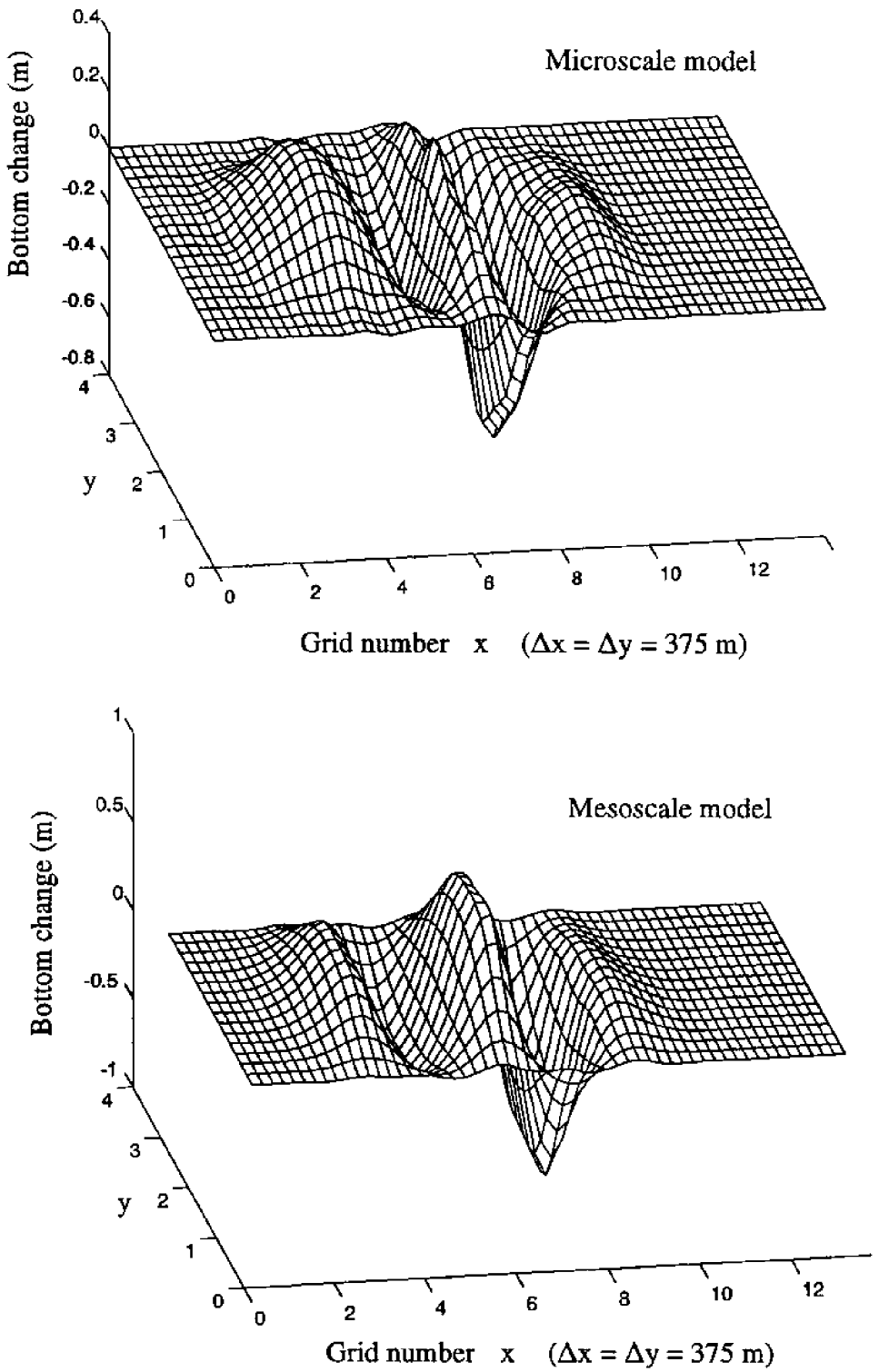

Figure 4.5 Comparison of mesoscale model results to microscale model results after 119 days.

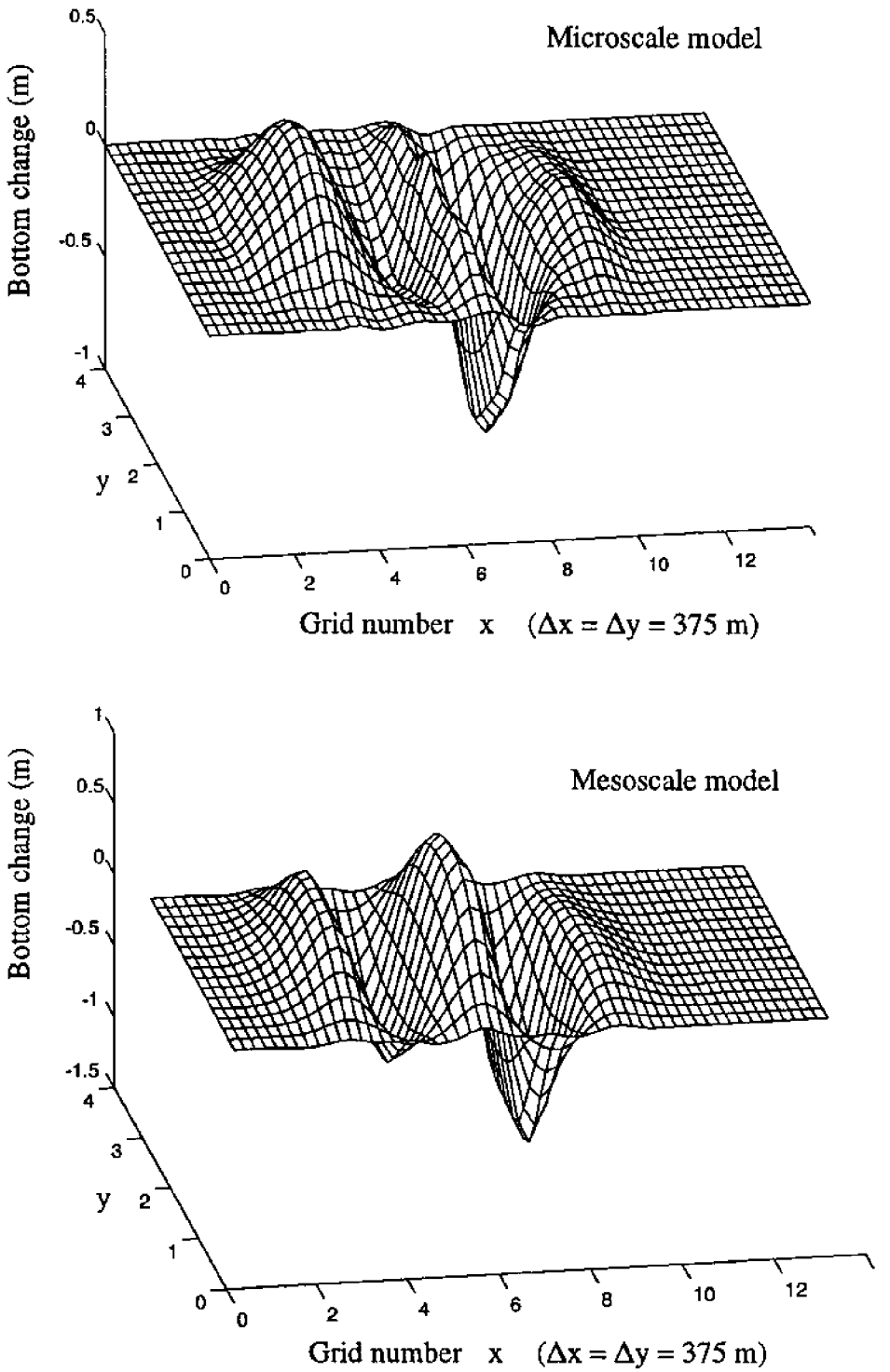

Figure 4.6 Comparison of mesoscale model results to microscale model results after 178 days.

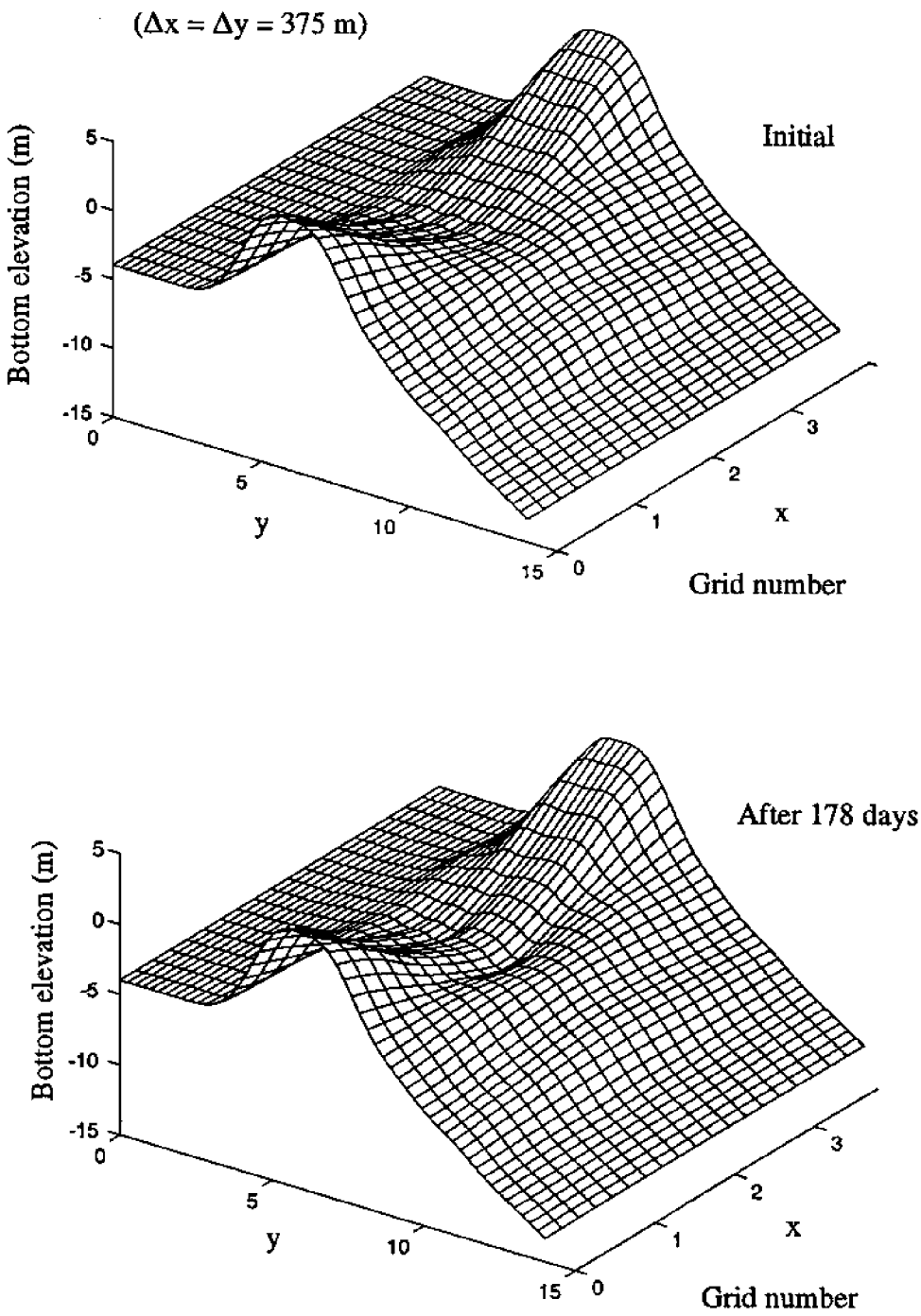

Figure 4.7 Initial bottom elevation and calculated bottom elevation by microscale model after 178 days.

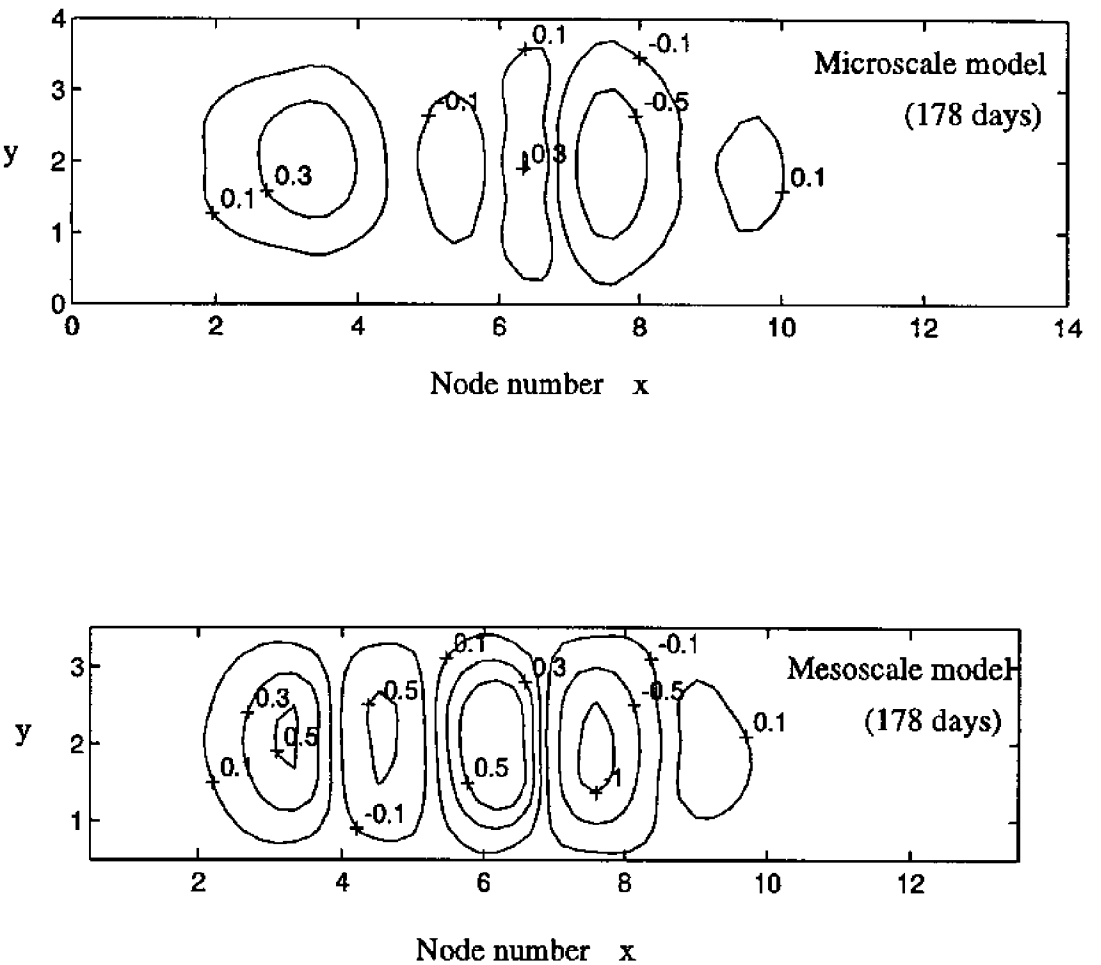

Figure 4.8 Bottom change comparison of mesoscale model to microscale model.

For the purpose of comparison, the sediment transport equation and the properties of the sediment used in the mesoscale modeling were identical to that used in the microscale model. The tidal ranges which are the boundary conditions to the mesoscale modeling were determined based on the tidal stage boundary conditions to the microscale model.

According to the mesoscale modeling approach described earlier, as a first step, the microscale model results (velocity and water depth) for one lunar month were saved at each node of the mesoscale model grid. Based on these hydrodynamic results, an empirical relation between the residual sediment transport over a tidal cycle and the corresponding tidal range was constructed in the quadratic form at each node using data regression methods.

As an example, Figures 4.9 and 4.10 show the relations and fitted curves at nodes A and B, respectively (see Figure 4.2). The solid lines represent best–fit quadratic relations; the dashed lines linear relations are shown for the purpose of comparison. The upper plot in each figure refers to the relations between the residual sediment transport over a tidal cycle in the positive x–direction and the tidal range, and the lower plots in the negative direction. It is seen from the figures that good relations are demonstrated in spite of the fact that the data points for the positive direction appear a little more scattered than for the negative direction at these two nodes. Additionally, there is no noticeable difference in the calculated bathymetric changes using the linear or quadratic relations for the hypothetical inlet case, based on several model tests.

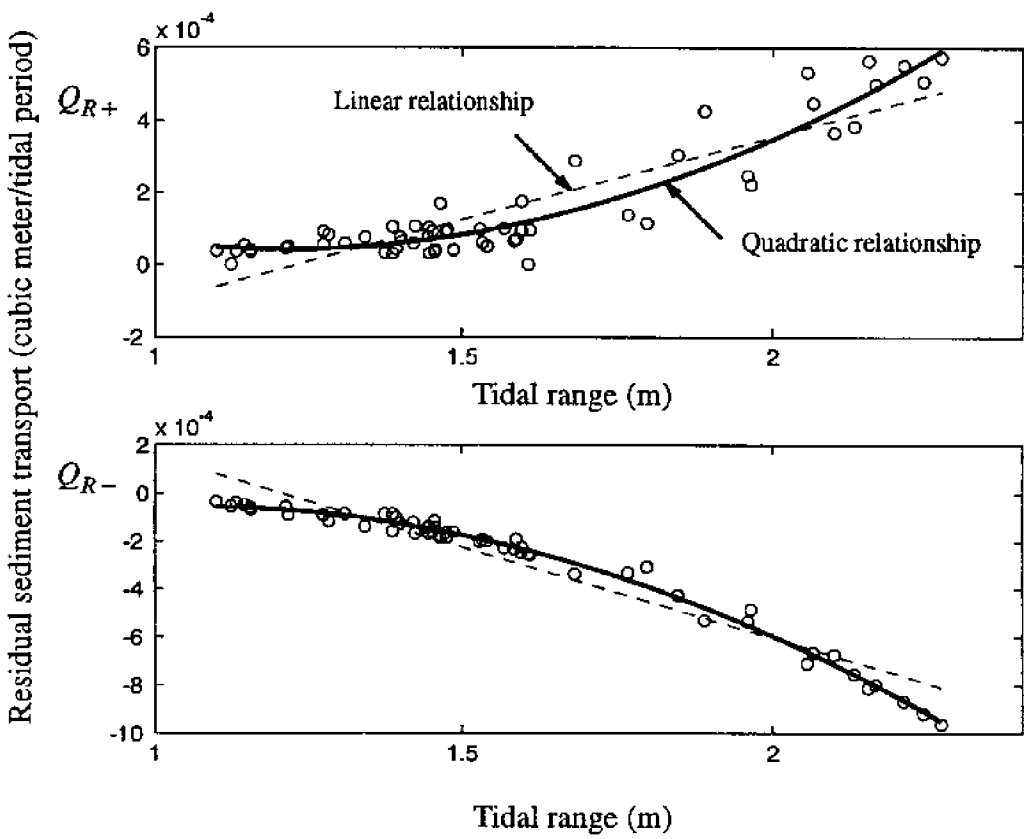

Figure 4.9 Residual sediment transports over a tidal cycle vs. tidal ranges at point A (see Figure 4.2).

After the empirical relations were constructed, the mesoscale model was run for 60 days. The output was the bottom change at each element of the mesoscale grid. It is somewhat

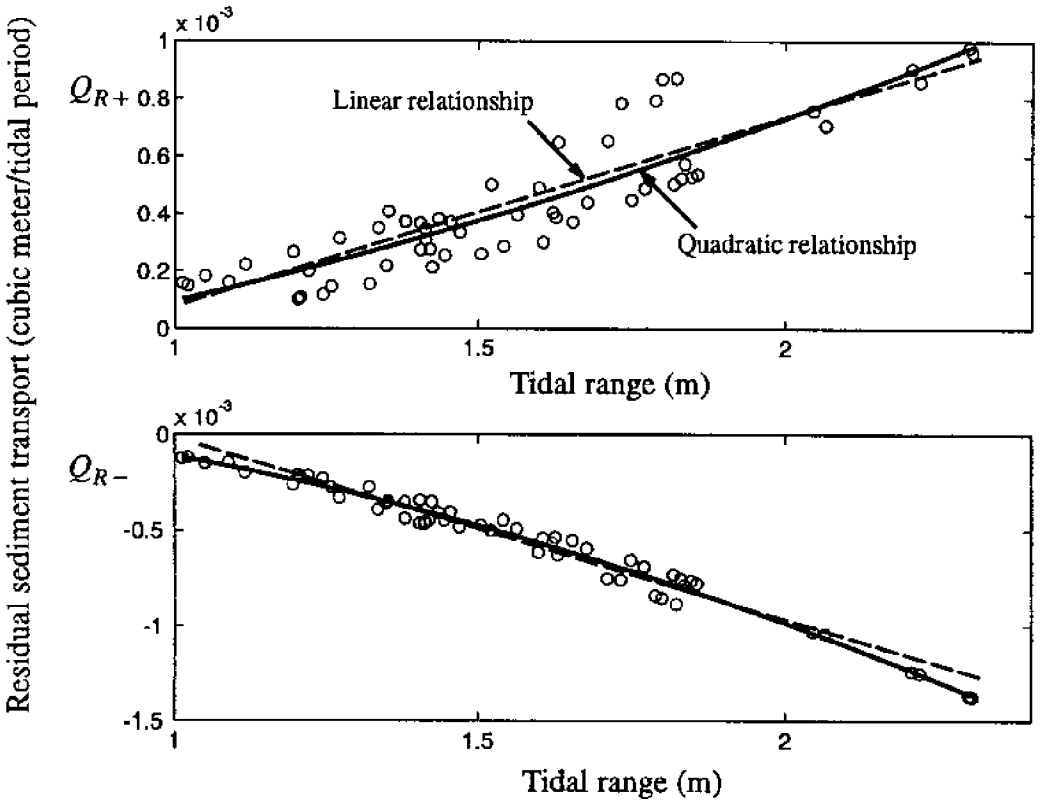

Figure 4.10 Residual sediment transports over a tidal cycle vs. tidal ranges at point B (see Figure 4.2).

arbitrary that a running time of 60 days was chosen. This implies the assumption that the empirical relations established previously were valid for a period of 60 days over which there was a 12% maximum relative bottom change. Similarly, the microscale model results from days 60–90 were saved and used for updating the required empirical relations. The mesoscale model was then run for 59 days starting from the 60th day. After this simulation cycle, the total running time of the mesoscale modeling was 119 days. By repeating this modeling procedure, the calculated bathymetric changes after 178 days were obtained. The lower plots in Figures 4.4, 4.5, and 4.6 show three–dimensional views of the calculated bathymetric change by the mesoscale model in the region of the inlet channel after 60, 119, and 178 days, respectively.

From these figures, a good similarity in the patterns of bottom changes between the two models is demonstrated. For instance, an ebb shoal and a flood shoal are formed on the bay side and the ocean side, respectively. The maximum scour occurs just behind the ebb shoal in the inlet

throat. By further comparing the three plots, both model results show that the flood shoal grows at a faster rate than the ebb shoal.

In addition to the comparison of the patterns of bottom changes, Figure 4.11 shows the history bottom changes calculated by the two models at two nodes, C and D, marked in Figure 4.2, where the maximum scour and deposition after 178 days are found in the microscale model results. The solid lines represent the results from the microscale model, and the dashed lines from the mesoscale model. It can be seen that the two model results are very close and demonstrate similar changing trends with tidal range. Table 4.1 and Figure 4.12 show the quantitative comparison of the maximum scour and deposition in the whole domain. The ratio of the maximum scour and deposition after 178 days from the microscale model to the mesoscale model are 0.70 and 0.83, respectively, i.e., the mesoscale model overpredicts maximum scour/deposition by 20–30%, compared to the microscale model. Through the comparisons of pattern and magnitude, the mesoscale model was found to give a satisfactory approximation to the microscale model.

Table 4.1 Comparison of maximum accretion and erosion between microscale and mesoscale model.

Model Run Time (Days)	Maximum Accretion (m)			Maximum Erosion (m)		
	Micro	Meso	$\frac{\text{Micro}}{\text{Meso}}$	Micro	Meso	$\frac{\text{Micro}}{\text{Meso}}$
60	0.247	0.372	0.66	0.465	0.550	0.85
119	0.334	0.558	0.60	0.748	0.889	0.84
178	0.452	0.648	0.70	0.941	1.128	0.83

4.C Results of Long–Term Simulation with Waves

A long–term simulation (3.3 years) of morphological changes of the hypothetical tidal inlet system subjected to tidal and wave forcing was conducted. The simulation includes the long–term bathymetric change at the inlet and the adjacent shoreline change.

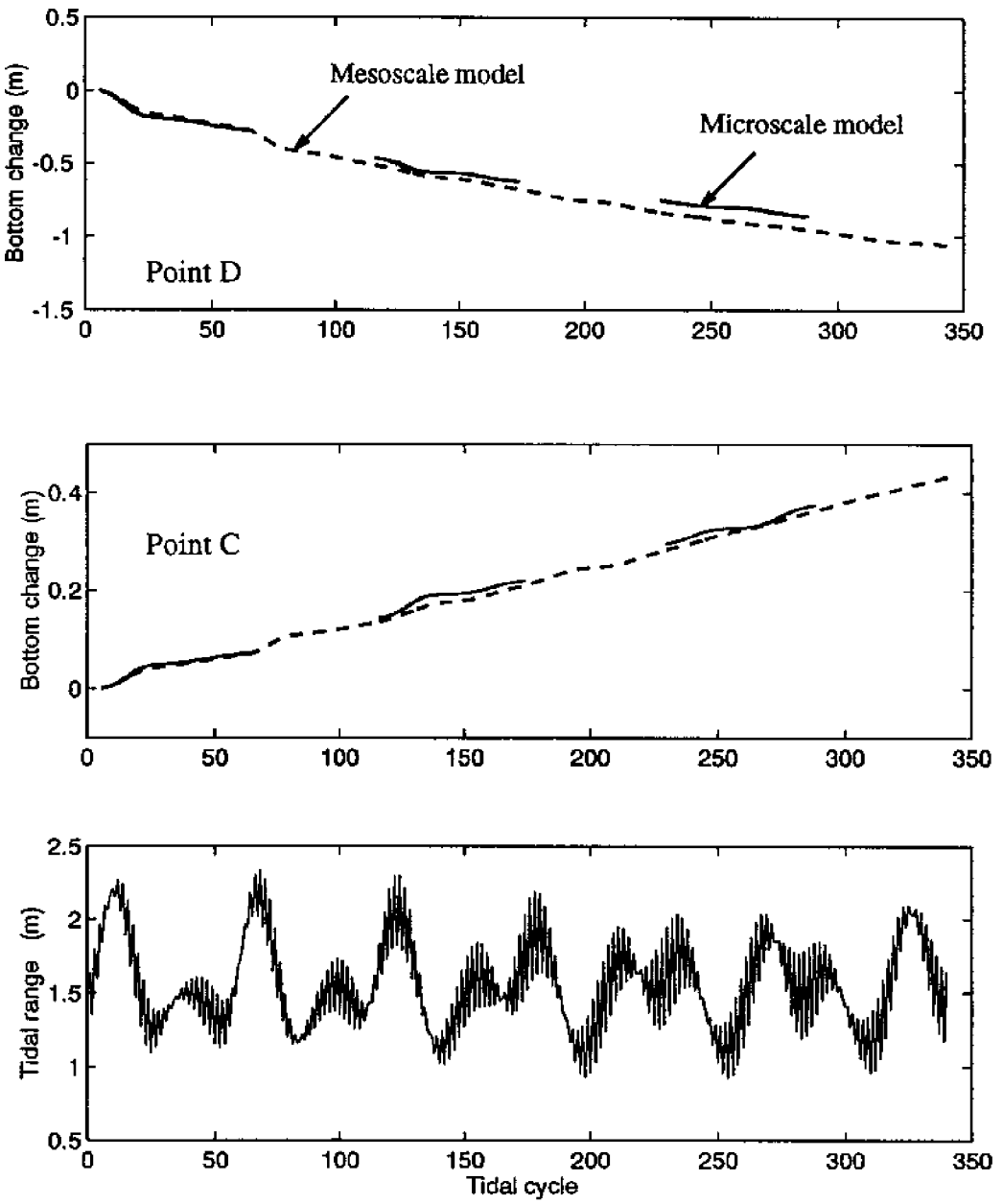

Figure 4.11 Comparison of bottom changes of mesoscale to microscale model at points C and D (see Figure 4.2).

The calculation of the shoreline change requires the breaking wave heights and directions as input to the shoreline change module. These wave parameters were provided by the wave transformation module. The area on the ocean side of the barrier islands, extending to the offshore boundary, was taken as the domain for wave modeling (shown in Figure 4.2 by dashed

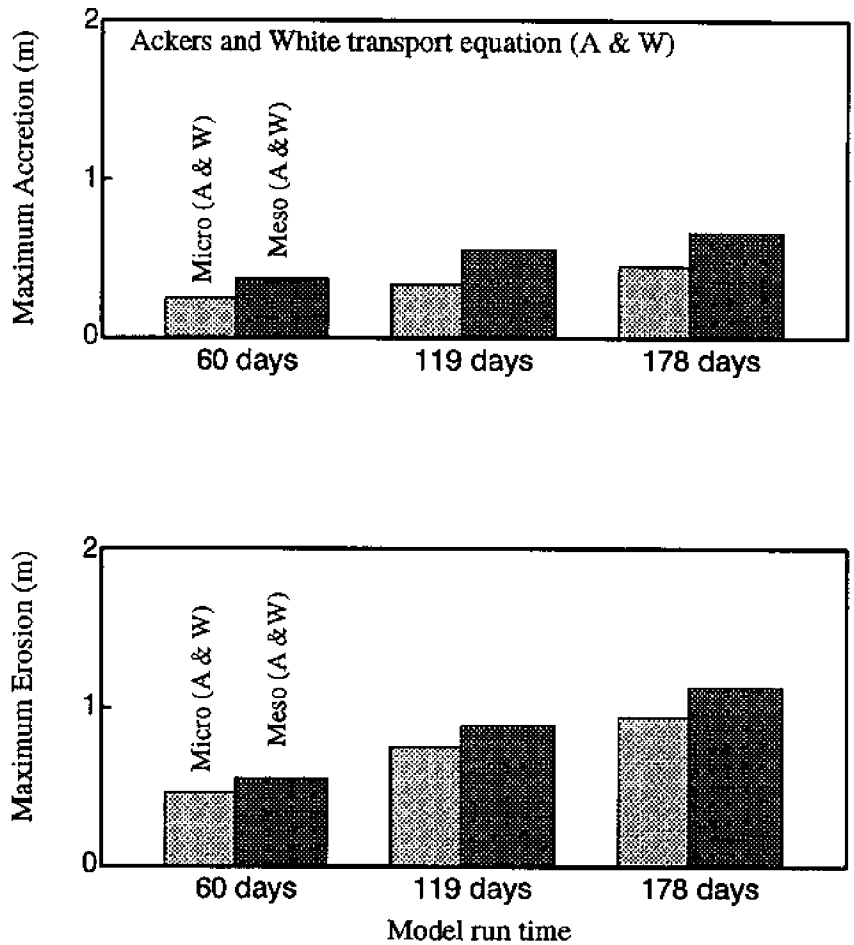

Figure 4.12 Comparison of calculated maximum bottom change between microscale and mesoscale model.

lines). Moreover, it was assumed that there are no waves on the bay side because of the shelter provided by the barrier islands. The grid size used in the wave modeling is the same as that of the mesoscale module, i.e., 375 m. The wave climate (wave height, direction, and period) was prescribed at the offshore boundary. Values were determined by random number generators, given mean values of wave height, direction, and period as well as the standard deviation of wave directions. It was assumed that wave heights and periods follow the Rayleigh probability distribution and that wave directions follow the normal distribution. The input wave condition was changed every 6 hours.

To more accurately determine the breaking wave heights and directions, the wave module automatically splits the grid of a sub–region of the wave domain into a finer one with a new grid size $\Delta y = 54$ m, where the wave breaking may occur. Figure 4.13 shows such a sub–region and the calculated wave vector fields along with bottom contours in the sub–region and the rest of the wave domain for the initial bathymetry.

The domain for the shoreline modeling consists of an updrift shoreline and a downdrift shoreline, each with a length of 5,250 m. The domain plus the inlet was divided into 32 computing cells, each 375 m long, matching the grid sizes of the other modules. The coordinate system and the grid are shown in Figure 4.14.

In the shoreline change calculation, the change of the water depth due to tides was not considered. The water depths at mean sea level were used. In the calculation of the amount of longshore sediment transport entering the inlet channel, it was assumed that a linear distribution of longshore sediment transport across the inlet was valid, and that Q_{out} in Equation 3.19 was equal to zero. Under this assumption, the sediment entering the inlet channel due to longshore sediment transport deposits uniformly in the four shadowed elements indicated in Figure 4.14.

A shoreline module test was done for investigating the responses of shoreline changes to constant and random input wave climate. Figure 4.15 shows the calculated shoreline changes after 60 days for random and constant wave input cases with an initially straight shoreline, and the distribution of longshore sediment transport rates for the constant wave input case. The mean wave height, period, and direction for the random wave case were used to represent the wave climate in the constant wave case. It is seen that the shoreline change under unchanging waves is less than under random waves with the same mean values of wave height and direction. This may be attributed to the nonlinear relationship between wave height and longshore sediment transport rate (Equation 3.14) and means that the mean wave height in a random field is not the "representative" wave.

In the bathymetric change simulation, the sediment transport equation and parameters related to sediment features are identical to those used in the model comparison described in the

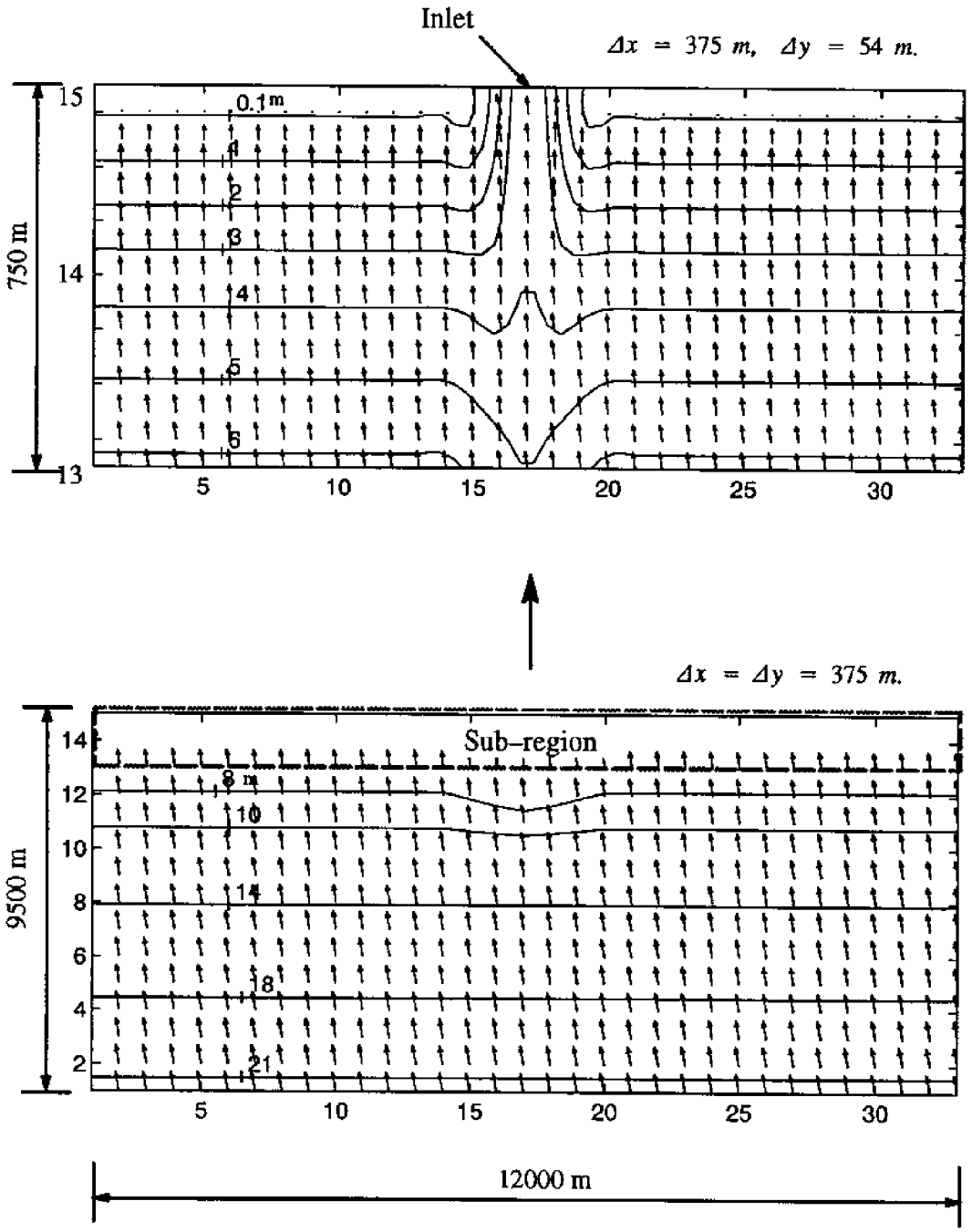

Figure 4.13 Calculated wave vectors over initial bathymetry (incident angle=10°, wave height=0.5 m, wave period = 6 sec. at offshore boundary). Upper plot shows sub–region of lower plot accented by dashed lines.

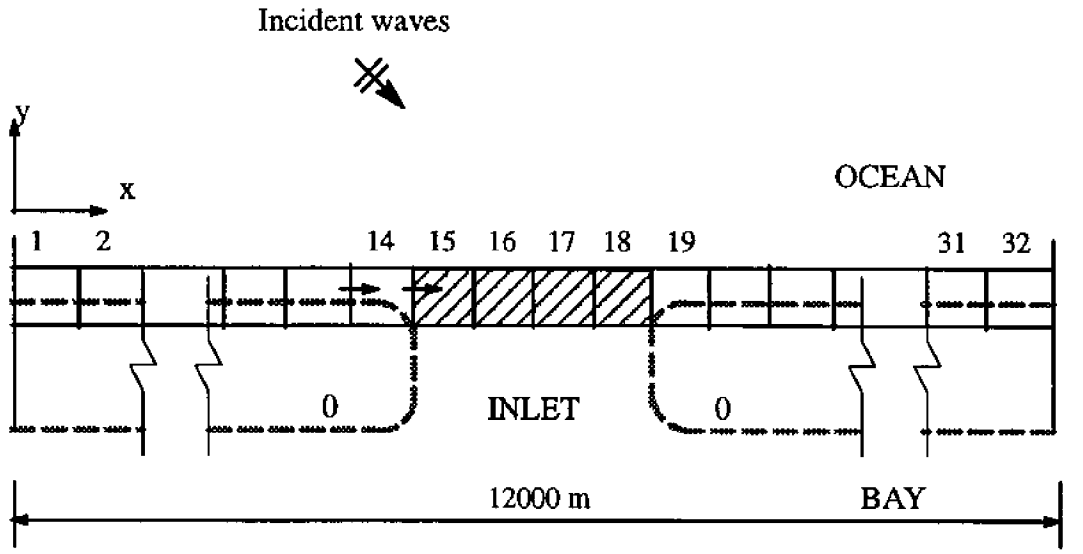

Figure 4.14 Shoreline change module grid.

previous section of this chapter. The time series of input tidal forcing (tidal range) in this simulation was extended by repeating the 202 day time series of tidal range used in the model comparison. In addition to the sediment transport due to tidal currents, the longshore sediment transport entering the inlet channel due to breaking waves was included in the calculation of the bathymetric changes.

Following the modeling procedure described in Chapter 3, the microscale hydrodynamic module was run for one lunar month for the construction of the empirical relations between the residual sediment transport over a tidal cycle and the tidal range at the offshore boundary. Based on the hydrodynamic results calculated by the microscale hydrodynamic module, the empirical relations were constructed. Using these empirical relations, the sediment transport module was then run for 59 days over which the maximum relative bottom change in the domain was 15%, a specified tolerance. And then, the wave transformation module and the shoreline change module were run for 59 days. A new bathymetry due to the tide–induced sediment transport and the longshore sediment transport entering the inlet channel was obtained. Using this new bathymetry, the microscale hydrodynamic module was re–run for one lunar month. Again, the sediment transport module was run until the maximum relative bottom change in the domain exceeds the specified tolerance, 15%. After this run, the total simulation time was 161 days.

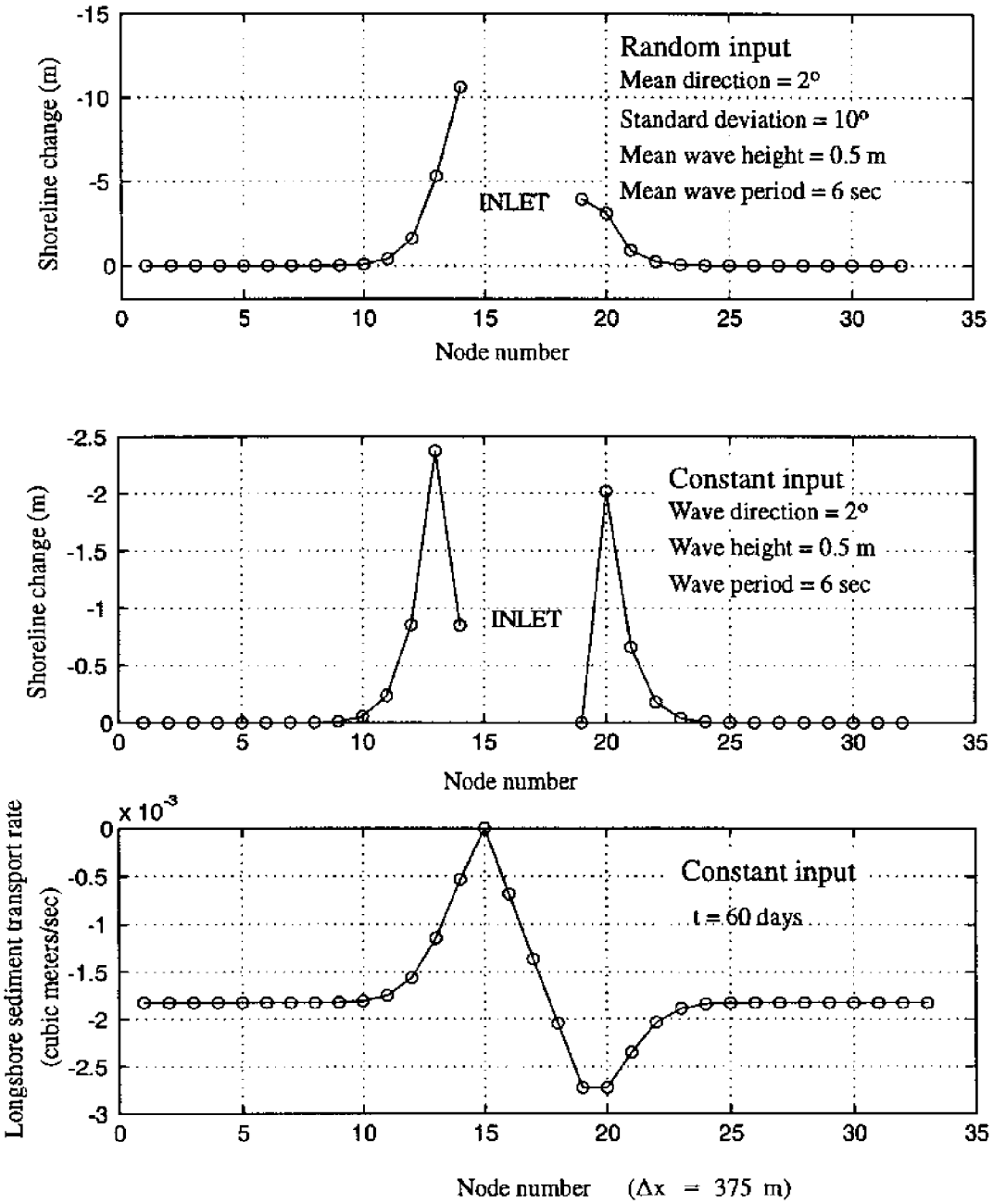

Figure 4.15 Comparison of calculated shoreline change using random and constant wave input conditions after 60 days.

Similarly, the wave transformation module and the shoreline change module were run for the same time period as that in the sediment transport module, and an updating bathymetry was obtained. By repeating this simulation procedure, the mesoscale model was run for 3.3 years.

Figure 4.16 presents calculated results of the shoreline change at selected points in time where the microscale hydrodynamic module was re–run for updating the empirical relations in the mesoscale modeling. The calculated shoreline changes indicate that both the updrift shoreline (i.e., the right shoreline in Figure 4.16) and downdrift shoreline retreat landward with time when a mean incident wave direction of 2 degrees was specified at the offshore boundary (see Figure 4.16). And, the downdrift shoreline retreats faster than does the updrift shoreline near the inlet. For a symmetric bathymetry with respect to the central line of the inlet channel, such shoreline change pattern is the result of a non–zero mean incident wave direction and the prescription of a permeable boundary condition which allows longshore sediment transport to enter the inlet channel from one adjacent beach and a "groin" boundary condition associated with the other adjacent beach. In addition, Table 4.2 summarizes the cumulative longshore sediment transport entering the inlet channel and the resulting cumulative bottom changes that would be found in the inlet channel if tidal currents did not redistribute sediment deposited by waves.

Figures 4.17 through 4.22 present the calculated bathymetry results in the vicinity of the inlet in the form of bottom contour and 3–D plots. Outside the region shown in the figures, where tidal currents are weaker due to large water depth and no considerable sediment transport is induced, no significant bathymetric change occurs. The calculated bathymetry shows the formation and evolution of ebb and flood shoals, important features of a tidal inlet. It is also shown that the longshore sediment entering the inlet channel is transported offshore and bayward by the inlet currents, and contributes to the formation of ebb and flood shoals. The calculated bathymetric change after 3.3 years is shown in Figure 4.23. The volume of the flood shoal is larger than that of the ebb shoal by a factor of 4. This is likely due to flood dominance of the inlet. The duration of the flood current exceeds that of the ebb. Comparing the calculated bathymetry at the end of 1,019 days to that at the end of 1,213 days (3.3 years), there is no

significant difference found except a small relocation of the ebb shoal. This indicates that an approach to equilibrium bathymetry of the hypothetical tidal inlet for the given tidal forcing and wave climate. This bathymetry development feature can be also seen in Figure 4.24 which shows the bottom change at point C at the inlet throat. Figure 4.24 indicates that the rate of bottom change decreases with time over the long term in spite of fluctuations within a short period of time (days).

The change of the empirical relation in time at the point E used in the mesoscale modeling is shown in Figure 4.25. The upper and lower plots show the change in the empirical relations in the positive and negative directions, respectively. Significant changes in the empirical relations in a short period of time (161 days) after the beginning of simulation can be found. After that, the rate of change is reduced considerably. Figure 4.26 shows changes of the empirical relation obtained by summing the empirical relations in the positive and negative directions at the point E.

Walton and Adams (1976) presented an empirical relationship between the volume of sediment stored in the ebb shoal and tidal prism. The relationship for moderately exposed coasts (Atlantic and Western gulf) in terms of average wave activity is expressed as:

$$V = 2.384 \times 10^{-4} P^{1.23} \qquad (4.1)$$

where V = volume of sediment stored in the ebb shoal (m^3).

Using Equation 4.1, the volume of sediment stored in the ebb shoal is $1.1 \times 10^6 m^3$. From the bathymetry calculated by the mesoscale model, the volume of sediment comprising the ebb shoal at the hypothetical inlet is $1.9 \times 10^6 m^3$ after 3.3 years. This comparison indicates that the volume of the ebb shoal calculated by the mesoscale model is roughly in agreement with that determined by Equation 4.1, a relationship determined with field data.

Table 4.2 Longshore transport entering inlet channel and resulting bottom change at inlet entrance on ocean side.

Run time (days)	Cumulative longshore sediment transport entering inlet channel (x 10^3 m^3)	Resulting bottom change (m)
60	59	0.1
161	160	0.3
325	349	0.6
548	601	1.1
817	936	1.7
1019	1,233	2.2
1213	1,443	2.6

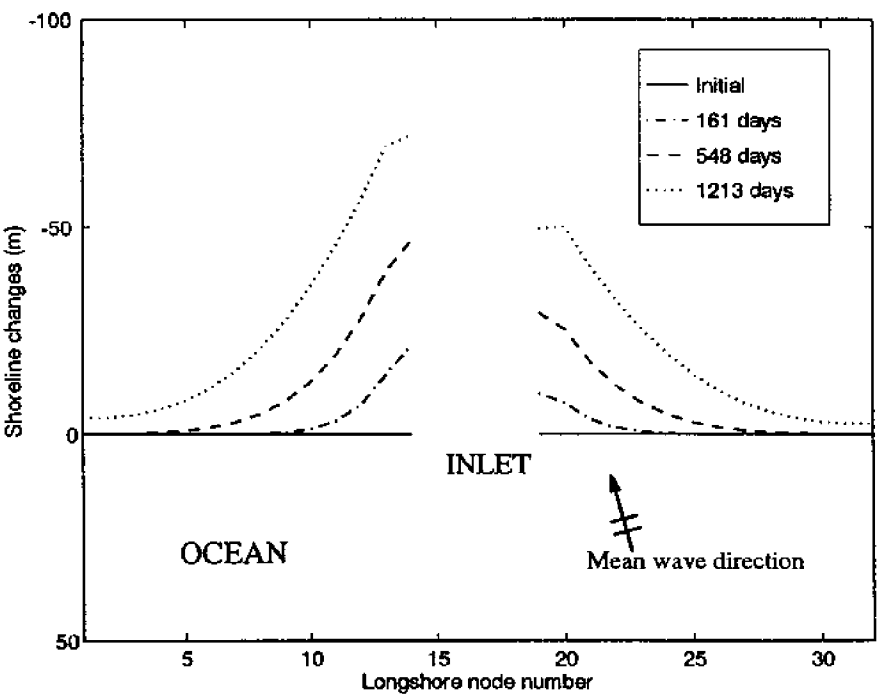

Figure 4.16 Calculated shoreline change with random waves (mean wave height = 0.5 m, period = 6 sec., mean angle = 2°, standard deviation of angle = 10°).

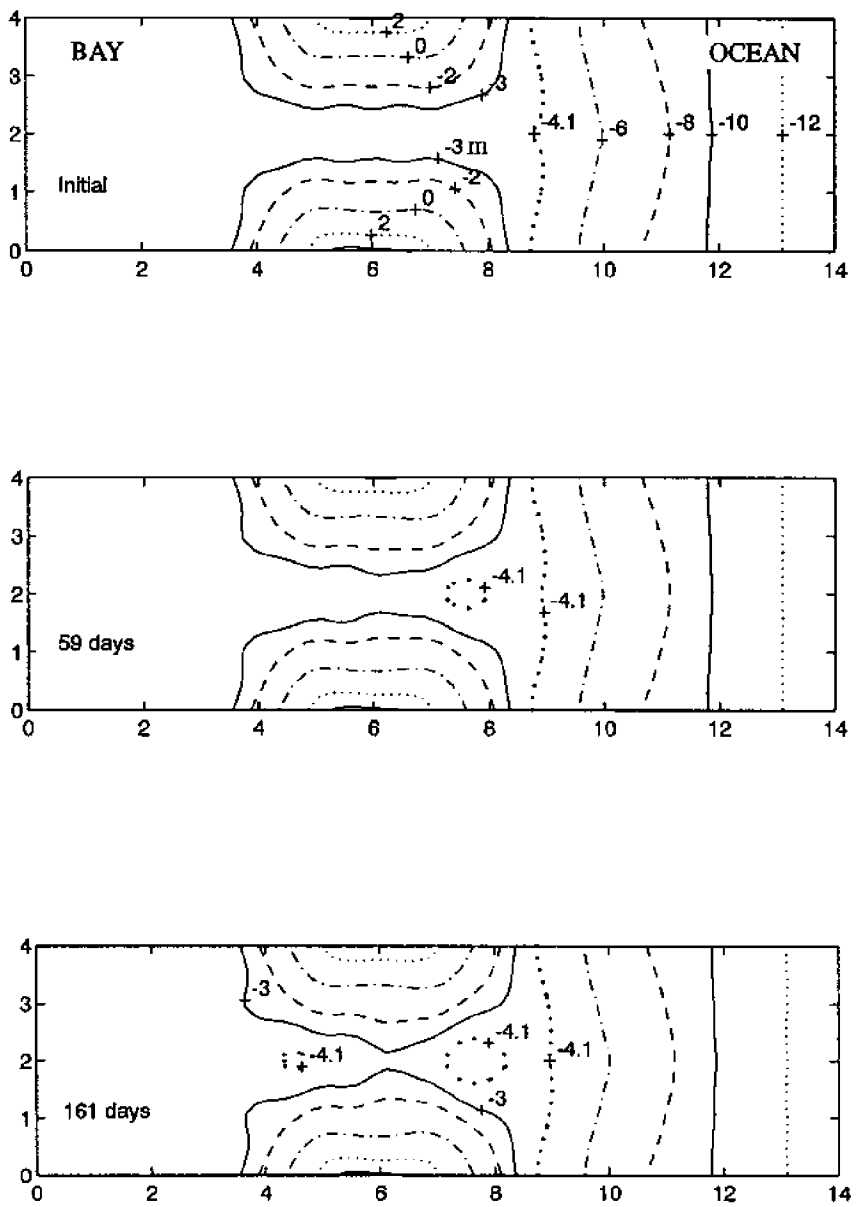

Figure 4.17 Initial and calculated bathymetry with random waves after 59 and 161 days (mean wave height = 0.5 m, period = 6 sec., mean angle = 2°, standard deviation of angle = 10°).

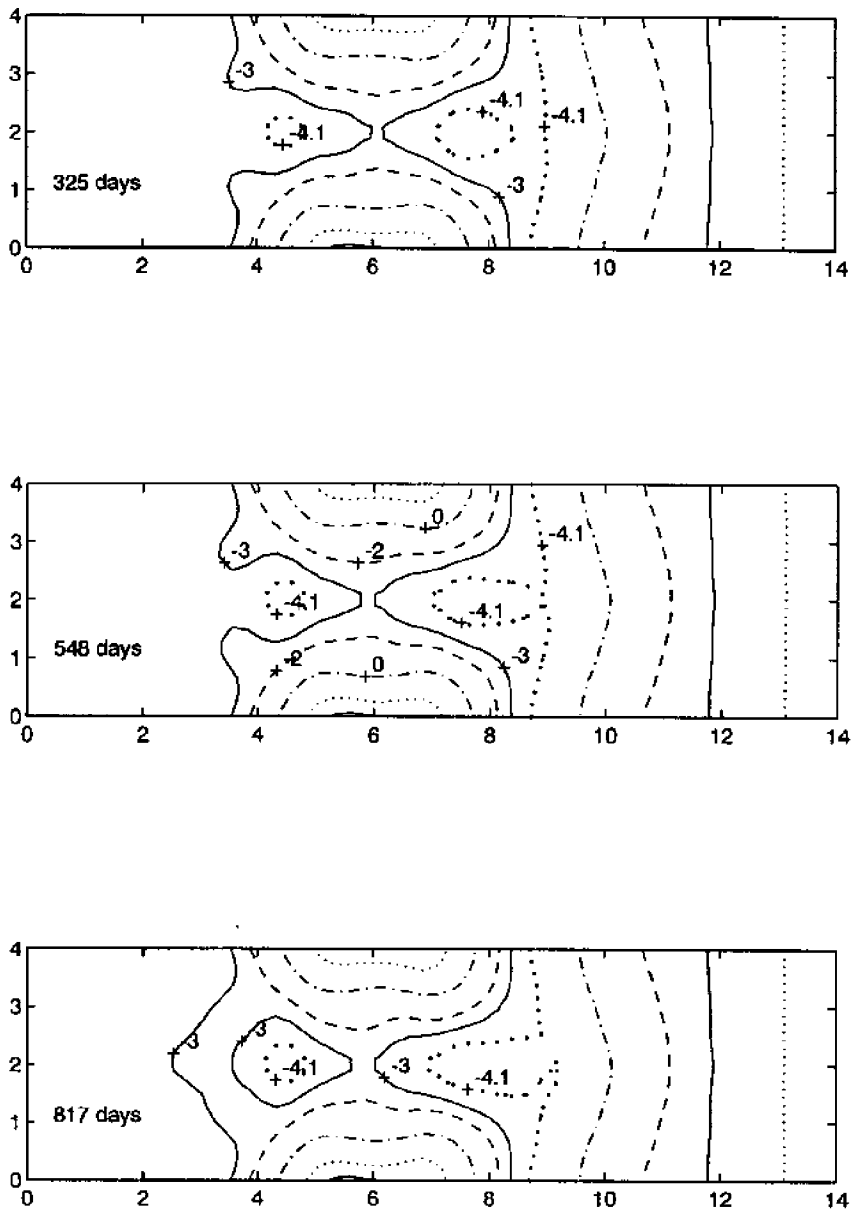

Figure 4.18 Calculated bathymetry with random waves after 325, 548, and 817 days (mean wave height = 0.5 m, period = 6 sec., mean angle = 2°, standard deviation of angle = 10°).

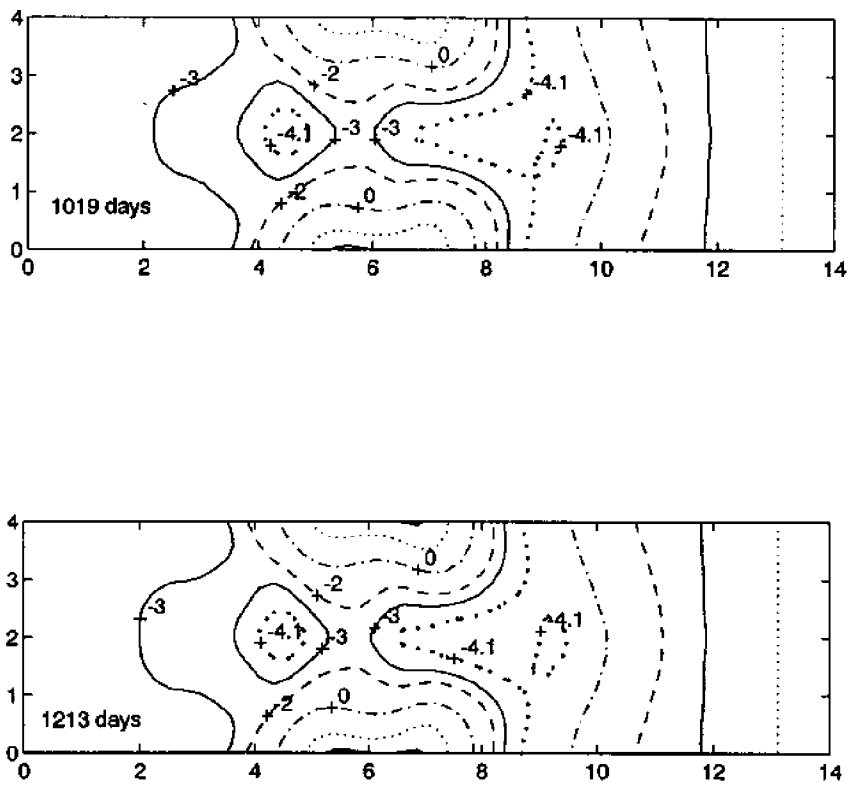

Figure 4.19 Calculated bathymetry with random waves after 1019 and 1213 days (mean wave height = 0.5 m, period = 6 sec., mean angle = 2°, standard deviation of angle = 10°).

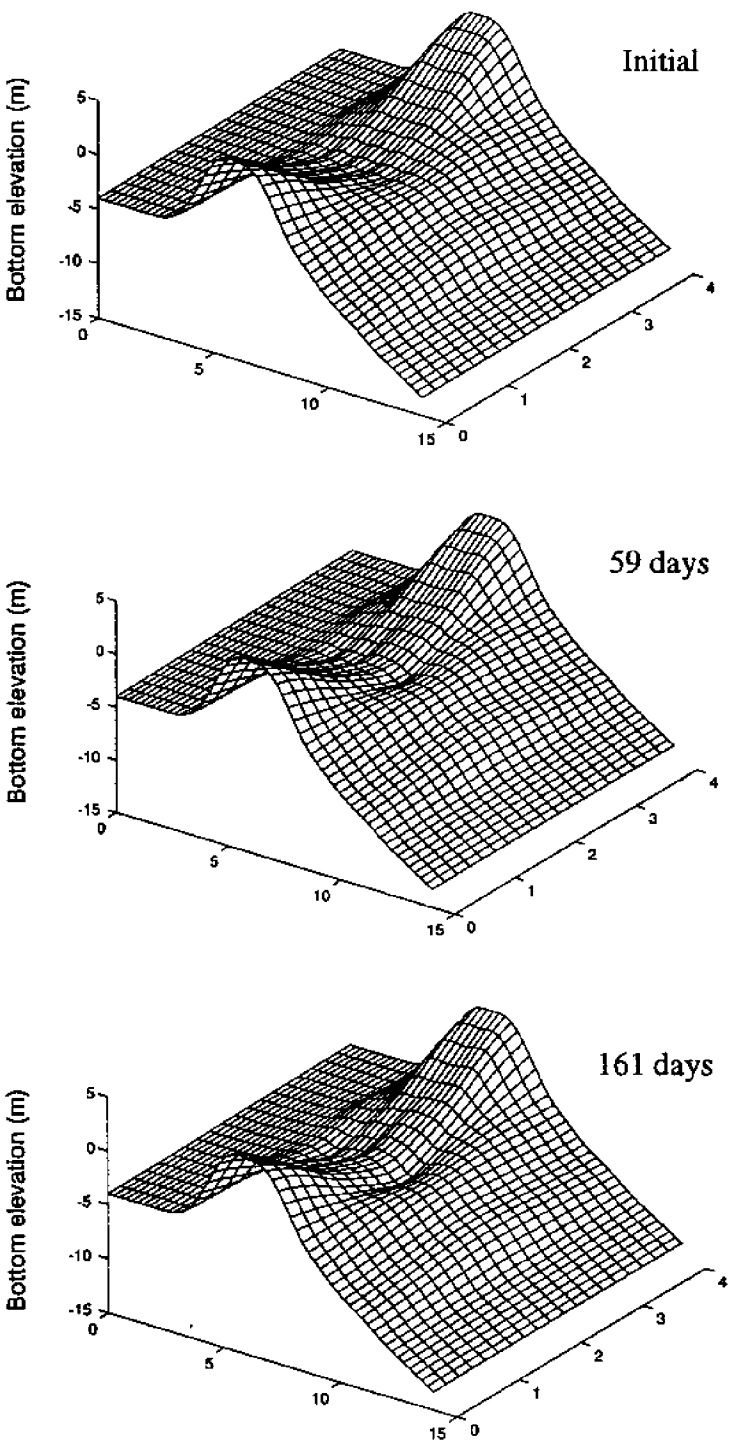

Figure 4.20 3–D view of initial and calculated bathymetry with random waves after 59 and 161 days (mean wave height = 0.5 m, period = 6 sec., mean angle = 2°, standard deviation of angle = 10°).

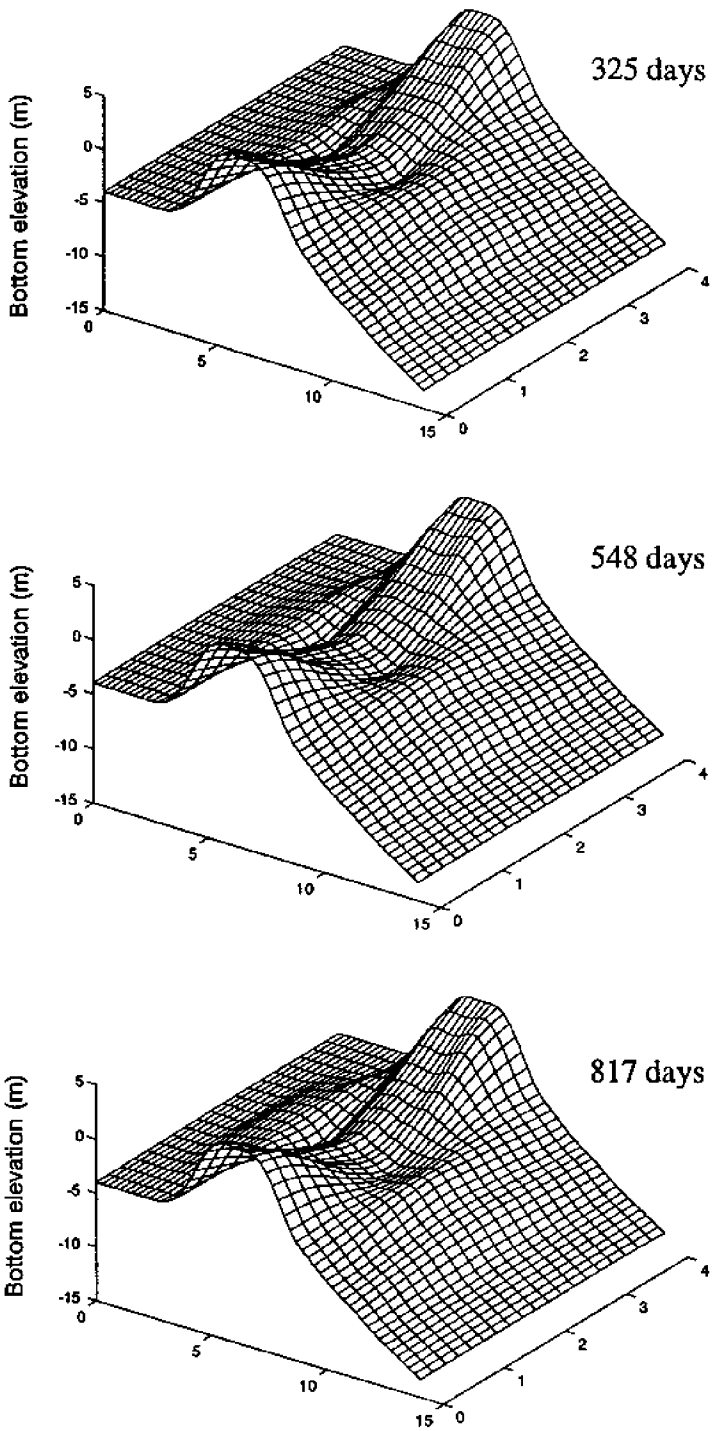

Figure 4.21 3–D view of calculated bathymetry with random waves after 325, 548, and 817 days (mean wave height = 0.5 m, period = 6 sec., mean angle = 2°, standard deviation of angle = 10°).

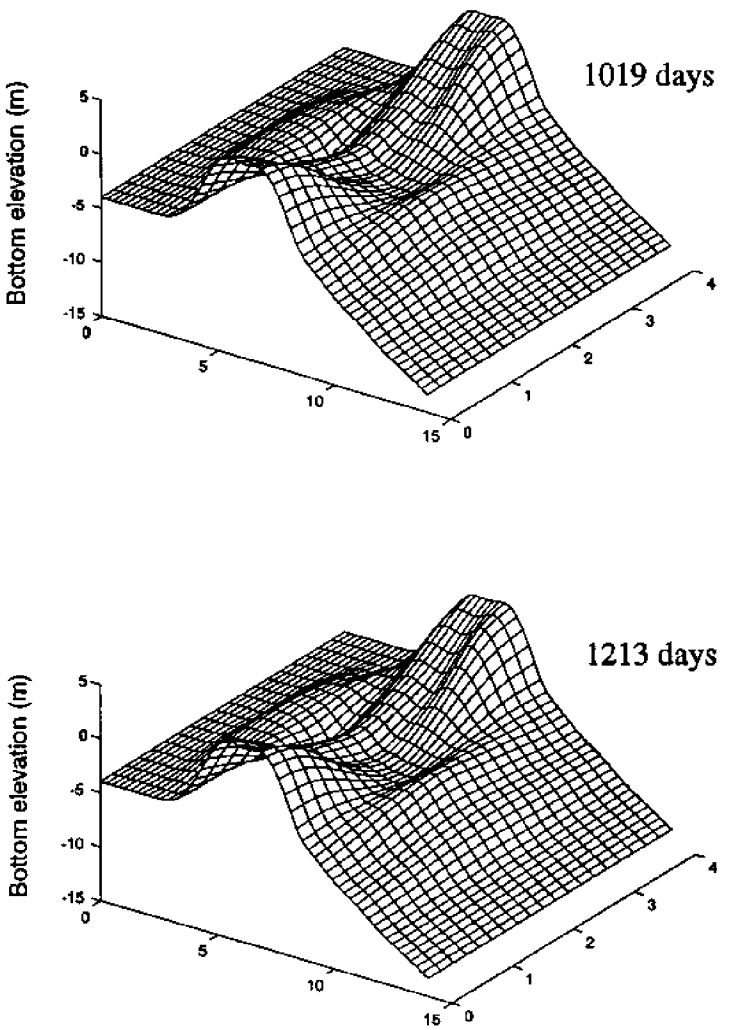

Figure 4.22 3–D view of calculated bathymetry with random waves after 1019 and 1213 days (mean wave height = 0.5 m, period = 6 sec., mean angle = 2°, standard deviation of angle = 10°).

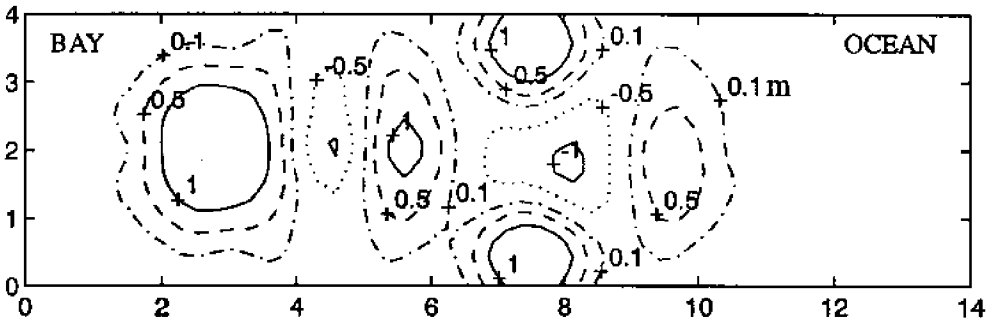

Figure 4.23 Calculated bathymetric change with random waves after 3.3 years (mean wave height = 0.5, period = 6 sec., mean angle = 2°, standard deviation of angle = 10°).

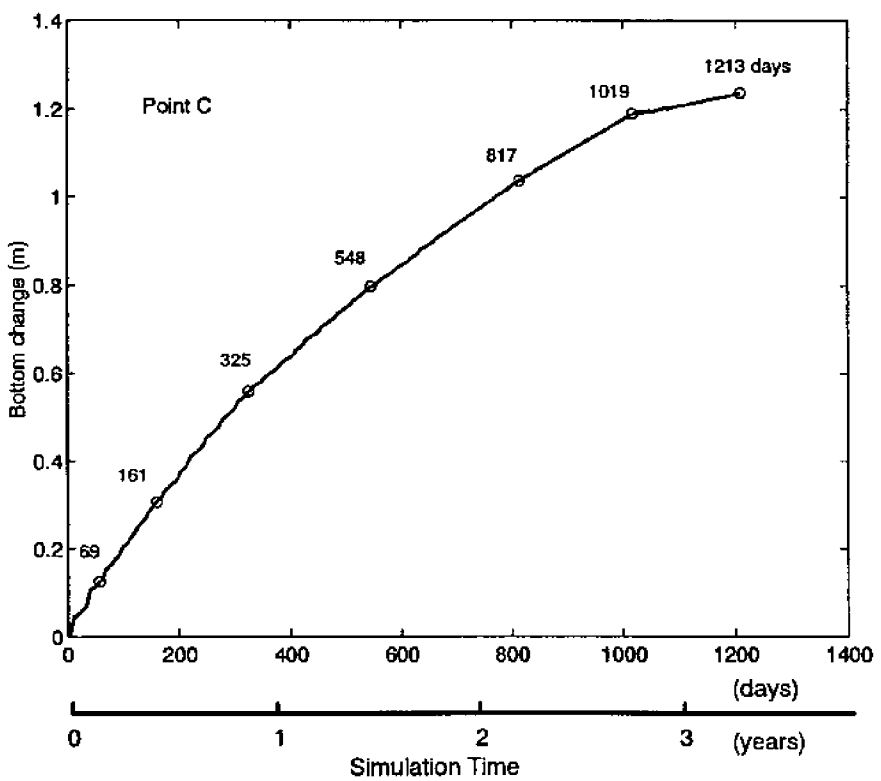

Figure 4.24 Calculated bottom change at point C (see Figure 4.2).

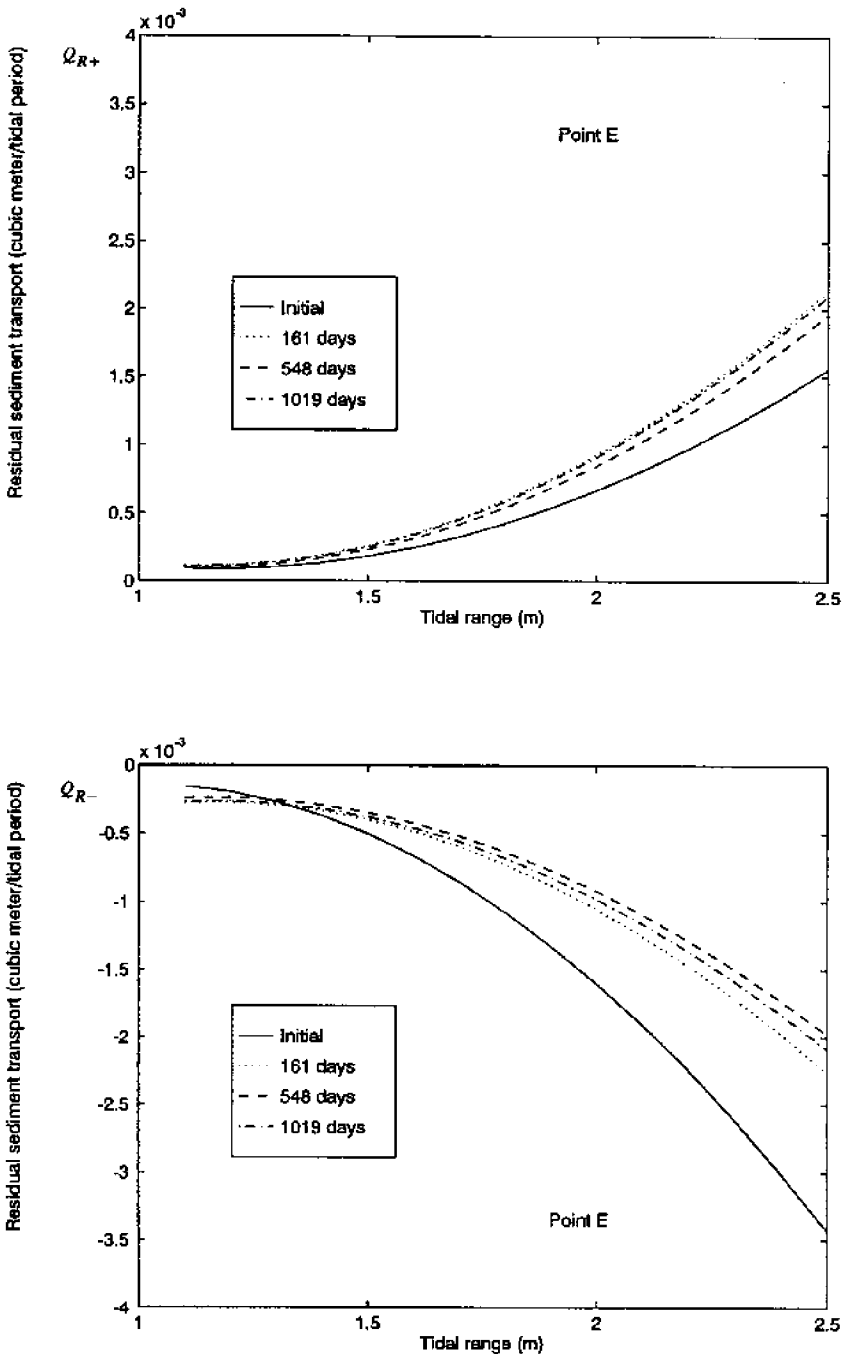

Figure 4.25 Changes of empirical relations in positive and negative directions at point E (see Figure 4.2).

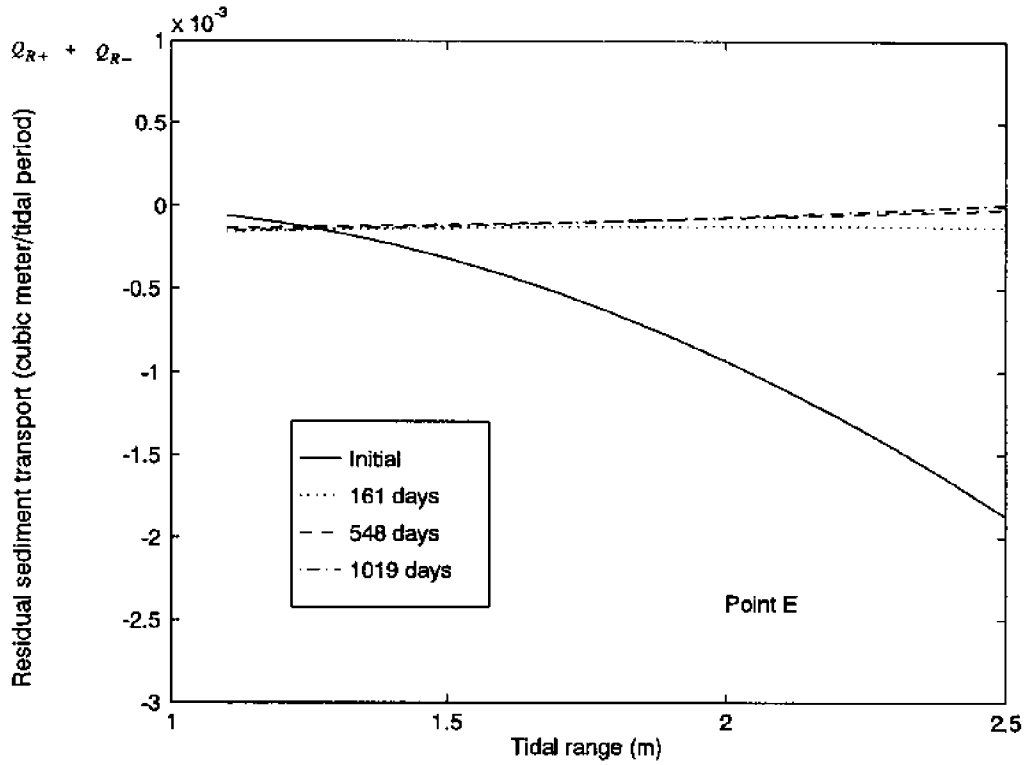

Figure 4.26 Change of empirical relation at point E (see Figure 4.2).

V CONCLUSIONS AND DISCUSSION

A mesoscale modeling approach for long–term (years to decades) simulation of the morphology (bathymetric and shoreline changes) of tidal inlets was addressed. The model includes tidal hydrodynamics, linear wave transformation, sediment transport by tidal currents, and shoreline change due to breaking waves. The validity of the overall mesoscale modeling approach was verified by comparing to results from a microscale model. The mesoscale model was applied to a hypothetical tidal inlet system at prototype scale under simulated wave and tidal input conditions. Additionally, a literature review of microscale and mesoscale modeling approaches as well as applicable sediment transport formulas was conducted. The following conclusions can be made based on the mesoscale model development and application to the hypothetical case.

1. The mesoscale modeling approach showed promising results through comparison to the microscale model results and a long–term simulation. From the calculated bathymetry results in a long–term (3.3 years) simulation, the ability of the mesoscale model to simulate the evolution of major features of a tidal inlet, such as ebb and flood shoals, was demonstrated. The pattern and magnitude of the calculated bathymetric changes appears reasonable compared to intuition, in spite of the lack of verification of field data. It, however, should be considered as a stepping stone rather than an end–point.

2. Since the mesoscale model relies on a microscale model and uses a large time step, the mesoscale model results basically are an "approximation" of the results of the microscale model. Moreover, the accuracy of the mesoscale model is controlled at least in part by that of the microscale model. For model verification, measured bathymetric changes within the domain to be modeled are essential. The other parameters must include tidal forcing and wave climate at the domain boundaries for input to the model, and measured currents and wave heights at a few locations within the domain for the model calibration and verification. The measured longshore sediment transport rate in the vicinity of a tidal inlet is also an important parameter in model verification.

3. The mesoscale modeling approach developed was limited to the cases where the sediment transport outside the surf zone is produced largely due to tidal currents. Wave action was not included. Under this circumstance, the tidal range can be taken as a representative parameter (independent variable) of the tidal driving force over a tidal period in constructing the empirical relations. This becomes the basis for use of a large time step, i.e., one tidal period, in the mesoscale modeling. If the action of waves is included, it is difficult to find a single parameter which represents the

effective wave action on sediment transport over a tidal period because the effect of waves has to be described by at least two parameters, the wave height and direction, if monochromatic waves are considered. In this case, at least two independent variables associated with waves are involved in the construction of the empirical relations even if the interaction of waves and currents is not considered. This may result in very complicated empirical relations. So, the method for including wave effect on sediment transport outside the surf zone in the mesoscale modeling approach needs further testing and improvement.

4. One lunar month of the microscale model run for the construction of the empirical relations still consumes a great deal of computer times. Improved methods for further reduction of the microscale model run time without considerably affecting the accuracy of empirical relations are desirable. For instance, the microscale model might be run for 3 days using a constant spring tidal range, then another 3 days using a constant mean and neap tidal ranges each. Three points can be obtained for construction of the empirical relations in a quadratic form.

5. The microscale module presently still is an independent model in terms of computing source code. The link between the microscale module and the other modules was conducted by transferring the output results from one module to another in data files "manually". An automatic link between the microscale module and the other modules should be made to improve modeling efficiency in the future, although that would make no difference in the calculated results.

6. The selection of a sediment equation suitable to such a study is difficult but important. In addition to the theoretical merits, the performance of the equation in prototype applications should be considered.

LITERATURE CITED

Abou–Seida, M.M. 1965. "Bedload Function due to Wave Action." Rep. HEL–2–11, Hydraul. Eng. Lab., Univ. Calif., 78.

Ackers, P. and W.R. White. 1973. "Sediment Transport: A New Approach and Analysis." J. of Hydraulic Division, ASCE, 99(HY11), 2041–2060.

Andersen, O.H., I.B. Hedegaard, R. Deigaard, P. de Girolamo, and P. Madsen. 1988. "Model for Morphological Changes under Waves and Currents." IAHR Symposium on Mathematical Modeling of Sediment Transport in the Coastal Zone, Copenhagen, Denmark.

Andersen, O.H., I.B. Hedegaad, J.K. Ronberg, R. Deigaard, and P. Madsen. 1991. "Model for Morphological Changes in the Coastal Zone." In: Preprints IAHR Symp. Math. Mod. Sed. Transp., Florence, 327–338.

Bagnold, R.A. 1966. "An Approach to the Sediment Transport problem form General Physics." USGS Professional Paper 422–J.

Bailard, J.A. 1981. "An Energetic Total Load Sediment Transport Model for A Plane Sloping Beach." J. Geophys. Res., Vol 86 (c11), 10938–10954.

Broker, I., H.K. Johnson, J.A. Zyserman, J.K. Ronberg, C. Pedersen, R. Deigaad, and J. Fredsoe. 1995. "Coastal Profile and Coastal Area Morphodynamic Modeling." MAST–G8M Final Report, 7–12.

Brown, C.B. 1950. "Sediment Transportation." in Engineering Hydraulics, H. Rouse, ed., John Wiley & Sons, New York, 1950, Chapter XII.

Bruun, P. 1978. Stability of tidal inlets. Elsevier Scientific Publishing Company. Amsterdam.

Buckingham, W.T. 1984. Coastal Engineering Investigation at Jupiter Inlet, UFL/COEL–84/004, Coastal and Oceanographic Engineering Department, University of Florida, Gainesville, Florida.

Butler, H.L. 1980. "Evolution of a Numerical Model for Simulating Long Wave Behavior in Ocean–Estuarine System." Estuarine and Wetlands Processes with Emphasis on Modeling, Marine Science Series, Vol. 11, Plenum, New York.

CERC. 1984. Shore Protection Manual. Dept. of the Army Waterways Experiment Station, Corps of Engineers, Vicksburg, Mississippi, Vol. 1 and 2.

Chesher, T.J., D.M. Price, and H.N. Southgate. 1995. "Long–term Morphodynamic Coastal Area Modeling." MAST–G8M Final Report, 7–25.

Chesher, T.J., and G.V. Miles. 1992. "The Concept of A Single Representative Wave." In: R.A. Falconer, S.N. Chandler–Wilde and S.Q. Liu (editors), Hydraulic and Environmental Modelling: Coastal Waters. Ashgate, Brookfield, VT, 371–380.

Chang, H.H. 1992. Fluvial Processes in River Engineering. Krieger Publishing Company, Malabar, Florida.

Chesher, T.J., D.M. Price, and H.N. Southgate. 1995. "Long–term Morphodynamic Coastal Area Modeling". MAST–G8M Final Report, 7–25.

Colby, B.R. 1964. "Discharge of Sands and Mean Velocity Relationships in Sand–Bed Streams." USGS Professional Paper 462–A.

Dally, W.R., R.G. Dean and R.A. Dalrymple. 1984. Modeling Wave Transformation in the Surf Zone, Miscellaneous papers CERC–84–8, U.S. Army Engineer Waterway Experiment Station, Vicksburg, Mississppi.

Dean, R.G., and R.A. Dalrymple. 1984. Water Wave Mechanics for Engineers and Scientists. World Scientific Publishing Co., Singapore.

DeVriend, H.J., M. Capobianco, T. Chesher, H.E. deSwart, B. Latteux and M.J.F. Stive. 1993. "Approaches to long–term modeling of coastal morphology: a review." Coastal Engineering, 21:225–269.

DeVriend, H.J. 1991. "Mathematical Modeling and Large–scale Coastal Behavior." J. of Hydraulic Research, Vol. 29, No. 6.

DeVriend, H.J. 1990. "Morphological Processes in Shallow Tidal Seas". In: R.T. Cheng (editor), Residual Currents and long–term Transport. Coastal and Estuarine Studies, Vol. 38. Springer–Verlag, New York, 276–301.

DuBoys, P. 1879. "Le Rhone et les Rivieres a Lit Affouillable." Annales des Ponts et Chaussees, 18, Series 5, 149–195.

Dalrymple, R.A. 1988. "Model for Refraction of Water Waves." J. Waterway, Port, Coastal and Ocean Engineering, Vol. 114, No. 4, ASCE, New York, NY, 423–435.

Ebersole, B.A., M.A. Cialone, and M.D. Prater. 1986. "Regional Coastal processes Numerical Modeling System Report 1: RCPWAVE–A Linear Wave Propagation Model for Engineering Use." Technical Report CERC–86–4, U.S. Army Corps of Engineers, Coastal Engineering Research Center, Vicksburg, MS.

Ebersole, B.A. 1985. "Refraction–Diffraction Model for Linear Water Waves". J. of Waterway, Port, Coastal and Ocean Engineering, Vol 111, No. 6, 939–953.

Ebersole, B.A. and R.A. Darymple. 1979. "A Numerical Model for Nearshore Circulation Including Convective Acceleration and Lateral Mixing." Ocean Engineering Rept. No. 21, Dept. of Civil Eng., University of Delaware, Newark, Delaware.

Engelund, F. and E. Hansen. 1967. A Monography on Sediment Transport in Alluvial Streams. Teknisk Vorlag, Copenhagen, Denmark.

Graf, W.H. 1971. Hydraulics of Sediment Transport. McGraw–Hill, New York.

Hanson, H. and N.C. Kraus. 1989. GENESIS: Generalized Model for Simulating Shoreline Change. U.S. Army Corps of Engineers, Waterways Experiment Station, Vicksburg, MS.

James, M.L. 1977. Applied Numerical Methods for Digital Computation with FORTRAN and CSMP, Harper & Row, New York.

Kaihatu, J.M. and J.T. Kirby. 1992. "Spectral Evolution of Directional Finite Amplitude Dispersive Waves in Shallow Water." Proc. Twenty–third Coastal Engineering Conf., ASCE, New York, NY.

Kalkanis, G. 1964. Transportation of Bed Material due to Wave Action. Technical Memorandum No. 2, U.S. Army Corps of Engineers.

Kirby, J.T. 1984. "A Note on Linear Surface Wave–Current Interaction over Slowly Varying Topography." J. Geophys. Res., Vol. 89, No. C1, 745–747.

Kirby, J.T. and H.T. Ozkan. 1994. "Combined Refraction/Diffraction Model for Spectral Wave Conditions." REF/DIF S, Version 1.1. Documentation and User's Manual. CACR Report No. 94–04, Center for Applied Coastal Research, Dept. of Civil Engineering, Univ. of Delaware, Newark, DE.

Koutitas, C.G. 1988. Mathematical Models in Coastal Engineering. Pentech Press, London.

Larson, M. and N.C. Kraus. 1989. SBEACH: Numerical Model for Simulating Storm–induced Beach Change. U.S. Army Corps of Engineers, Coastal Engineering Research Center, Vicksburg, Mississippi.

Larson, M., H. Hanson, and N.C. Kraus. 1987. "Analytical solution of the one–line model of shoreline change." Technical Report CERC–87–15, U.S. Army Corps of Engineers, Coastal Engineering Research Center, Vicksburg, Mississippi.

Letteux, B. 1992. "Long–term morphological simulation under tidal current with non–cohesive sediment." MAST G6–M Final Workshop, paper 5.18.

Latteux, B., C. Le Normant, and E. Peltier. 1995. "Long–term morphological simulation under–tidal current with non–cohesive sediment." MAST–G8M Final Report, 7–11.

Lee, J.L. and H. Wang. 1992. "Evaluation of Numerical Models on Wave–Currents Interactions." Proc. 23rd Inter. Coastal Eng. Conf., ASCE, Venice, Italy.

Manohar, M. 1955. Mechanics of Bottom Sediment Movement due to Wave Action. Technical Memorandum No. 75, Beach Erosion Board, U.S. Army Corps of Engineers.

Maruyama, K., and T. Takagi. 1988. "A Simulation System of Nearshore Sediment Transport for the Coupling of the Sea–bottom Topography, Waves and Currents." IAHR Symposium on Mathematical modeling of Sediment Transport in the Coastal Zone, Copenhagen, Denmark.

McCowan, J. 1894. "On the Highest Wave of Permanent Type." Philos. Mag. J. Sci., Vol. 38.

Mehta, A.J., and P.B. Joshi. 1984. Review of Tidal Inlet Hydraulics. UFL/COEL–TR/054, Coastal and Oceanographic Engineering Department, University of Florida, Gainesville, Florida.

Meyer–Peter, E. and R. Muller. 1948. "Formulas for Bed–Load Transport." Paper No. 2, Proc. of the Second Meeting, IAHR, 1984, 39–64.

Nielsen, P. 1992. Coastal Bottom Boundary Layers and Sediment Transport. World Scientific, Singapore.

Nishimura, H. 1982. "Numerical Simulation of Nearshore Circulation." Proc. of 29th Conf. on Coastal Engineering in Japan, 333–337 (in Japanese).

O'Brien, M.P. 1969. "Equilibrium Flow Areas of Inlets on Sandy Coasts." J. Waterways and Harbors Div., ASCE, New York, N.Y., Vol. 95, 43–52.

O'Connor, B.A. and J. Nicholson. 1992. "An Estuarine and Coastal Sediment Transport Model." In: D. Prandle (editor), Dynamics and Exchanges in Estuaries and the Coastal Zone. Springer Verlag, New York.

Ohnaka, S. and A. Watanabe. 1990. "Modeling of Wave–Current Interaction and Beach Change." Proc. 22nd Inter. Coastal Eng. Conf., ASCE, Delft, The Netherlands, 2443–2456.

Raudkivi, A.J. 1976. Loose Boundary Hydraulics. 2nd edition, Pergamon, Oxford, England.

Resio, D.T. 1993. "Program STWAVE: Wave Propagation Simulation Theory, Testing, and Application." Draft Report, U.S. Army Engineer Waterways Experiment Station, Coastal Engineering Research Center, Vicksburg, MS.

Seelig, W.N. and R.M. Sorensen. 1978. "Numerical Model Investigation of Selected Tidal Inlet–Bay System Characteristics." Proc. of 16th ICCE, 1302–1319.

Shen, H.W. and C.S. Hung. 1972. "An Engineering Approach to Total Bed Material Load by Regression Analysis." in Sedimentation, H.W. Shen, ed., Fort Collins, Colorado, Chapter 14.

Shields, A. 1936. "Anwendung Aenlich Keitsmenchanik und der Trubulenzfor–schung auf Die Geschiebewegun," Mitteilungen de Preussischen Versuchsanstalt fur Wasserbau und Schiffbau, Berlin, Germany.

Sill, B.L., J.S. Fisher, and S.D. Whiteside. 1981. "Laboratory Investigation of Ebb Tidal Shoals." J. of Waterway, Port, Coastal and Ocean Engineering, ASCE, Vol. 107, 233.

Simons, D.B. and F. Senturk. 1977. Sediment Transport Technology. Water Resources Publishing, Litteton, Colorado.

Steijn, R.C., T. Louters, A.J.F. van der Spek and H.J. deVriend. 1989. "Numerical model hindcast of the ebb–tidal delta evolution in front of the Deltaworks." In: R.A. Falconer et al. (eds.), Hydraulic and Environmental Modeling of Coastal, Estuarine and River Waters. Gower Technical, Aldershot, 255–264.

Stive, M.J.F. and H.J. DeVriend. 1995. "Advances in Modeling of Large Scale Coastal Evolution." MAST–G8M Final Report, 7–6.

Van Rijn, L.C. 1984. "Sediment Transport, Part I: Bed Load Transport." J. of Hydraulic Engineering, No. 10.

Van Rijn, L.C. 1984. "Sediment Transport, Part II: Suspended Load Transport." J. of Hydraulic Engineering, No. 11.

Veeramachaneni, R., and E.J. Hayter. 1988. "Mathematical modelling of sediment transport at tidal inlets." In Proc. IAHR Symposium on Mathematical Modelling of Sediment Transport in the Coastal Zone, Copenhagen, Denmark, 23–32.

Vemulakonda, S.R., J.R. Houston, and A. Swain. 1988. "Development and application of a coastal and inlet process modeling system." In D.G. Aubrey and L. Weishar (eds.), Hydrodynamics and Sediment Dynamics of Tidal Inlets, Springer–Verlag, New York, 54–70.

Vemulakonda, S.R., and N.W. Scheffner. 1987. Application of CIP Modeling System to St. Marys Inlet, Florida. U.S. Army Corps of Engineers, Coastal Engineering Research Center, Vicksburg, Mississippi.

Vincent, C.L., and M.J. Briggs. 1989. "Refraction–Diffraction of Irregular Waves over A Mound." J. Waterway, Port, Coastal and Ocean Engineering, Vol. 115, No. 2, ASCE, New York, NY, 269–284.

Vincent, C.E., R.A. Young, and D.J.P. Swift. 1981. "Bed–Load Transport under Waves and Currents." Marine Geology, Vol. 39, 71–80.

Vincent, M.S. 1992. "A Numerical Scour–Deposition Model for Tidal Inlets." Master's thesis, Department of Civil Engineering and Mechanics, University of South Florida.

Walton, T.L., and W.D. Adams. 1976. "Capacity of Inlet Outer Bars to Store Sand." Fourteenth International Coastal Engineering Conference, Honolulu, Hawaii.

Wang, H., G. Miao, and L.–H. Lin. 1992. "A time–dependent nearshore morphological response model." 23rd International Coastal Engineering Conference, Vol. 3, 2513.

Wang, H., L. Lin, H. Zhong, and G. Miao. 1991. Sebastian Inlet Physical Model Studies. Part I: Fixed Bed Model. Coastal and Oceanographic Engineering Department, University of Florida. UFL/COEL–91/001.

Wang, H., L. Lin, H. Zhong, and G. Miao. 1992. Sebastian Inlet Physical Model Studies. Part II: Movable Bed Model. Coastal and Oceanographic Engineering Department, University of Florida, UFL/COEL–92/014.

Watanabe, A., K. Maruyama, T. Shimizu, and T. Sakakiyama. 1984. "Numerical Simulation Model of Horizontal Topography Change Due to Artificial Structures", Proc. of 31th Conf. on Coastal Eng. in Japan, 406–410 (in Japanese).

Watanabe, A., K. Maruyama, T. Shimizu, and T. Sakakiyama. 1986. "Numerical prediction model of three–dimensional beach deformation around a structure". Coastal Eng. Jpn., 29: 179–194.

Wells, W.J. 1988. Ebb Tidal Shoal Formation under Oscillatory Tidal Flow on A Sloping Bottom and Waves, M.S. Thesis, Dept. of Civil Engineering, Clemson University, Clemson, South Carolina.

Work, P.A. and W.E. Rogers. 1994. Laboratory Study of Beach Nourishment Behavior. Project Rept. to SC Sea Grant Consortium, Dept. of Civil Engineering, Clemson University, Clemson, South Carolina.

Work, P.A. and R.G. Dean. 1995. "Assessment and Prediction of Beach Nourishment Evolution." J. of Waterway, Port, Coastal and Ocean Engineering, 121(3), ASCE, 182–189.

Work, P.A., Y. Zhang, E.J. Hayter, and T.W. Kana. 1996. "Mesoscale Modeling of Sediment Transport and Morphologic Changes at Tidal Inlets: Years 1 & 2." Project Report to SC Sea Grant Consortium, Dept. of Geological Science, Univ. of South Carolina.

Yang, C.T. 1972. "Unit Stream Power and Sediment Transport." J. Hydraulic Division, ASCE, 98 (HY10), 1805–1826.

Yang, C.T. 1984. "Unit Stream Power Equation for Gravel." J. Hydraul. Eng. ASCE, 110(HY12), 1783–1798.

Zhang, Y. 1996. Long–Term Numerical Simulation of Morphology of Tidal Inlets, M.S. Thesis, Dept. of Civil Engineering, Clemson University, Clemson, South Carolina.